

1 **The Genetic Architecture of Biological Age in Nine Human Organ** 2 **Systems**

3 Junhao Wen^{1*}, Ye Ella Tian², Ioanna Skampardoni³, Zhijian Yang³, Yuhan Cui³, Filippos
4 Anagnostakis⁴, Elizabeth Mamourian³, Bingxin Zhao⁵, Arthur W. Toga⁶, Andrew Zalesky²,
5 Christos Davatzikos³

6
7 ¹Laboratory of AI and Biomedical Science (LABS), Stevens Neuroimaging and Informatics Institute, Keck School
8 of Medicine of USC, University of Southern California, Los Angeles, California, USA

9 ²Melbourne Neuropsychiatry Centre, Department of Psychiatry, Melbourne Medical School, The University of
10 Melbourne, Melbourne, Victoria, Australia

11 ³Artificial Intelligence in Biomedical Imaging Laboratory (AIBIL), Center for AI and Data Science for Integrated
12 Diagnostics (AI²D), Perelman School of Medicine, University of Pennsylvania, Philadelphia, USA

13 ⁴Department of Medical and Surgical Sciences, University of Bologna, 40126 Bologna, Italy

14 ⁵Department of Statistics and Data Science, University of Pennsylvania, Philadelphia, PA, USA

15 ⁶Laboratory of Neuro Imaging (LONI), Stevens Neuroimaging and Informatics Institute, Keck School of Medicine
16 of USC, University of Southern California, Los Angeles, California, USA

17
18 *Corresponding author:

19 Junhao Wen, junhaowe@usc.edu

20 2025 Zonal Ave, Los Angeles, CA 90033, United States

21

22 **eMethod 1: The definition of genomic loci, independent significant SNP, lead SNP,**
23 **candidate SNP**

24 **eText1: Sensitivity check analyses for the main GWAS of the nine BAGs using European**
25 **ancestry**

26 **eText2: Phenome-wide association query using the GWAS Atlas platform**

27 **eText3: Sensitivity check analyses for the causality between the hepatic BAG and**
28 **musculoskeletal BAG**

29 **eFigure 1: GWAS Manhattan plots for the brain BAG**

30 **eFigure 2: GWAS Manhattan plots for the cardiovascular BAG**

31 **eFigure 3: GWAS Manhattan plots for the eye BAG**

32 **eFigure 4: GWAS Manhattan plots for the hepatic BAG**

33 **eFigure 5: GWAS Manhattan plots for the immune BAG**

34 **eFigure 6: GWAS Manhattan plots for the metabolic BAG**

35 **eFigure 7: GWAS Manhattan plots for the musculoskeletal BAG**

36 **eFigure 8: GWAS Manhattan plots for the pulmonary BAG**

37 **eFigure 9: GWAS Manhattan plots for the renal BAG**

38 **eFigure 10: Bayesian colocalization analysis for the locus on chromosome 6 between the**
39 **hepatic and musculoskeletal BAGs**

40 **eFigure 11: Exemplary genomic locus for each BAG in the nine human organ systems**

41 **eFigure 12: SNP-based heritability, beta coefficients, and alternative allele frequency using**
42 **the brain-BAG comparable populations and different inclusion criteria for the SNPs**

43 **eFigure 13: Trumpet plots of the alternative allele frequency vs. the beta coefficient of the**
44 **nine BAG GWASs**

45 **eFigure 14: Manhattan of and QQ plots for the four pulmonary features used to compute**
46 **the pulmonary BAG**

47 **eFigure 15: Bayesian colocalization signal between the pulmonary BAG and FEV/FVC**

48 **eFigure 16: Beta coefficients of the significant colocalization signal between the pulmonary**
49 **BAG and the four pulmonary features**

50 **eFigure 17: GSEA using sex-stratified GWAS results**

51 **eFigure 18: TEA correlations using sex-stratified GWAS results**

52 **eFigure 19: Genetic correlations using sex-stratified GWAS results**

53 **eFigure 20: Mendelian randomization sensitivity check for the hepatic BAG on the**
54 **musculoskeletal BAG**

55 **eFigure 21: Mendelian randomization sensitivity check for the musculoskeletal BAG on the**
56 **hepatic BAG**

57 **eFigure 22: Mendelian randomization sensitivity check for AD on the brain BAG**

58 **eFigure 23: Mendelian randomization sensitivity check for AD on the hepatic BAG**

59 **eFigure 24: Mendelian randomization sensitivity check for Crohn's disease on the hepatic**
60 **BAG**

61 **eFigure 25: Mendelian randomization sensitivity check for body weight on the immune**
62 **BAG**

63 **eFigure 26: Mendelian randomization sensitivity check for type 2 diabetes on the metabolic**
64 **BAG**

65 **eFigure 27: Mendelian randomization sensitivity check for AD on the musculoskeletal BAG**

66 **eFigure 28: Mendelian randomization sensitivity check for IBD on the musculoskeletal**
67 **BAG**

- 68 **eFigure 29: Mendelian randomization sensitivity check for PBC on the musculoskeletal**
69 **BAG**
- 70 **eFigure 30: Mendelian randomization sensitivity check for weight on the musculoskeletal**
71 **BAG**
- 72 **eFigure 31: Mendelian randomization sensitivity check for weight on the pulmonary BAG**
- 73 **eFigure 32: Mendelian randomization sensitivity check for AD on the renal BAG**
- 74 **eFigure 33: Mendelian randomization sensitivity check for weight on the renal BAG**
- 75 **eFigure 34: Mendelian randomization sensitivity check for the brain BAG on sleep**
76 **duration**
- 77 **eFigure 35: Mendelian randomization sensitivity check for the cardiovascular BAG on**
78 **triglycerides to lipids ratio in very large VLDL**
- 79 **eFigure 36: Mendelian randomization sensitivity check for the metabolic BAG on weight**
- 80 **eFigure 37: Mendelian randomization sensitivity check for the pulmonary BAG on weight**
- 81 **eFigure 38: Causal multi-organ network between the nine biological age gaps and 17**
82 **clinical traits of chronic diseases, lifestyle factors, and cognition**
- 83 **eTable 1: Heritability estimates using the GCTA software**
- 84 **eTable 2: The beta coefficient and its SE estimate from the full sample vs. the down-**
85 **sampled brain BAG comparable sample**
- 86 **eTable 3: Genetic correlation analyses between the pulmonary BAG and the four features**
87 **used to derive the BAG.**
- 88 **eTable 4: Selected 41 clinical traits for genetic correlation analyses**
- 89 **eTable 5: Genetic correlations analyses between the nine BAGs and longevity, household**
90 **income, and telomere length**
- 91 **eTable 6: Causal analysis using the LCV method**
- 92 **eTable 7: Selected 17 clinical traits for Mendelian randomization analyses**

93 **eMethod 1: The definition of genomic loci, independent significant SNP, lead SNP,**
94 **candidate SNP**

95 FUMA defined the significant independent SNPs, lead SNPs, candidate SNPs, and genomic risk
96 loci as follows (<https://fuma.ctglab.nl/tutorial#snp2gene>):

97 *Independent significant SNPs*

98 They are defined as SNPs with $P \leq 5 \times 10^{-8}$ that are independent of each other at the user-defined
99 r^2 (set to 0.6 in the current study). We further describe *candidate SNPs* as those in linkage
100 disequilibrium (LD) with independent significant SNPs. FUMA then queries each candidate SNP
101 in the GWAS Catalog to check whether any clinical traits have been reported to be associated with
102 previous GWAS studies.

103 *Lead SNPs*

104 Lead SNPs are defined as independent significant SNPs that are also independent of each other at
105 $r^2 < 0.1$. If multiple independent significant SNPs are correlated at $r^2 \geq 0.1$, then the one with the
106 lowest individual P -value becomes the lead SNP. If r^2 threshold is set to 0.1 for the independent
107 significant SNPs, then they would constitute the identical set as the lead SNPs by definition.
108 FUMA thus advises setting r^2 to be 0.6 or higher.

109 *Genomic risk loci*

110 FUMA defines genomic risk loci to include all independent signals physically close or overlapping
111 in a single locus. First, independent significant SNPs dependent on each other at $r^2 \geq 0.1$ are
112 assigned to the same genomic risk locus. Then, independent significant SNPs with less than the
113 user-defined distance (250 kb by default) away from one another are merged into the same
114 genomic risk locus - the distance between two LD blocks of two independent significant SNPs is
115 the distance between the closest points from each LD block. Each locus is represented by the SNP
116 within the locus with the lowest P -value.
117

118 **eText 1: Sensitivity check analyses for the main GWAS of the nine BAGs using European**
 119 **ancestry**

120 We fully considered linkage disequilibrium and only included the independent significant SNPs
 121 in this sensitivity check analysis. We exemplified this analysis in the split-sample GWAS. We
 122 first used the Plink *clump* command (*--clump-p1 0.00000005 --clump-p2 0.05 --clump-r2 0.60 --*
 123 *clump-kb 250*) to define the independent significant SNPs for the split1 and split2 GWAS. We
 124 then included all the unique independent significant SNPs in either of the two split GWASs. We
 125 then calculated three statistics to scrutinize the concordance of the two split GWASs:

- 126 • $r\text{-}\beta$: Pearson's r between the two sets of β coefficients from the two splits;
- 127 • $C\text{-}\beta$: concordance rate of the sign of the β coefficients from the two splits – if the same
 128 SNP exerts the same protective/risk effect between the two splits;
- 129 • $P\text{-}\beta$: the difference between the two sets of β coefficients from the two splits – if the two
 130 sets of β coefficients (mean) statistically differ.

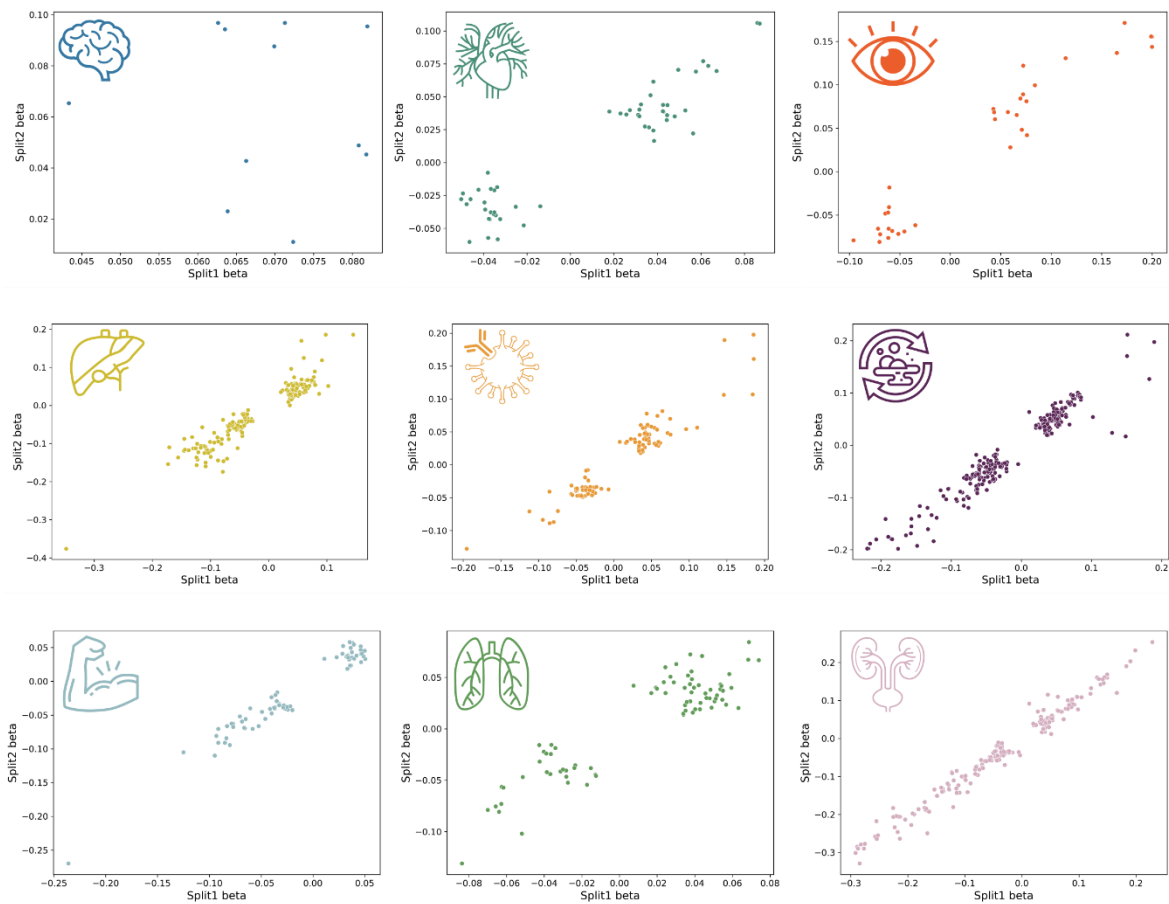
131 The two metrics were calculated for sex-stratified, fastGWA, and non-European GWAS
 132 sensitivity check analyses.

133
 134 **Split-sample GWAS**

135 **P-values:**

136 In the split1 GWAS, we found 6, 28, 20, 117, 62, 160, 37, 40, and 127 independent significant
 137 SNPs for the brain, cardiovascular, eye, hepatic, immune, metabolic, musculoskeletal,
 138 pulmonary, and renal BAGs, and 5, 30, 21, 110, 55, 164, 45, 43, and 139 independent significant
 139 SNPs in split2 GWAS.

140 For the brain BAG, we obtained an $r\text{-}\beta$ of -0.06 (P-value=0.84; $N=11$), but the two sets of
 141 coefficients did not statistically differ ($P\text{-}\beta=0.70$). All the 11 independent significant SNPs
 142 showed the same direction of effect ($C\text{-}\beta=1$). The low $r\text{-}\beta$ was likely due to small sample sizes in
 143 the brain BAG. For all the other 8 BAGs, we obtained significantly high $r\text{-}\beta$ estimates ($0.90 < r\text{-}\beta < 0.99$;
 144 $P\text{-value} < 1 \times 10^{-19}$). The two sets of coefficients did not statistically differ ($P\text{-}\beta > 0.48$). All
 145 independent significant SNPs showed the same direction of effect ($C\text{-}\beta=1$). Detailed results of
 146 these SNPs are presented in **Supplementary eFile 2** for split-sample GWAS. The scatter plot of
 147 the independent SNPs' β coefficients is shown below.



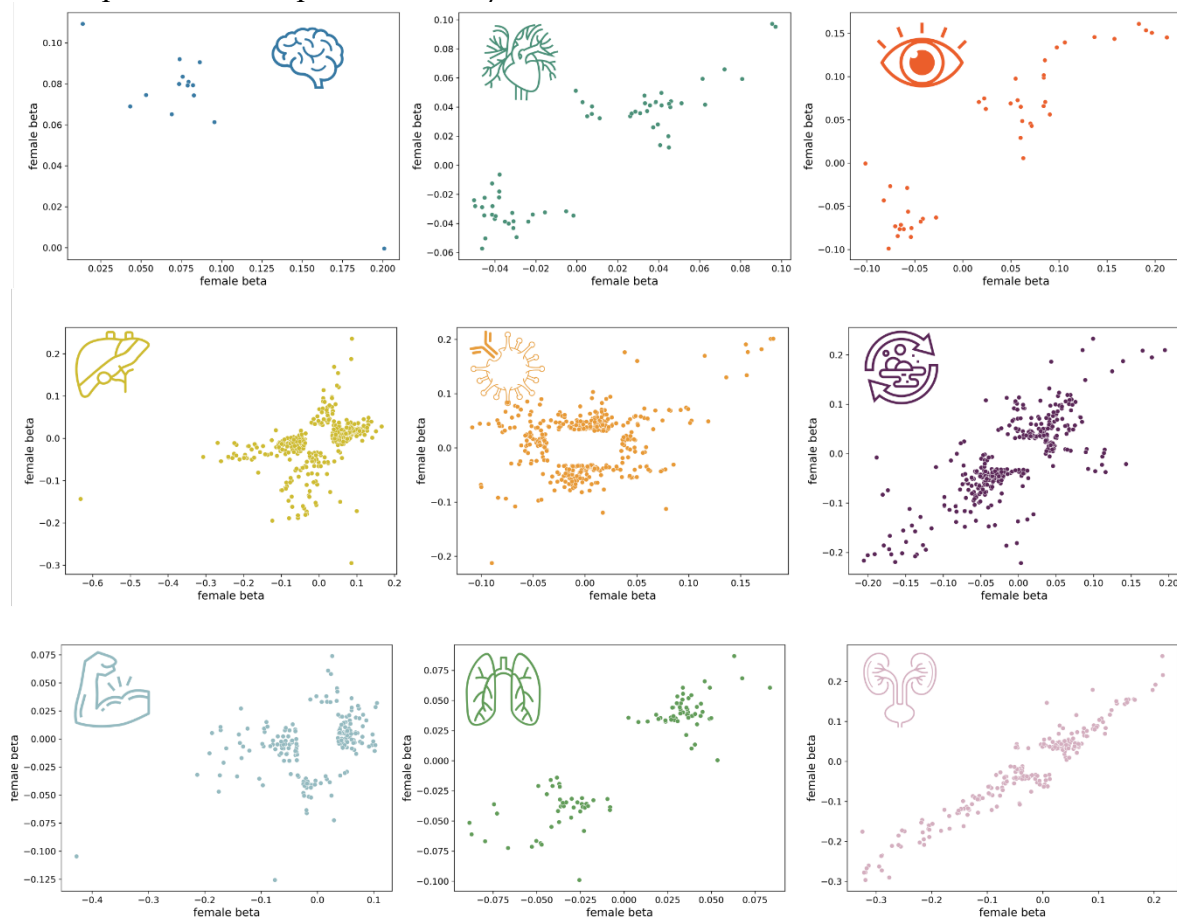
148
149
150

The figures present the scatter plots for the two sets of beta coefficients estimated from different splits.

151 Sex-stratified GWAS

152 In the female GWAS, we found 7, 24, 23, 286, 116, 142, 153, 30, and 131 independent
 153 significant SNPs for the brain, cardiovascular, eye, hepatic, immune, metabolic, musculoskeletal,
 154 pulmonary, and renal BAGs, and 7, 38, 22, 126, 275, 286, 42, 71, and 167 independent
 155 significant SNPs in the male GWAS.

156 For the brain BAG, we obtained an $r\text{-}\beta$ of -0.869 ($P\text{-value}=5.29\times 10^{-5}$, $N=14$), but the two
 157 sets of coefficients did not statistically differ ($P\text{-}\beta=0.66$). 13 out of the 14 independent significant
 158 SNPs showed the same direction of effect ($C\text{-}\beta=0.93$). The one independent significant SNP
 159 (rs1634777) that had the opposite β sign in males compared to females was because the β
 160 coefficient was close to 0 ($\beta=-0.000417162$) and was not statistically significant ($P\text{-value}=0.99$).
 161 For all the other 8 BAGs, we obtained significantly high $r\text{-}\beta$ estimates ($0.30 < r\text{-}\beta < 0.96$; $P\text{-}$
 162 $\text{value} < 2.57\times 10^{-7}$). The two sets of coefficients did not statistically differ ($P\text{-}\beta > 0.40$), except for
 163 the immune BAG ($P\text{-}\beta=0.013$). Most independent significant SNPs showed the same direction of
 164 effect ($C\text{-}\beta > 0.89$), except for the immune (0.54) and musculoskeletal BAGs (0.70). Detailed
 165 results of these SNPs are presented in **Supplementary eFile 3** for sex-stratified GWAS. The
 166 scatter plot of the independent SNPs' β coefficients is shown below.

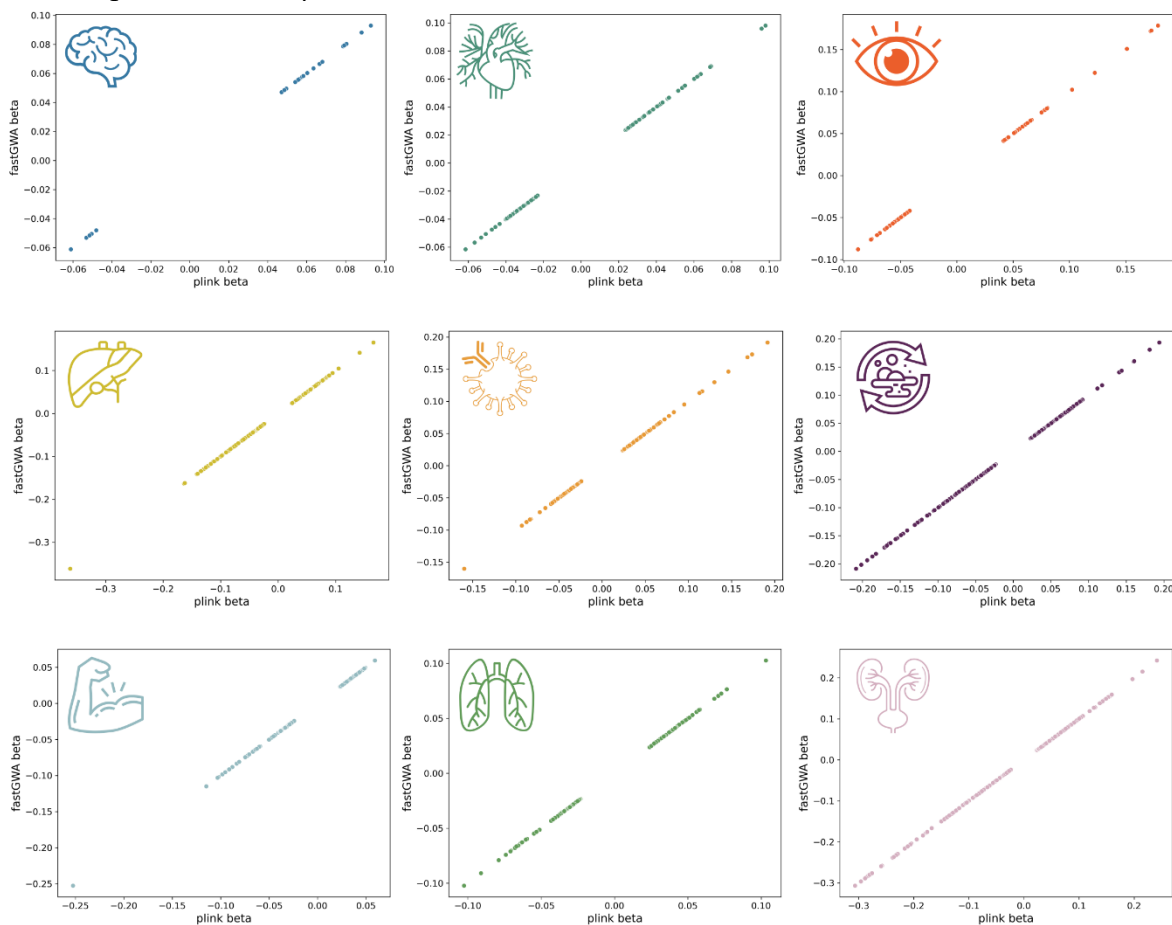


167 The figures present the scatter plots for the two sets of beta coefficients estimated from different
 168 genders.
 169

170 **fastGWA vs PLINK GWAS**

171 In the PLINK GWAS, we found 27, 124, 69, 289, 217, 422, 147, 272, and 331 independent
 172 significant SNPs for the brain, cardiovascular, eye, hepatic, immune, metabolic, musculoskeletal,
 173 pulmonary, and renal BAGs, and 27, 124, 69, 292, 218, 422, 148, 269, and 333 independent
 174 significant SNPs in fastGWA GWAS.

175 For all the nine BAGs, we found almost perfect concordance between the PLINK and
 176 fastGWA GWASs using the three proposed metrics ($r\text{-}\beta=1$; $C\text{-}\beta=1$; $P\text{-}\beta=1$). Detailed results of
 177 these SNPs are presented in **Supplementary eFile 4** for method-specific GWAS. The scatter plot
 178 of the independent SNPs' β coefficients is shown below.

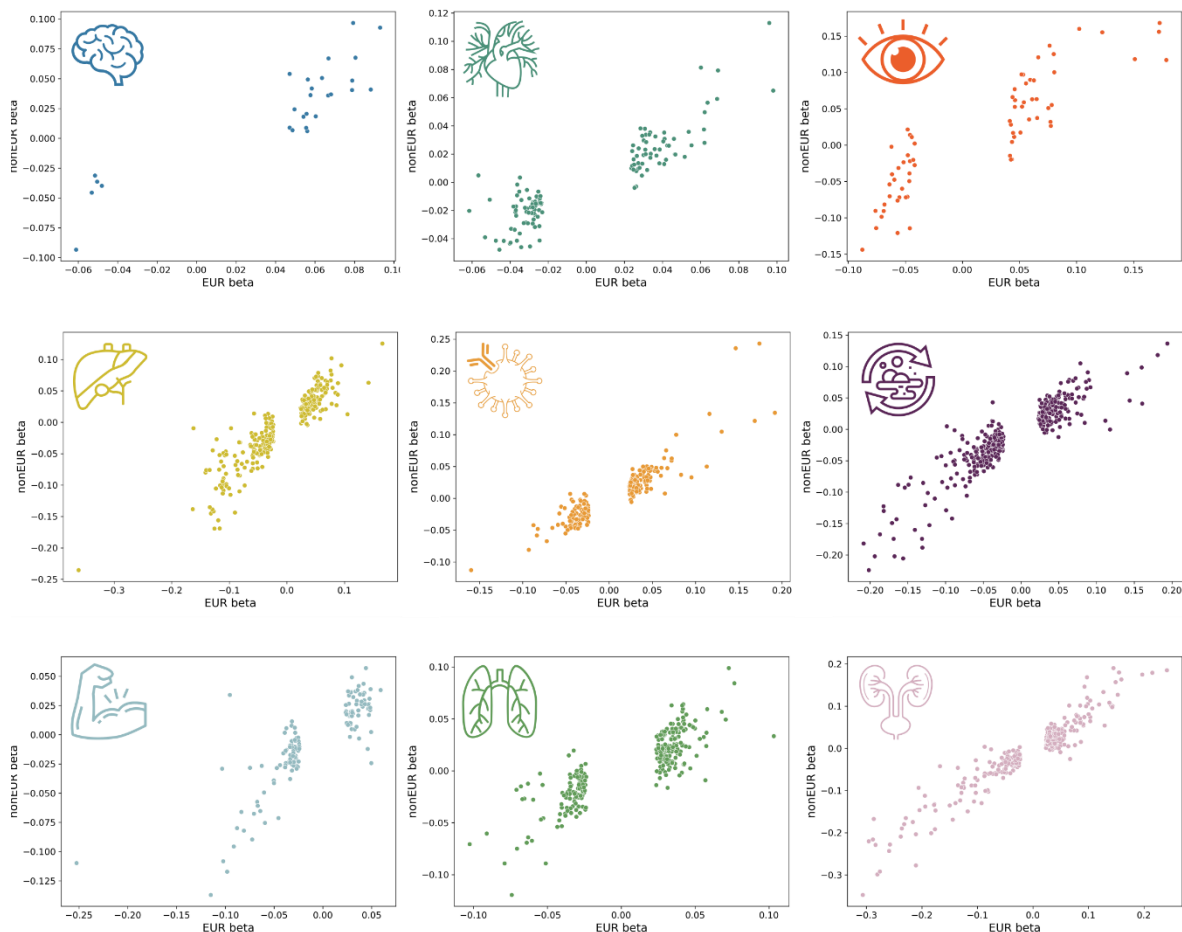


179 The figures present the scatter plots for the two sets of beta coefficients estimated from different
 180 GWAS methods.
 181

182 European vs. non-European GWAS

183 In the European GWAS, we found 27, 124, 69, 289, 217, 422, 147, 272, and 331 independent
 184 significant SNPs for the brain, cardiovascular, eye, hepatic, immune, metabolic, musculoskeletal,
 185 pulmonary, and renal BAGs, and 0, 2, 1, 16, 2, 23, 1, 1, and 35 independent significant SNPs in
 186 non-European GWAS (with much smaller sample sizes).

187 For all the nine BAGs, we found a high concordance between the European and non-
 188 EuroEuropean GWASs using the three proposed metrics ($0.85 < r\text{-}\beta < 0.95$; $0.89 < C\text{-}\beta < 1$). The two
 189 sets of β coefficients did not significantly differ ($P\text{-}\beta > 0.12$). Detailed results of these SNPs are
 190 presented in **Supplementary eFile 5** for ancestry-specific GWAS. The scatter plot of the
 191 independent SNPs' β coefficients is shown below.



192 The figures present the scatter plots for the two sets of beta coefficients estimated from different
 193 GWAS ancestry groups.
 194

195 **eText 2: Phenome-wide association query using the GWAS Atlas platform**

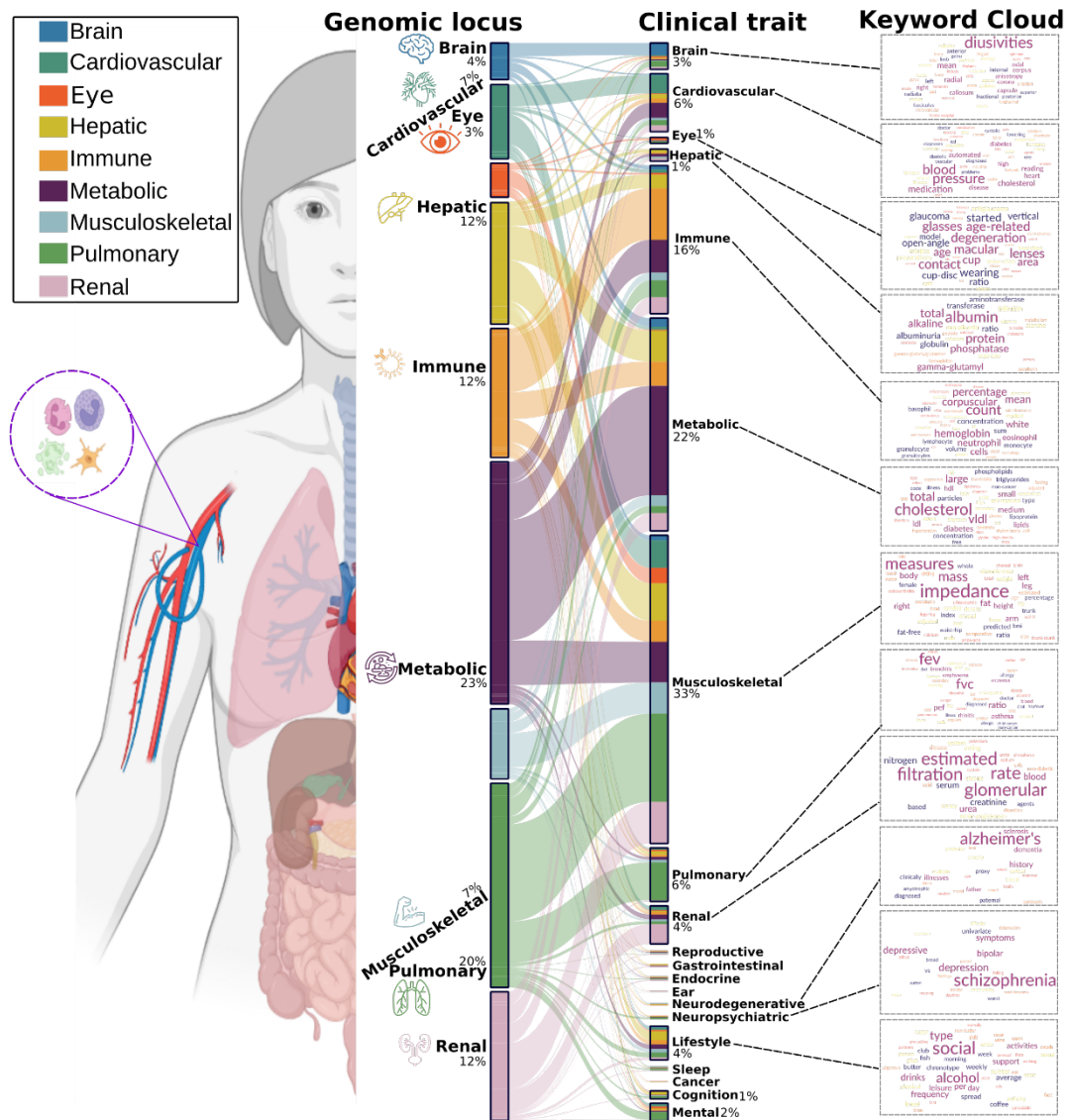
196 To comprehensively encompass the genetic landscape reported in previous literature, we
197 comparatively conducted a phenome-wide association query using the GWAS Atlas platform
198 (<https://atlas.ctglab.nl/PheWAS>). We applied the same P-value threshold search criteria as those
199 used in the EMBL-EBI GWAS Catalog ($P\text{-value} < 1 \times 10^{-5}$). These findings are presented as a
200 supplementary search to complement the results shown in **Fig. 2a**. The details of this
201 comparative search are presented in **Supplementary eFile 7**.

202 It's important to note that the two platforms may exhibit variations in their curated
203 GWAS datasets, the genome build versions utilized, and the specific P-value thresholds set for
204 their search analyses by default. We tried our best to harmonize the query criteria. Hence, this
205 comparative search was not exhaustive, and the results may differ. Rather, we intend to offer a
206 broad overview of the two platforms commonly employed for phenome-wide association studies
207 (PheWAS). Given the rapid updates in GWAS summary statistics in the field, it's worth
208 mentioning that this comparative search was originally conducted on October 23, 2023, and
209 revised on January 13, 2024, based on the reviewer's comments. The results from the GWAS
210 Atlas are shown in the figure below.

211 In the GWAS Atlas platform, we identified 8,576 significant associations between the
212 identified loci in our GWAS and clinical traits. The genomic loci associated with the brain BAG
213 exhibited the highest proportion of associations (109 out of 308) with traits related to the brain.
214 The brain BAG loci were also largely linked to many other traits related to other organ systems,
215 evidencing inter-organ connections, including metabolic ($N=78/308$), lifestyle factor ($N=13/308$),
216 neurodegenerative traits ($N=5/308$), and immune ($N=35/308$). For the eye BAG loci, most
217 associations were found in the musculoskeletal ($N=139/279$), eye ($N=14/279$), and mental traits
218 ($N=19/279$), among many others.

219 For the seven body organ systems, among the loci associated with the cardiovascular
220 BAG, most associations were observed with musculoskeletal traits ($N=249/611$) and
221 cardiovascular traits (166/611). 29 out of 1009 associations were related to hepatic traits (e.g.,
222 blood protein, cirrhosis, and bilirubin) for the hepatic BAG loci. Among the loci associated with
223 the immune BAG, abundant associations were found enriched in immune ($N=467/1062$) traits.
224 For the metabolic BAG loci, most associations were observed in metabolic traits ($N=993/1990$).
225 We found a significant intertwining of musculoskeletal systems with other organ systems in the
226 GWAS Atlas platform. Details of the phenome-wide associations are presented in
227 **Supplementary eFile 7**.

228



229
230
231
232

Figure. We queried the clumped independent significant SNPs using the PheWAS functionality provided by the GWAS Atlas platforms.

233 **eText 3: Sensitivity check analyses for the causality between the hepatic BAG and**
 234 **musculoskeletal BAG**

235
 236 **A) Sensitivity analyses on body weight for the bi-directional causality between the hepatic**
 237 **and musculoskeletal BAGs**

238 We conducted a revised Mendelian randomization analysis by introducing body weight as a
 239 covariate in the split-sample GWASs for hepatic and musculoskeletal BAGs. In this approach,
 240 we employed hepatic BAG as the exposure variable in split1 GWAS and musculoskeletal BAG
 241 as the outcome variable in split2 GWAS. Likewise, we reversed the roles, using musculoskeletal
 242 BAG as the exposure variable in split1 GWAS and hepatic BAG as the outcome variable in
 243 split2 GWAS, thus assessing the inverse causal relationship. This methodology ensured the
 244 absence of overlapping populations while effectively controlling for the influence of body
 245 weight.

246 Compared to the original results, this bi-directional causality persisted while adjusting the
 247 body weight as a covariate, shown in the tables below:

248
 249 **1) GWAS without and with body weight as a covariate for the causal relationship from**
 250 **the hepatic BAG to the musculoskeletal BAG.**

| Weight | Outcome (split2) | Exposure (split1) | Method | nSNP | BETA | SE | P | OR | CI_low | CI_high |
|--------|------------------|-------------------|---------------------------|------|------------|------------|------------|------------|------------|------------|
| N | Musculoskeletal | Hepatic | MR Egger | 19 | 0.51783336 | 0.14070786 | 0.00185593 | 1.67838725 | 1.27385274 | 2.21138886 |
| | Musculoskeletal | Hepatic | Weighted median | 19 | 0.35295633 | 0.06606437 | 9.16E-08 | 1.42326899 | 1.25040832 | 1.62002649 |
| | Musculoskeletal | Hepatic | Inverse variance weighted | 19 | 0.38344296 | 0.07834137 | 9.85E-07 | 1.46732785 | 1.25846644 | 1.71085295 |
| | Musculoskeletal | Hepatic | Simple mode | 19 | 0.15733154 | 0.10700058 | 0.15872332 | 1.17038357 | 0.94895908 | 1.44347395 |
| | Musculoskeletal | Hepatic | Weighted mode | 19 | 0.46614953 | 0.08121762 | 1.93E-05 | 1.59384531 | 1.35929067 | 1.86887391 |
| Y | Musculoskeletal | Hepatic | MR Egger | 18 | 0.51517011 | 0.14245065 | 0.00231711 | 1.67392323 | 1.26613232 | 2.21305338 |
| | Musculoskeletal | Hepatic | Weighted median | 18 | 0.35613857 | 0.06002398 | 2.97E-09 | 1.42780539 | 1.26933301 | 1.60606258 |
| | Musculoskeletal | Hepatic | Inverse variance weighted | 18 | 0.38926537 | 0.0792834 | 9.12E-07 | 1.47589615 | 1.2634801 | 1.72402356 |
| | Musculoskeletal | Hepatic | Simple mode | 18 | 0.24697399 | 0.11293776 | 0.04302518 | 1.28014581 | 1.02594689 | 1.59732761 |
| | Musculoskeletal | Hepatic | Weighted mode | 18 | 0.47542746 | 0.06925444 | 2.74E-06 | 1.60870171 | 1.40451037 | 1.84257891 |

251
 252 **2) GWAS without and with body weight as a covariate for the causal relationship from**
 253 **the musculoskeletal BAG to the hepatic BAG.**

| Weight | Outcome (split2) | Exposure (split1) | Method | nSNP | BETA | SE | P | OR | CI_low | CI_high |
|--------|------------------|-------------------|---------------------------|------|------------|------------|------------|------------|-----------|------------|
| N | Hepatic | Musculoskeletal | MR Egger | 9 | 1.8282501 | 0.24293965 | 0.00013439 | 6.22298749 | 3.8654897 | 10.0182839 |
| | Hepatic | Musculoskeletal | Weighted median | 9 | 0.92114305 | 0.13768954 | 2.23E-11 | 2.51216028 | 1.9179781 | 3.2904178 |
| | Hepatic | Musculoskeletal | Inverse variance weighted | 9 | 1.02402966 | 0.18103365 | 1.54E-08 | 2.78439235 | 1.9526818 | 3.97035541 |

| | | | | | | | | | | |
|---|---------|-----------------|----------------------------------|---|------------|------------|------------|------------|------------|------------|
| | Hepatic | Musculoskeletal | Simple mode | 9 | 1.20577311 | 0.18620161 | 0.000193 | 3.33933976 | 2.31826245 | 4.81014995 |
| | Hepatic | Musculoskeletal | Weighted mode | 9 | 1.25833413 | 0.13034769 | 1.10E-05 | 3.51955347 | 2.7260472 | 4.54403601 |
| | Hepatic | Musculoskeletal | MR Egger | 9 | 1.69092352 | 0.35916855 | 0.00218827 | 5.42448802 | 2.68304718 | 10.9670342 |
| | Hepatic | Musculoskeletal | Weighted median Inverse variance | 9 | 0.85408009 | 0.13197703 | 9.71E-11 | 2.34921232 | 1.81376558 | 3.04272978 |
| Y | Hepatic | Musculoskeletal | Weighted mode | 9 | 0.99179962 | 0.19767923 | 5.24E-07 | 2.69608204 | 1.83005923 | 3.97192521 |
| | Hepatic | Musculoskeletal | Simple mode | 9 | 1.23665687 | 0.15851732 | 5.23E-05 | 3.44408019 | 2.52429777 | 4.6990052 |
| | Hepatic | Musculoskeletal | Weighted mode | 9 | 1.27628794 | 0.15385855 | 3.36E-05 | 3.58331353 | 2.65043899 | 4.84453174 |

254

255

B) Sensitivity analysis for the hepatic BAG on musculoskeletal BAG excluding the *APOE* gene

256

We conducted a revised Mendelian randomization analysis by excluding SNPs within the *APOE*

gene for the causal relationship from the hepatic BAG to the musculoskeletal BAGs; all other

significant causality did not involve the two common *APOE* gene SNPs (rs429358 and rs7412).

In this approach, we employed hepatic BAG as the exposure variable in split1 GWAS and

musculoskeletal BAG as the outcome variable in split2 GWAS.

Compared to the original results, this causality persisted while excluding the SNP (rs429358)

as an IV, shown in the tables below:

GWAS without and with rs429358 as an IV for the causal relationship from the hepatic

BAG to the musculoskeletal BAG.

265

| rs429358 | Outcome (split2) | Exposure (split1) | Method | nSNP | BETA | SE | P | OR | CI_low | CI_high |
|----------|------------------|-------------------|----------------------------------|------|------------|------------|------------|------------|------------|------------|
| | Musculoskeletal | Hepatic | MR Egger | 18 | 0.51522659 | 0.12736616 | 0.00093844 | 1.67401778 | 1.30419881 | 2.14870271 |
| | Musculoskeletal | Hepatic | Weighted median Inverse variance | 18 | 0.36478773 | 0.06339608 | 8.71E-09 | 1.44020827 | 1.27192489 | 1.63075657 |
| N | Musculoskeletal | Hepatic | Simple mode | 18 | 0.41660503 | 0.07146014 | 5.55E-09 | 1.5168033 | 1.31856385 | 1.74484706 |
| | Musculoskeletal | Hepatic | Simple mode | 18 | 0.15924454 | 0.09710274 | 0.11938508 | 1.17262466 | 0.96940109 | 1.41845167 |
| | Musculoskeletal | Hepatic | Weighted mode | 18 | 0.45942325 | 0.07899932 | 2.07E-05 | 1.58316063 | 1.35606155 | 1.84829191 |
| | Musculoskeletal | Hepatic | MR Egger | 19 | 0.51783336 | 0.14070786 | 0.00185593 | 1.67838725 | 1.27385274 | 2.21138886 |
| | Musculoskeletal | Hepatic | Weighted median Inverse variance | 19 | 0.35295633 | 0.06606437 | 9.16E-08 | 1.42326899 | 1.25040832 | 1.62002649 |
| Y | Musculoskeletal | Hepatic | Weighted mode | 19 | 0.38344296 | 0.07834137 | 9.85E-07 | 1.46732785 | 1.25846644 | 1.71085295 |
| | Musculoskeletal | Hepatic | Simple mode | 19 | 0.15733154 | 0.10700058 | 0.15872332 | 1.17038357 | 0.94895908 | 1.44347395 |
| | Musculoskeletal | Hepatic | Weighted mode | 19 | 0.46614953 | 0.08121762 | 1.93E-05 | 1.59384531 | 1.35929067 | 1.86887391 |

266

267

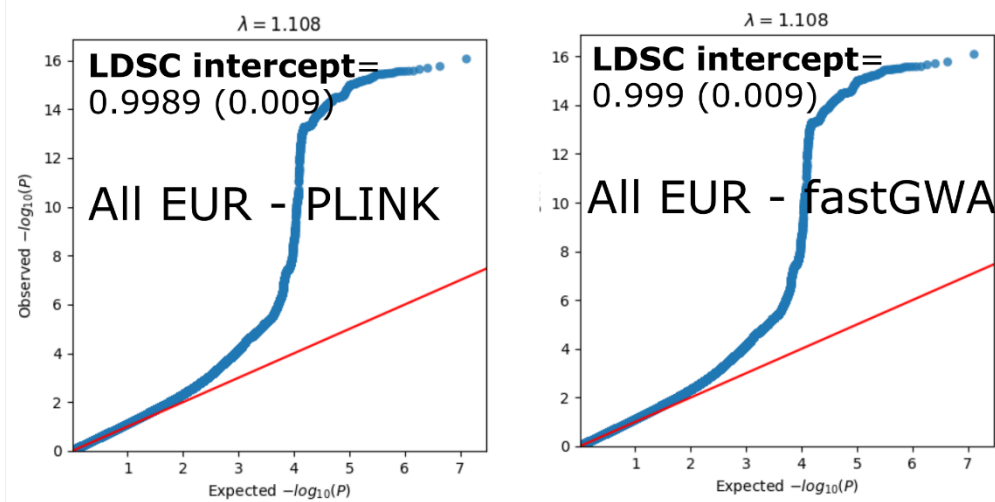
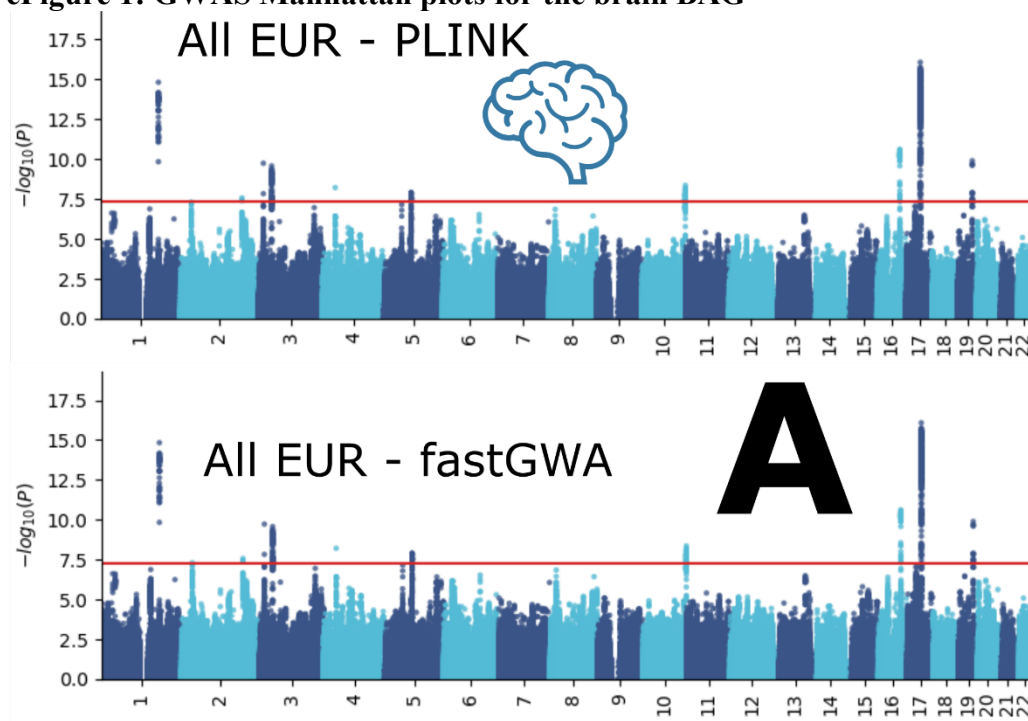
C) Sensitivity analyses for metabolic BAG on body weight

We showcased sensitivity analyses to investigate potential violations of the three IV assumptions

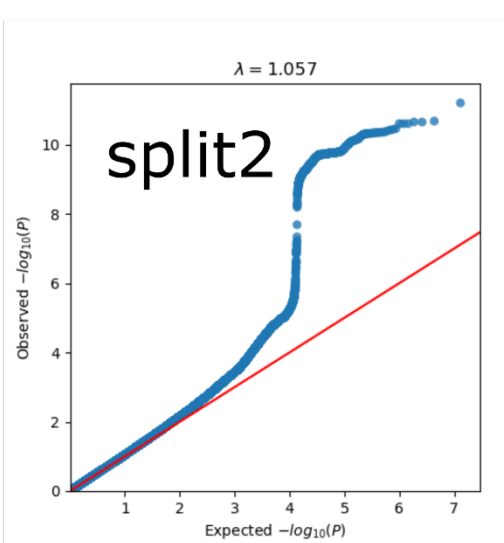
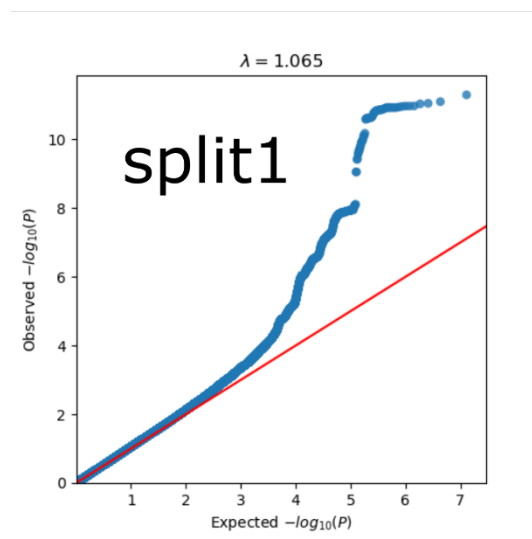
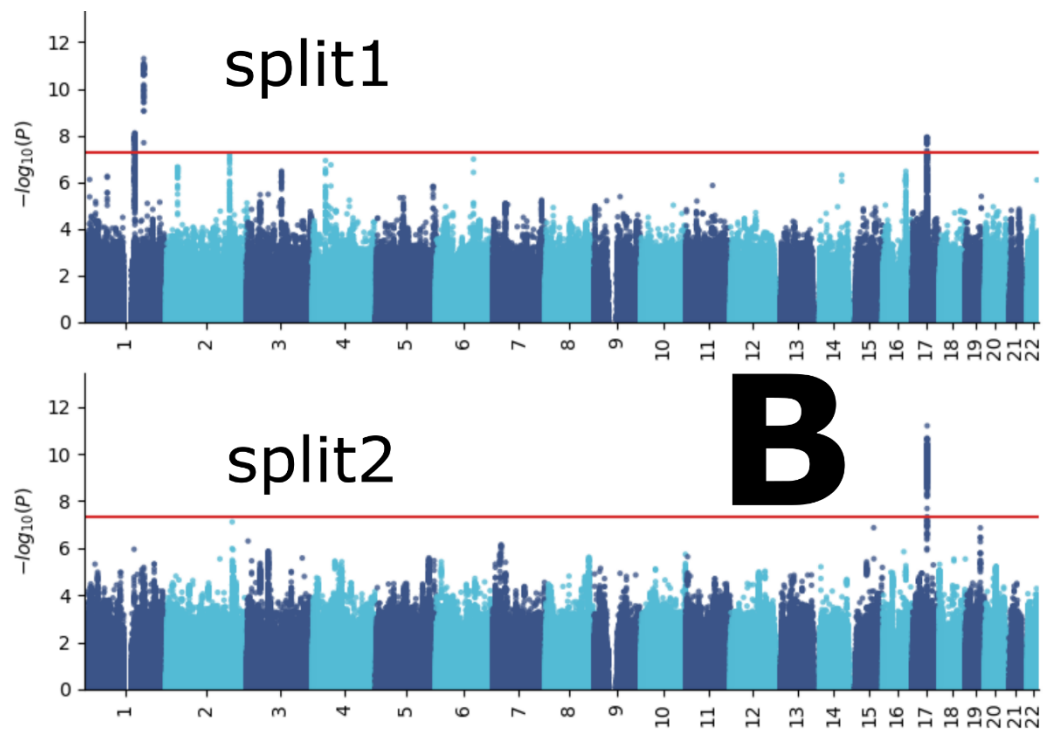
(Method 3j). To illustrate this, we showcased the sensitivity analysis results for the causal effect

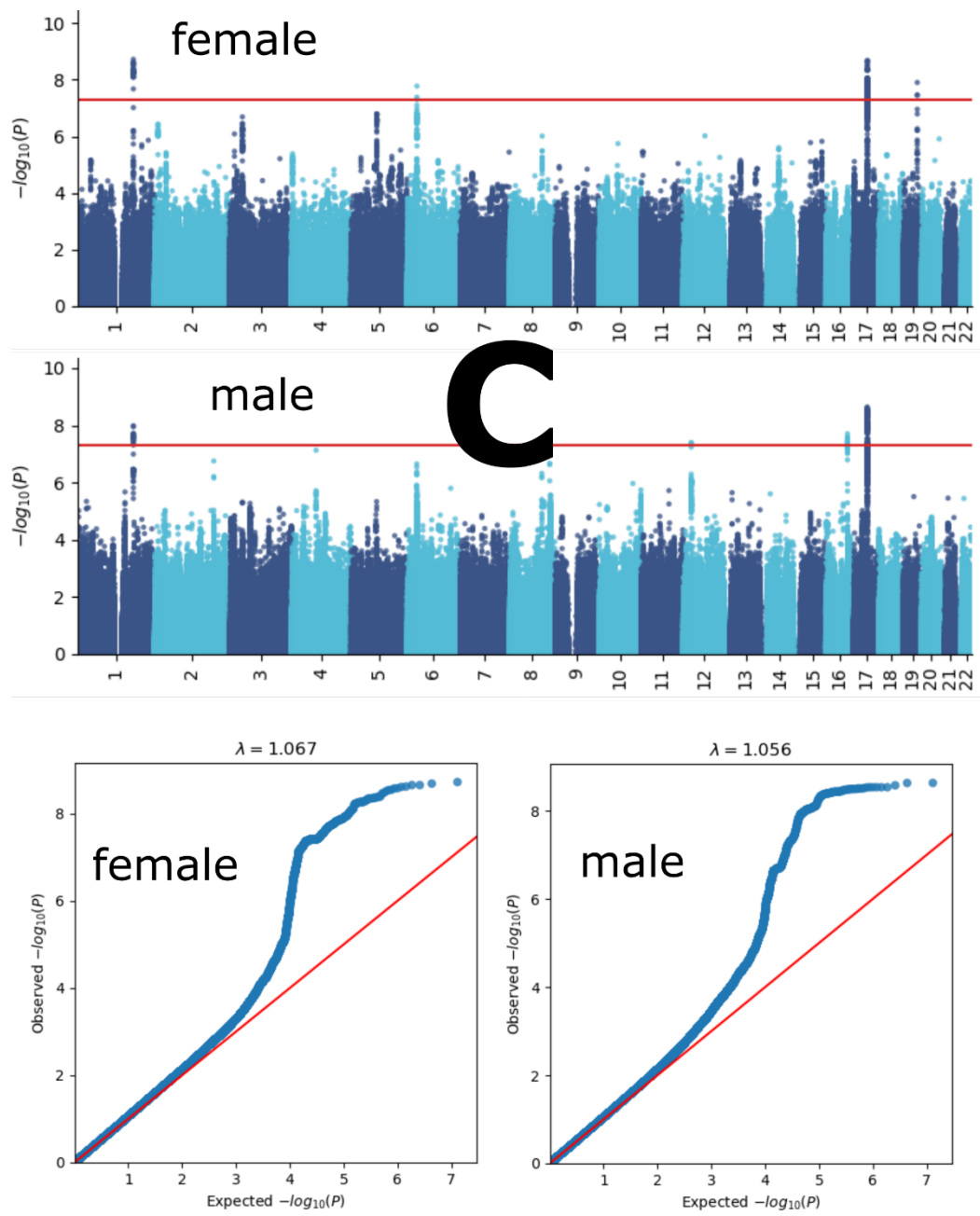
270

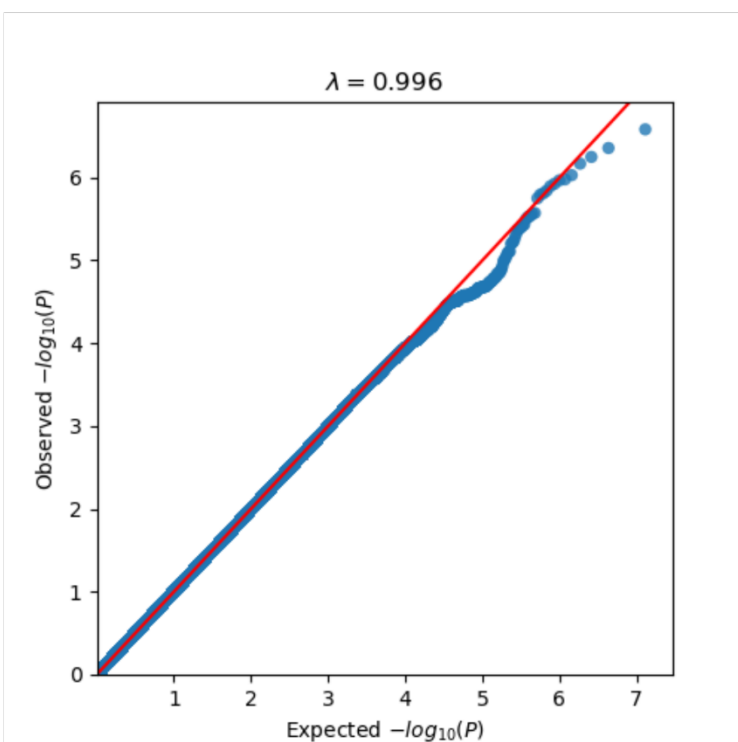
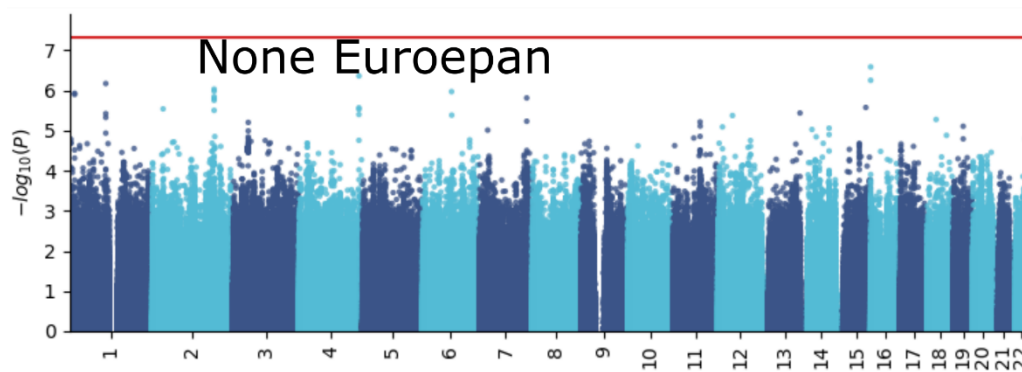
271 of the metabolic BAG on body weight (**Supplementary eFigure 33**). In a leave-one-out
272 analysis, no single SNP overwhelmingly drove the overall effect. There was evidence for minor
273 heterogeneity¹ of the causal effect amongst SNPs (Cochran's Q value=57.33, P-value<1x10⁻⁵).
274 Some SNPs exerted opposite causal effects compared to the model using all SNPs. The scatter
275 plot indicated two obvious SNP outliers (rs117233107 and rs33959228), and the funnel plot
276 showed slight asymmetry. Finally, the MR Egger estimator allows for pleiotropic effects
277 independent of the effect on the exposure of interest (i.e., the InSIDE assumption²). Our results
278 from the Egger estimator showed a small but not significant positive intercept ($3.62 \times 10^{-4} \pm 1.67 \times 10^{-3}$, P-value=0.83), which may indicate that the IVW estimate is not likely biased². We
279 re-analyzed the IVW MR analyses by excluding the two outliers identified in **Supplementary**
280 **eFigure 33** (rs117233107 and rs33959228), which led to a similar OR [0.94 (0.91, 0.97) vs. 0.95
281 (0.92, 0.98)] and a less significant P-value [6.9×10^{-4} vs. 1.2×10^{-3}].
282
283

284 **eFigure 1: GWAS Manhattan plots for the brain BAG**

285

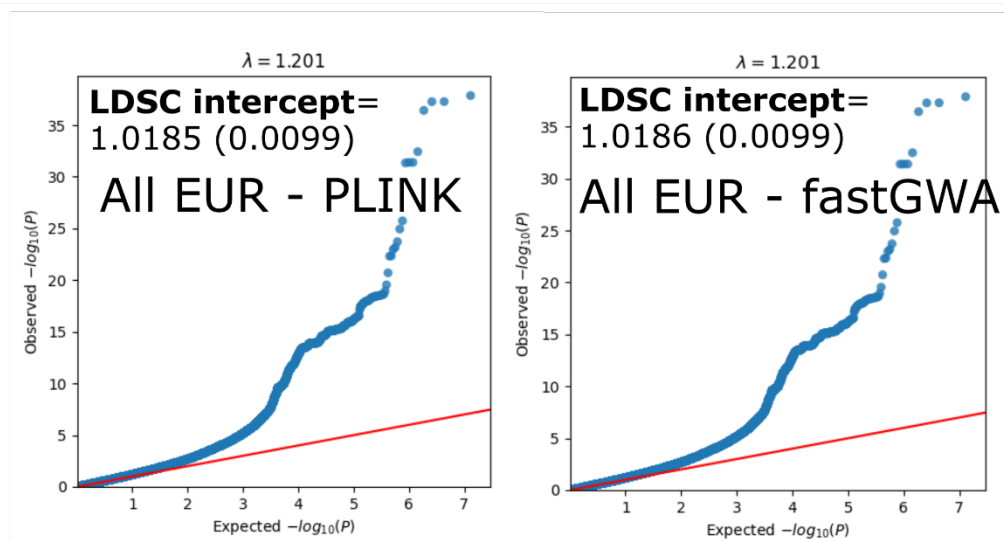
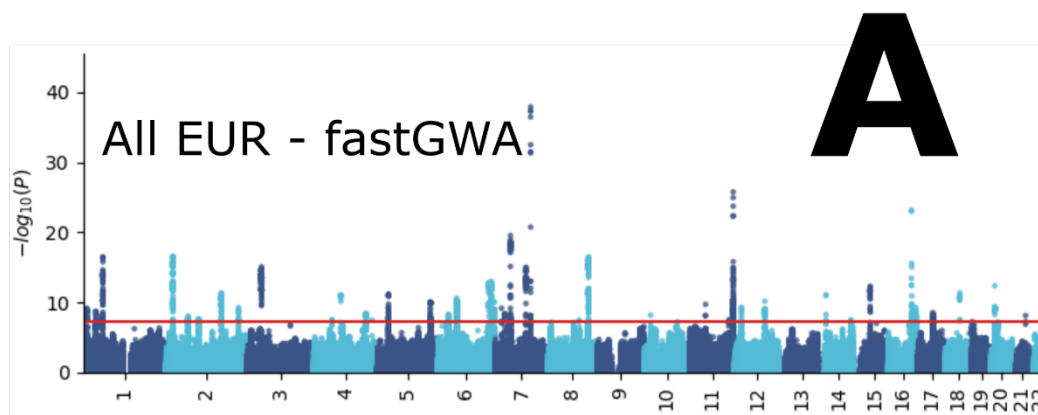
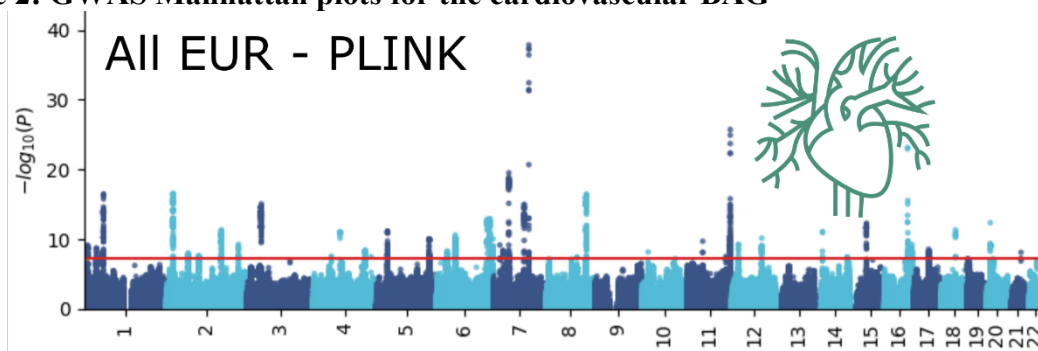


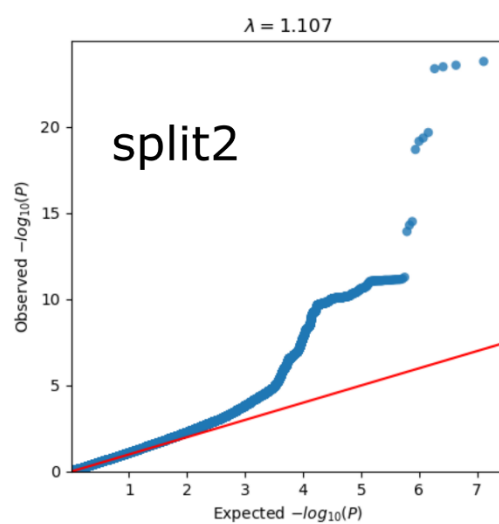
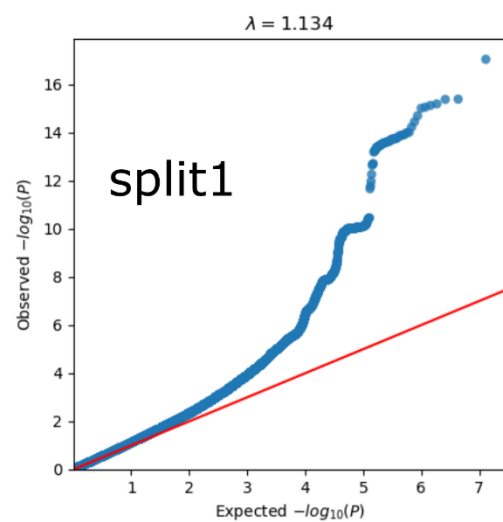
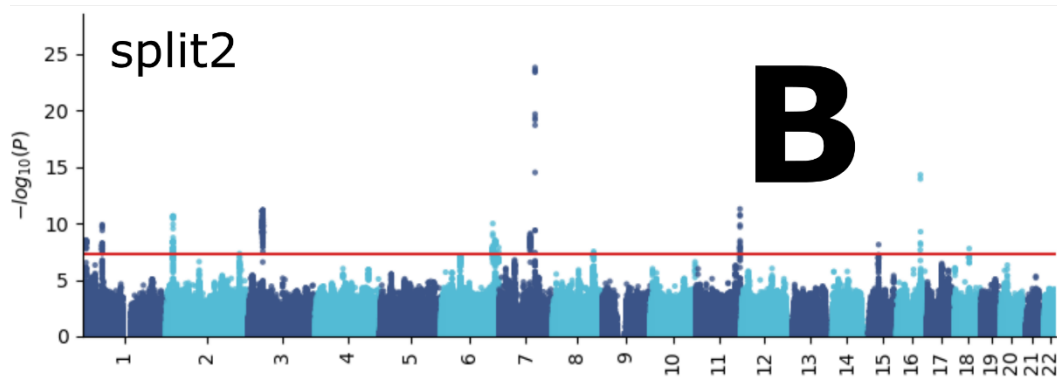
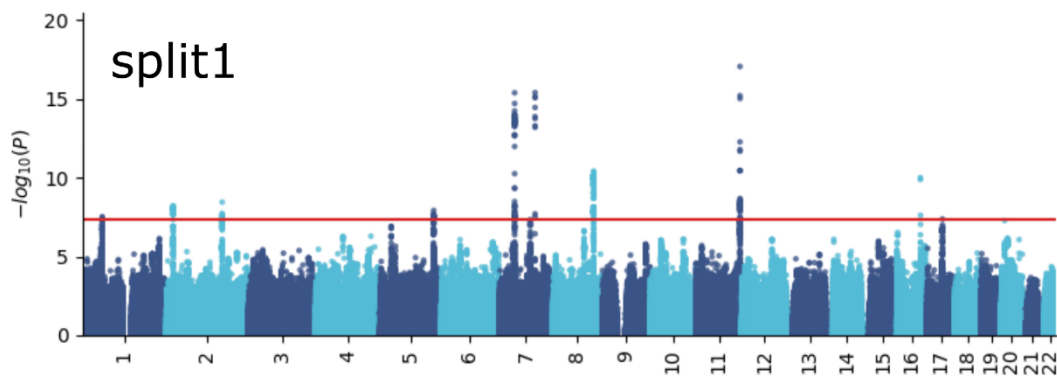


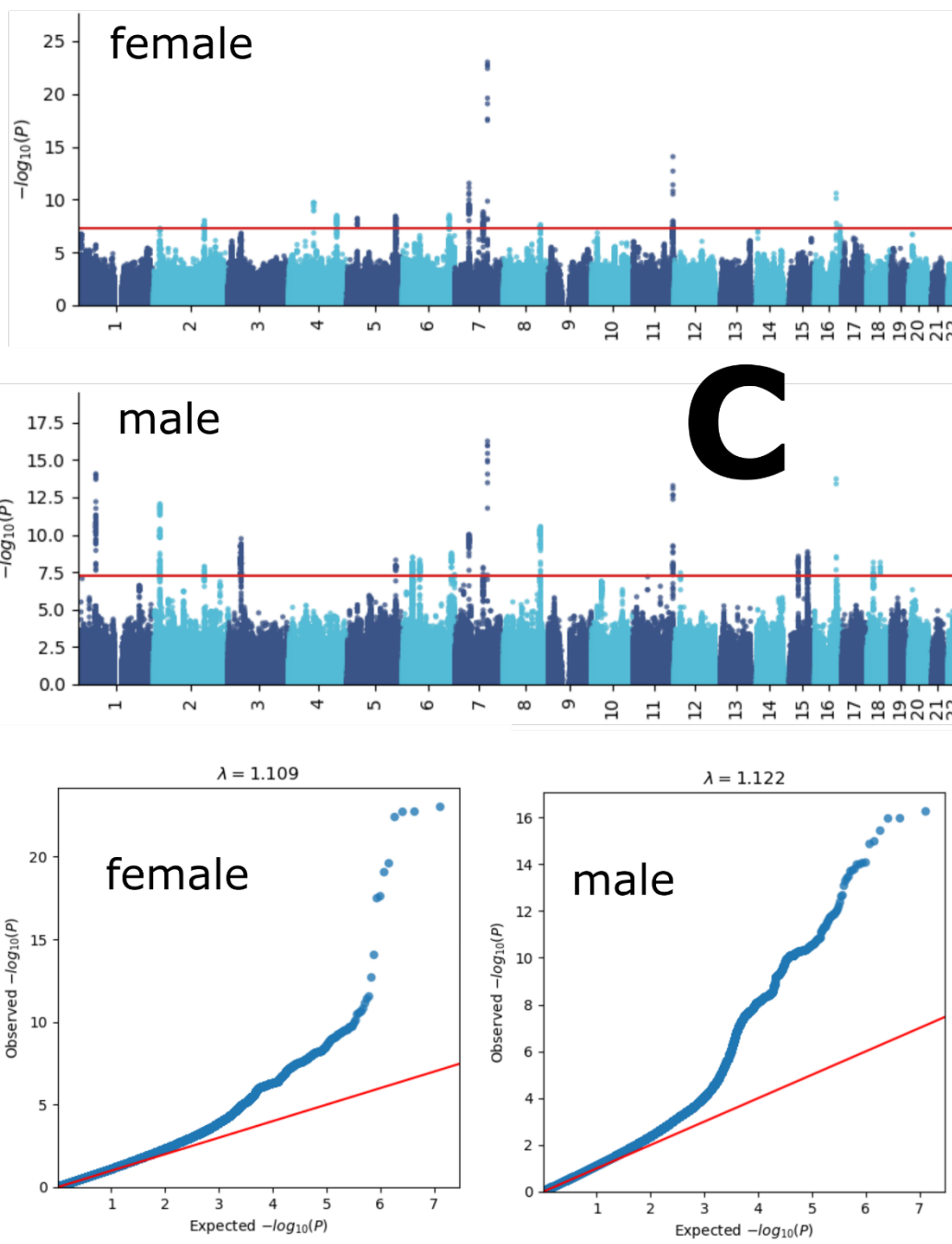


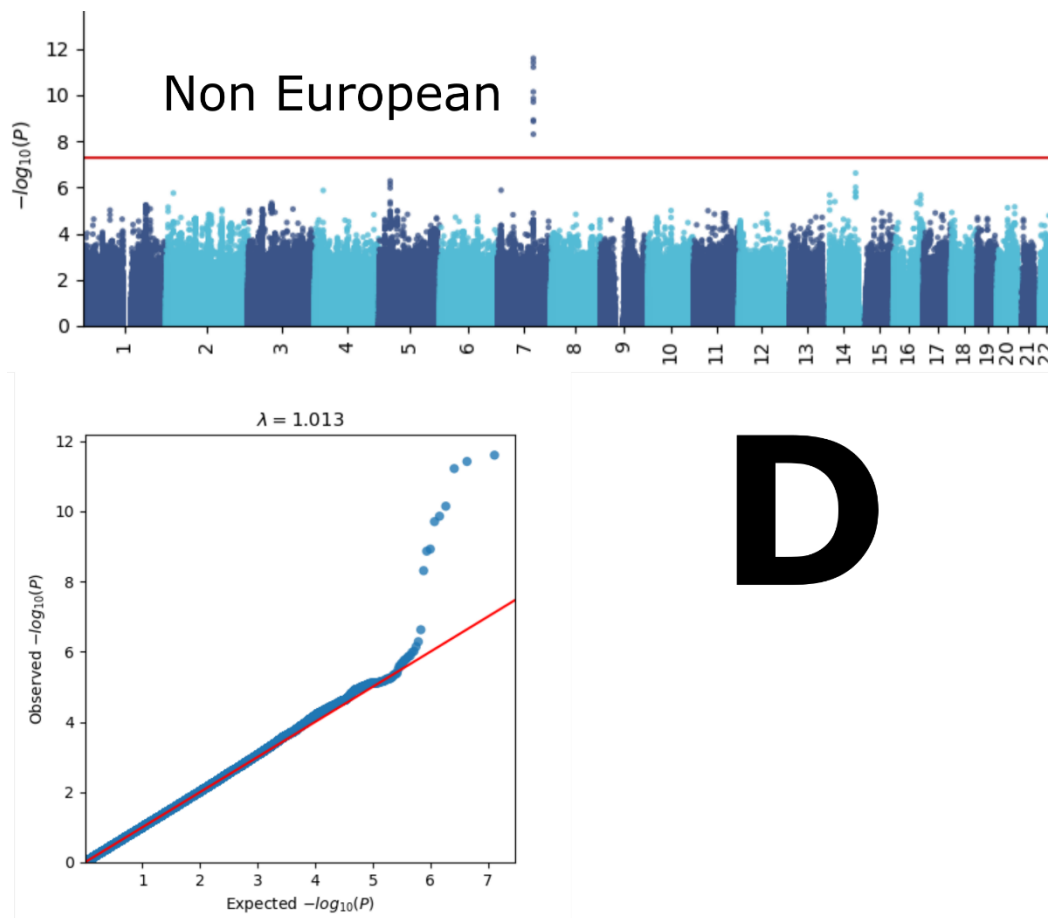
D

288
 289 Manhattan and QQ plots, along with genomic inflation factors and LDSC intercepts, are
 290 displayed for the primary GWAS conducted on individuals of European ancestry ($N=30,062$)
 291 using PLINK and fastGWA (**A**). Additionally, results are presented for split-sample GWAS
 292 (split1 and split2, **B**), sex-stratified GWAS (female and male, **C**), and GWAS involving non-
 293 European ancestry populations ($N=4465$, **D**).

294 **eFigure 2: GWAS Manhattan plots for the cardiovascular BAG**

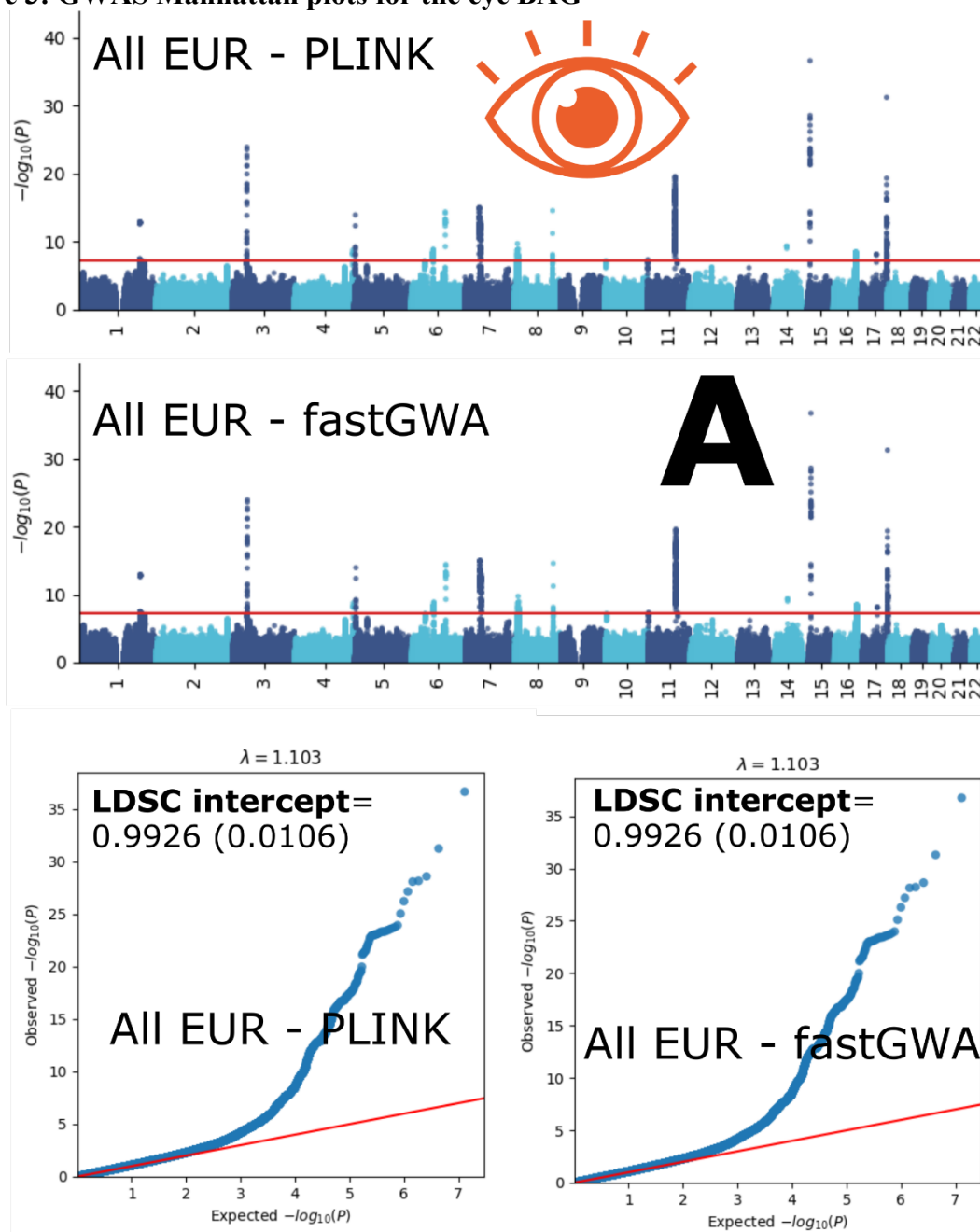




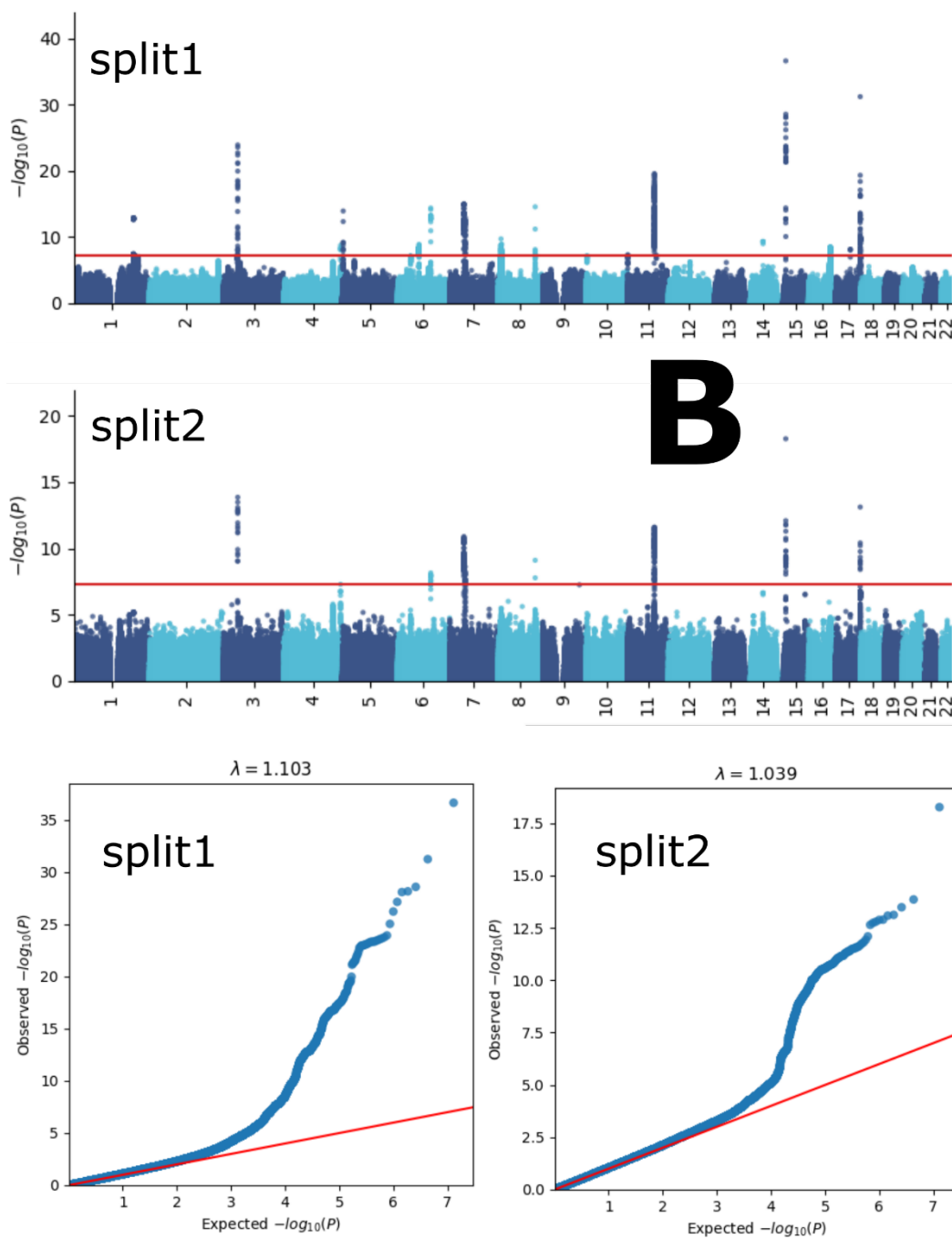


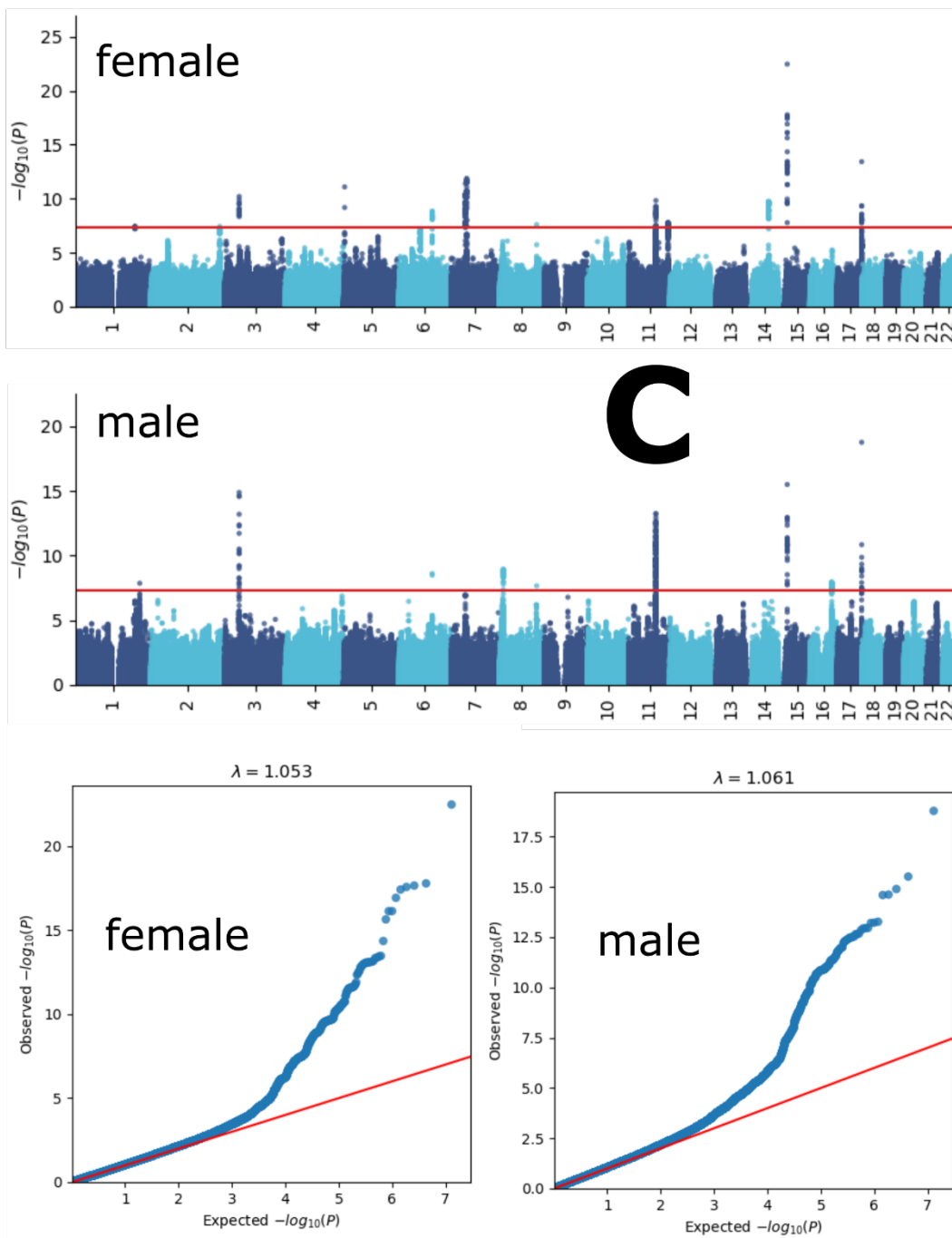
298
 299 Manhattan and QQ plots, along with genomic inflation factors and LDSC intercepts, are
 300 displayed for the primary GWAS conducted on individuals of European ancestry ($N=111,386$)
 301 using PLINK and fastGWA (**A**). Additionally, results are presented for split-sample GWAS
 302 (split1 and split2, **B**), sex-stratified GWAS (female and male, **C**), and GWAS involving non-
 303 European ancestry populations ($N=20,408$, **D**).

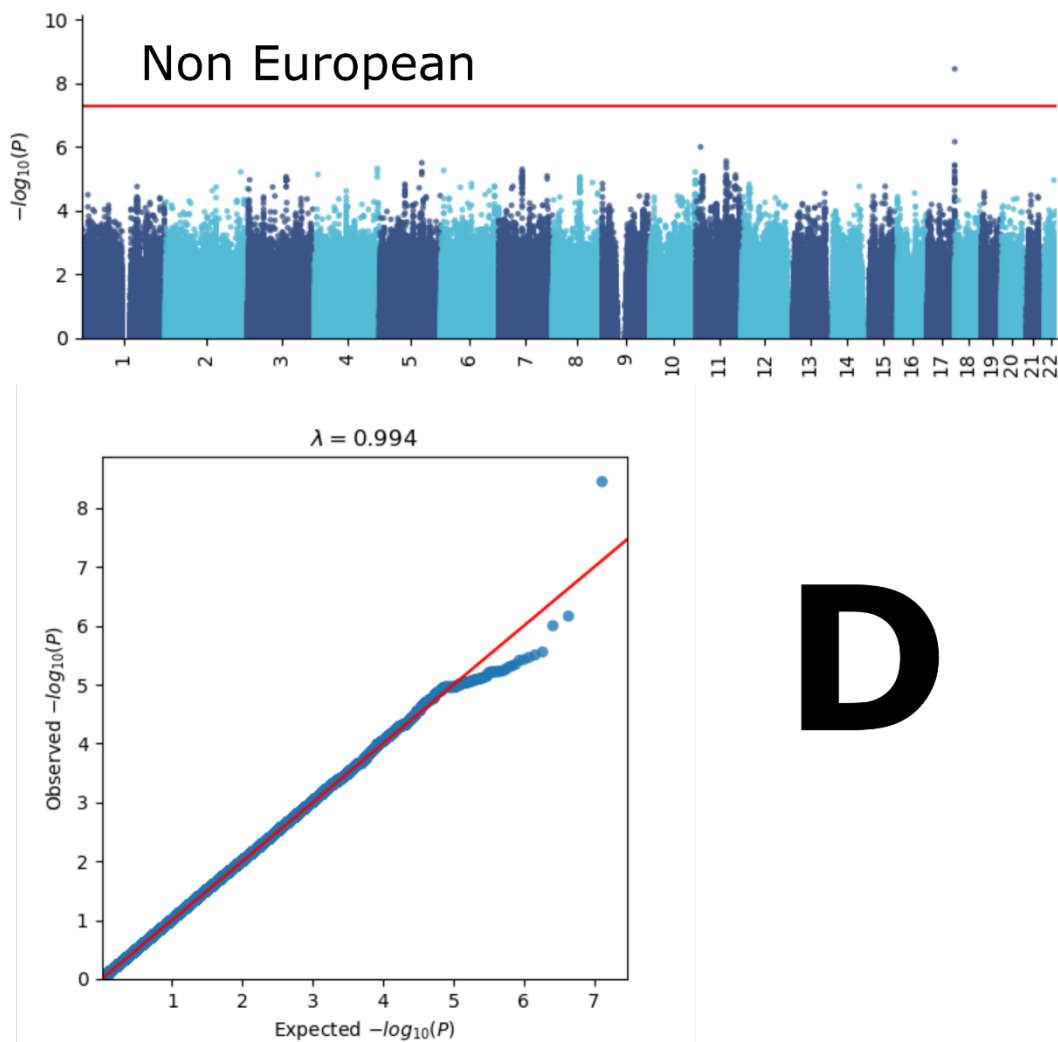
304 eFigure 3: GWAS Manhattan plots for the eye BAG



305

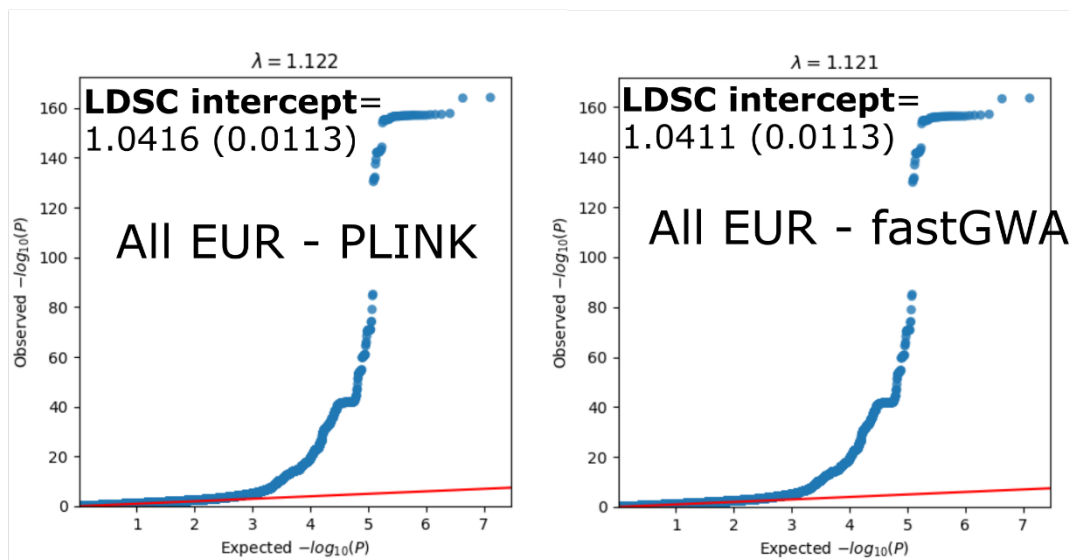
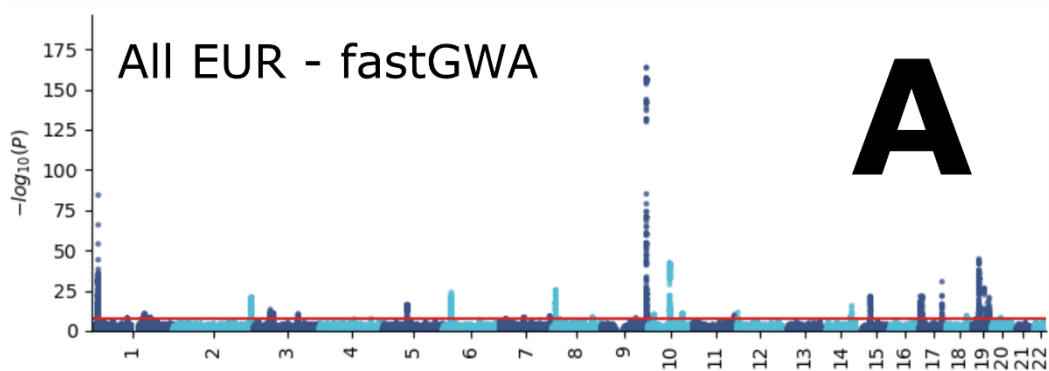
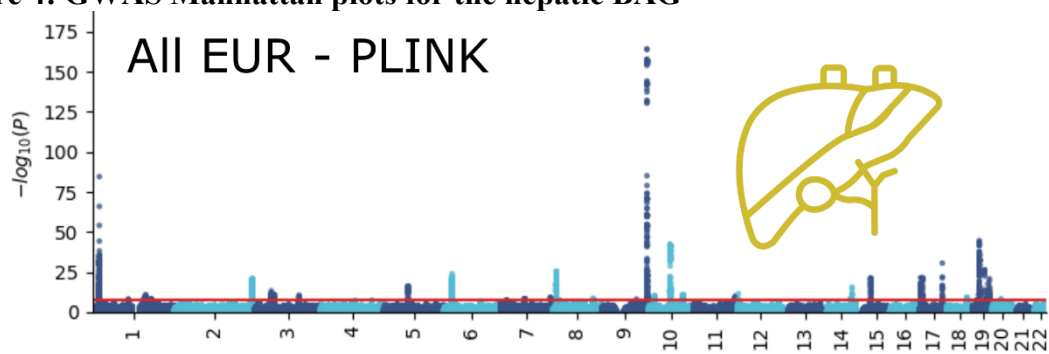


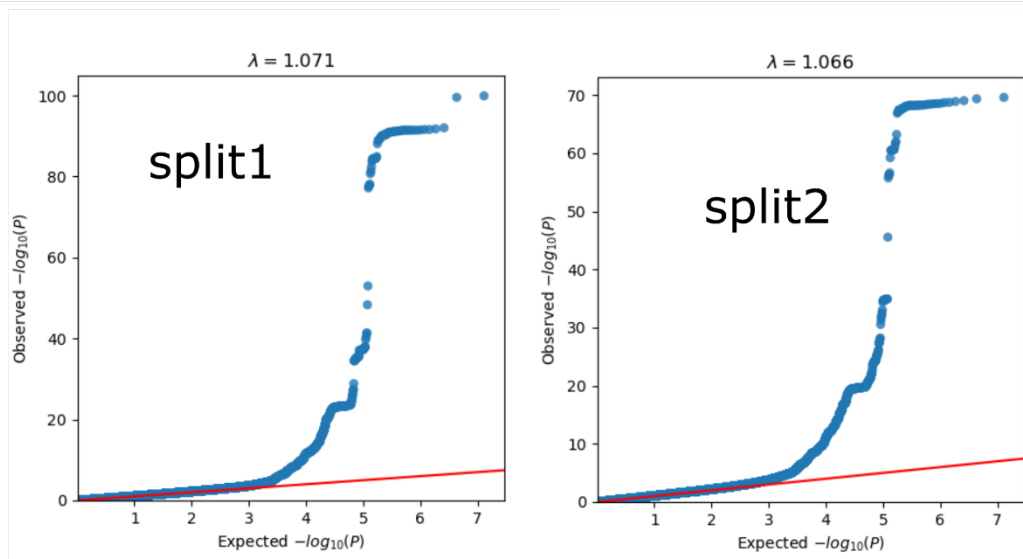
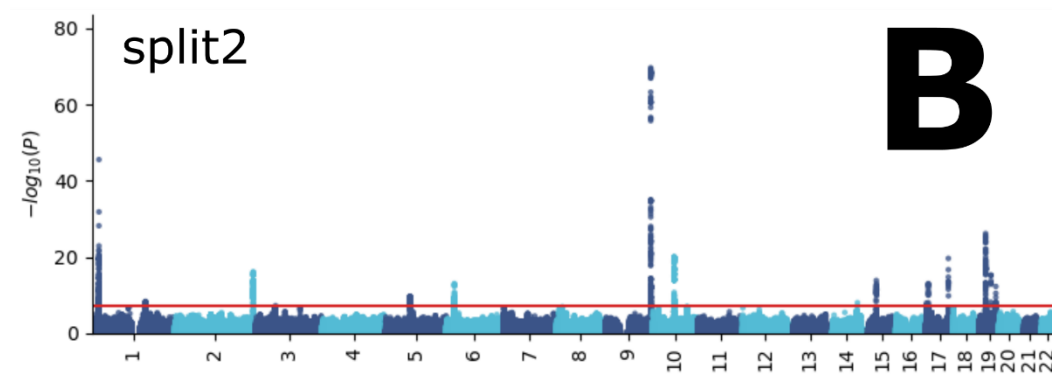
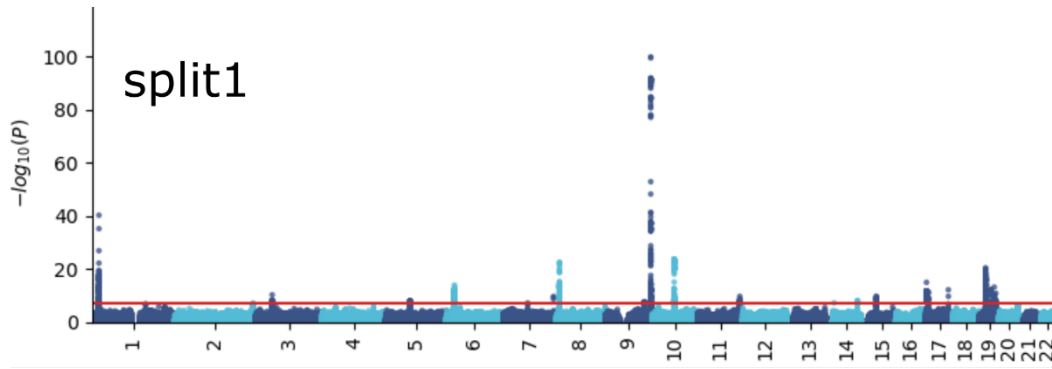


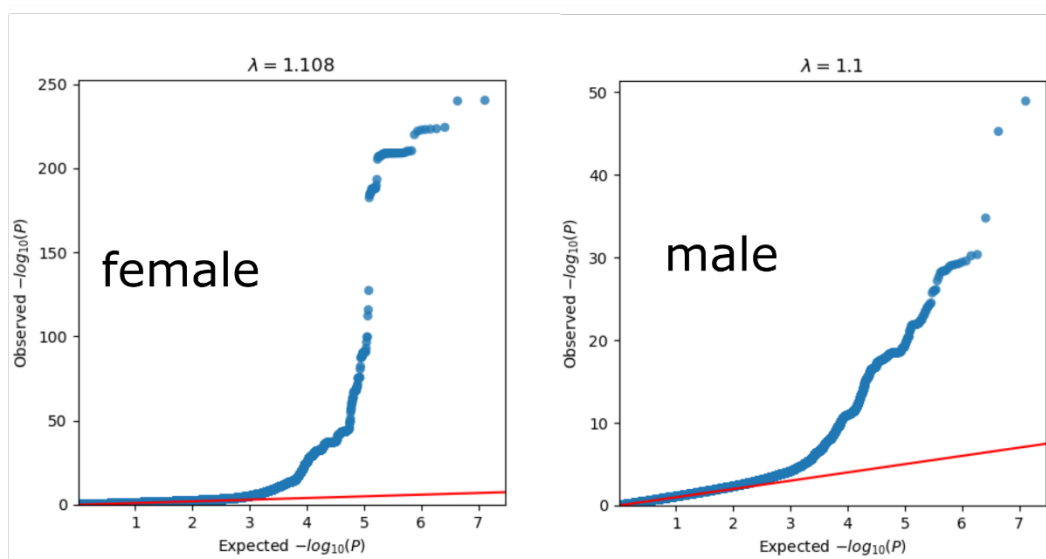
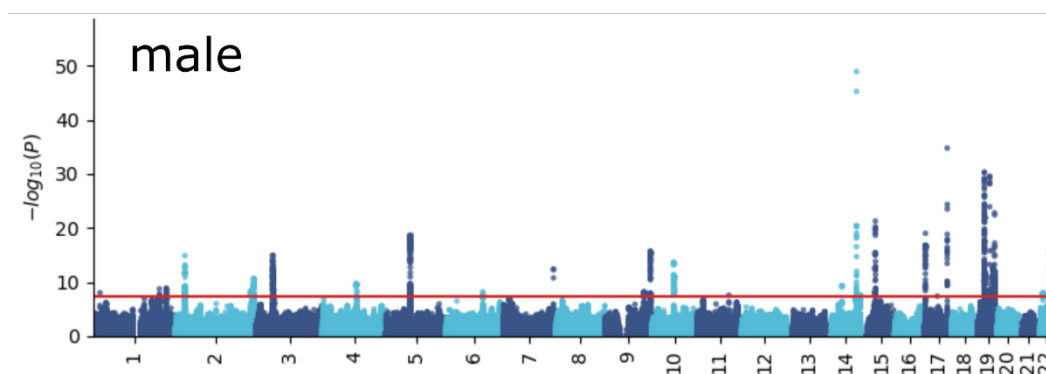
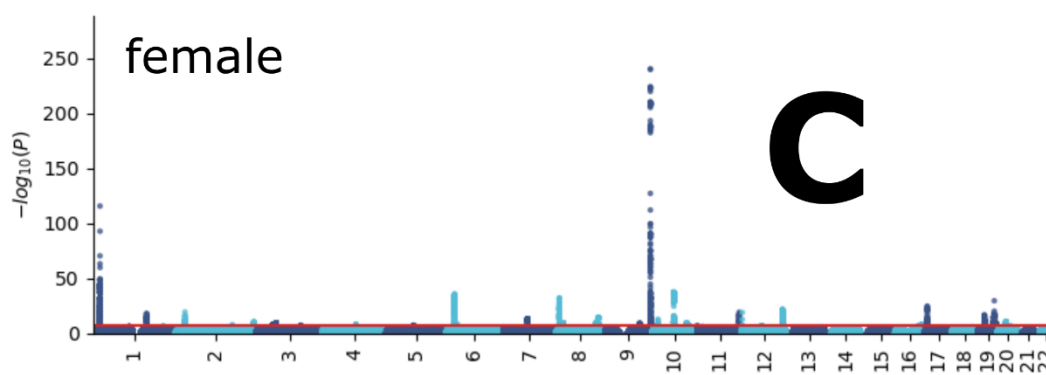


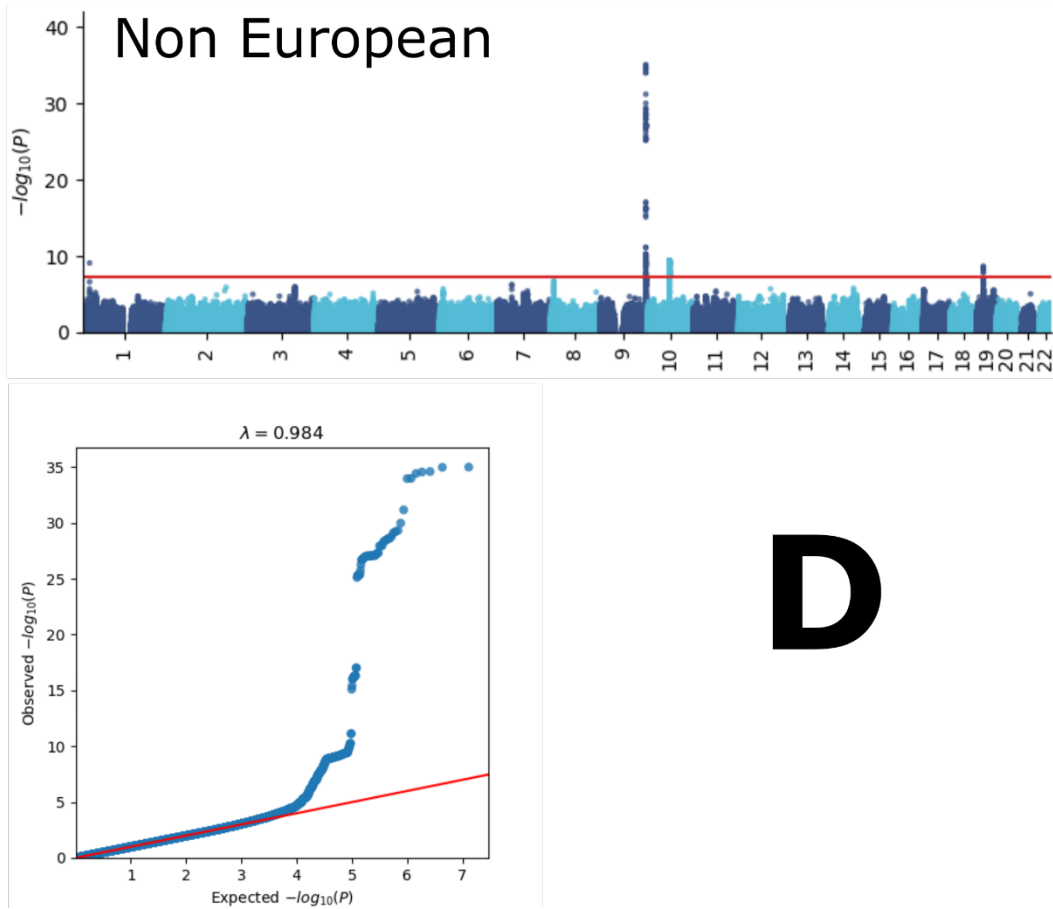
308
 309 Manhattan and QQ plots, along with genomic inflation factors and LDSC intercepts, are
 310 displayed for the primary GWAS conducted on individuals of European ancestry ($N=36,004$)
 311 using PLINK and fastGWA (A). Additionally, results are presented for split-sample GWAS
 312 (split1 and split2, B), sex-stratified GWAS (female and male, C), and GWAS involving non-
 313 European ancestry populations ($N=3407$, D).

314 eFigure 4: GWAS Manhattan plots for the hepatic BAG







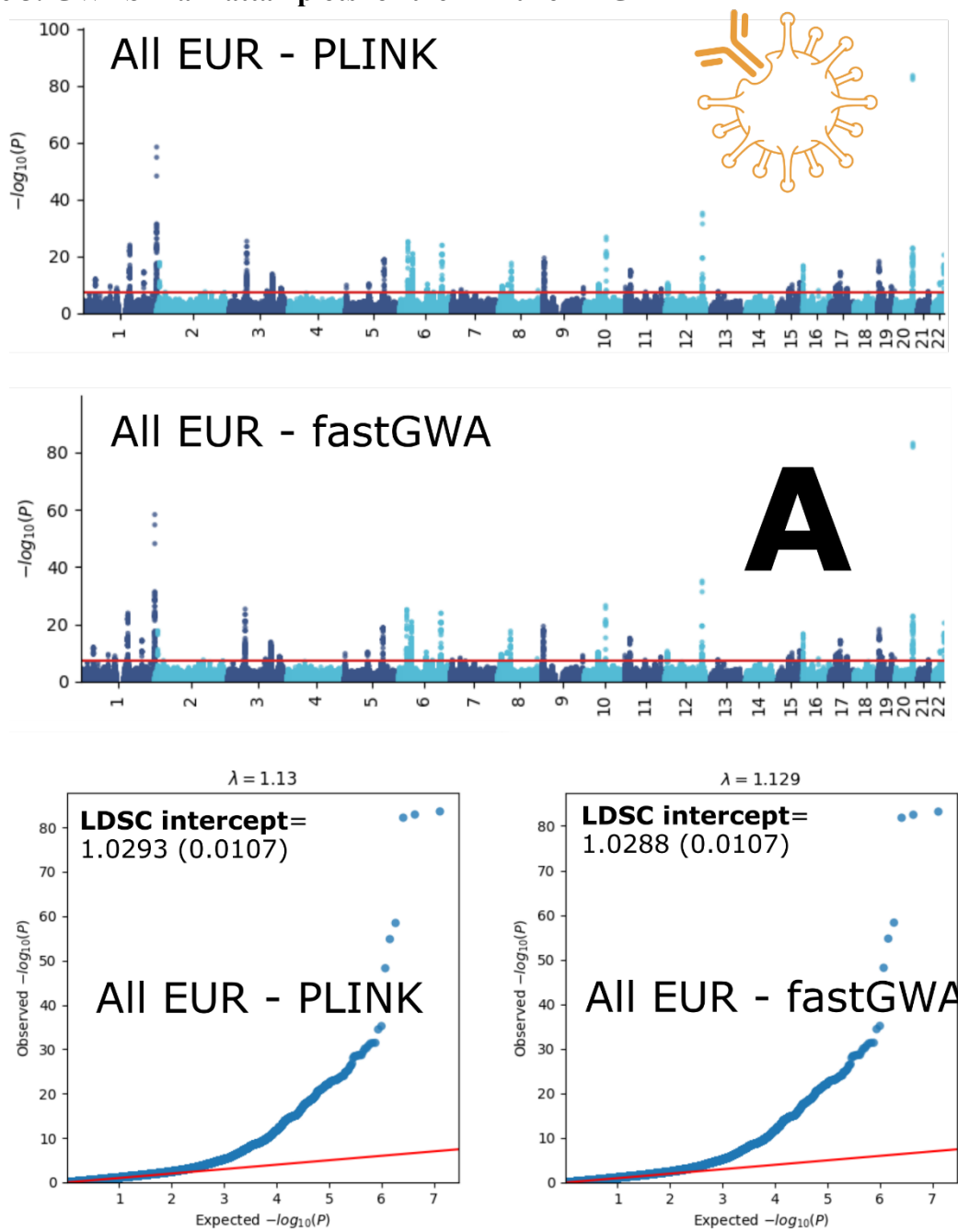


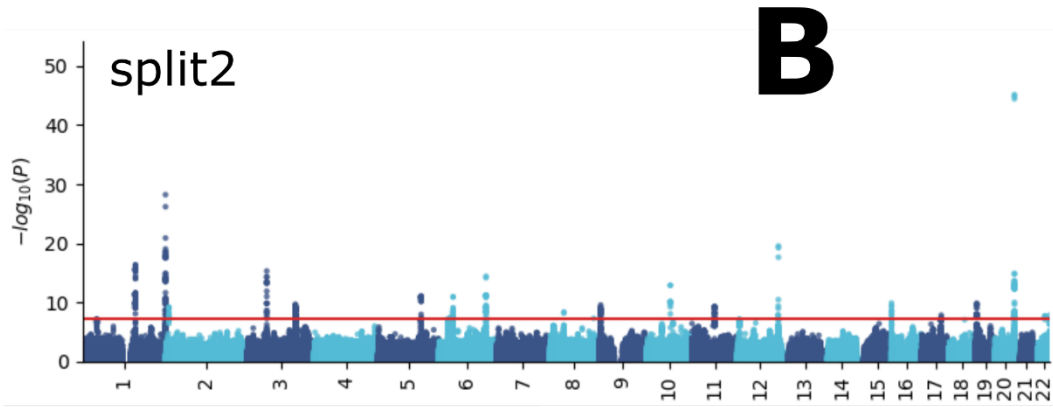
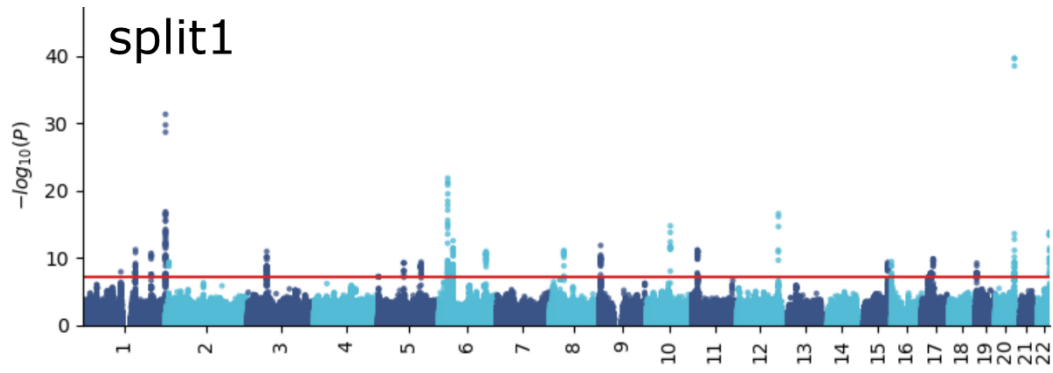
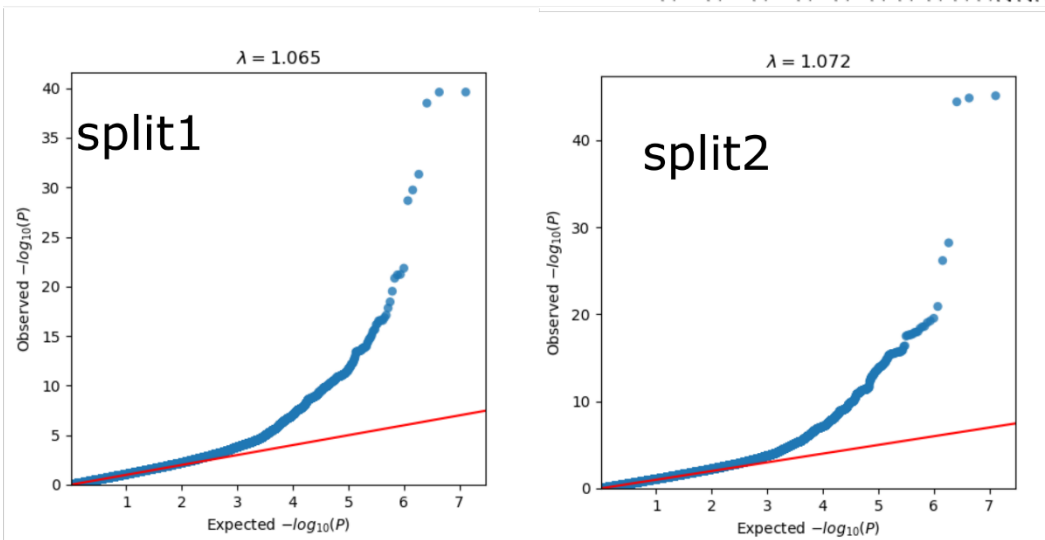
D

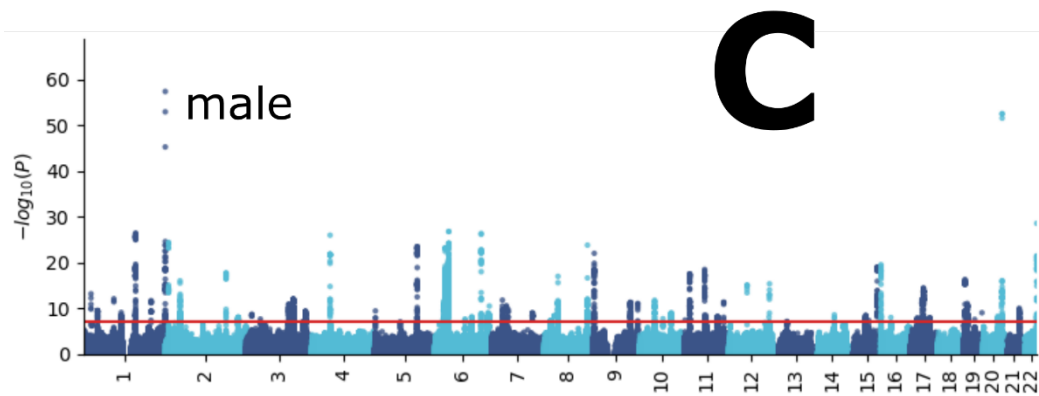
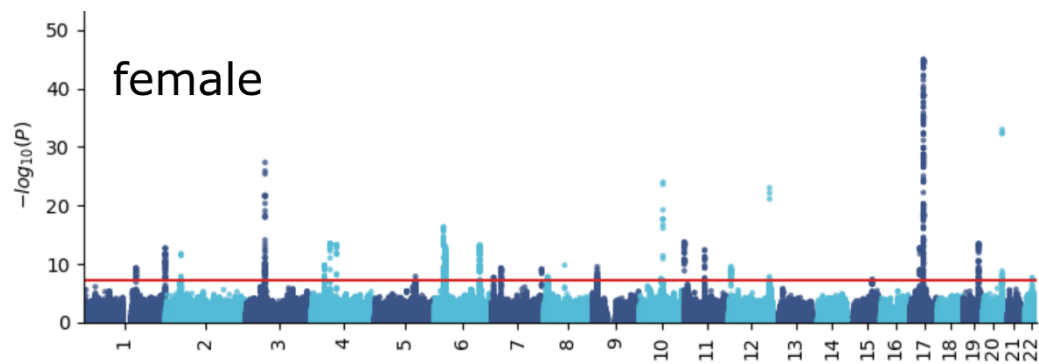
318
319
320
321
322
323

Manhattan and QQ plots, along with genomic inflation factors and LDSC intercepts, are displayed for the primary GWAS conducted on individuals of European ancestry ($N=111,386$) using PLINK and fastGWA (**A**). Additionally, results are presented for split-sample GWAS (split1 and split2, **B**), sex-stratified GWAS (female and male, **C**), and GWAS involving non-European ancestry populations ($N=20,408$, **D**).

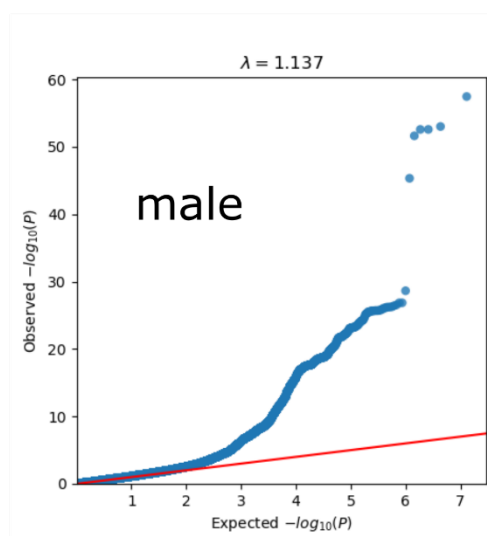
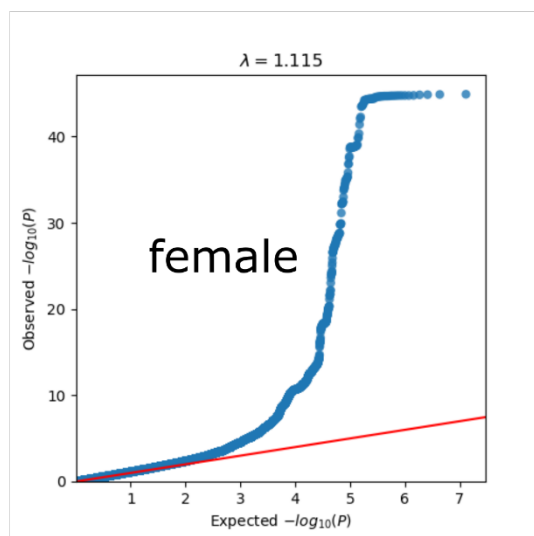
324 eFigure 5: GWAS Manhattan plots for the immune BAG

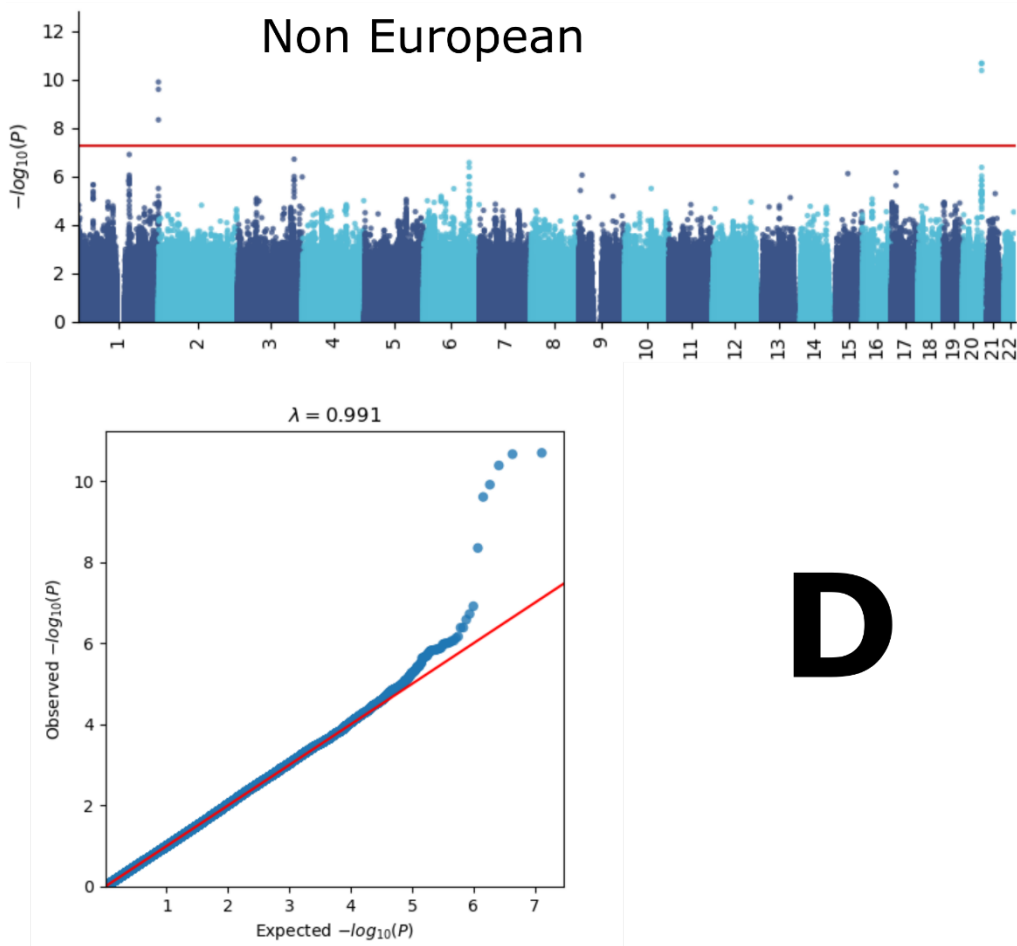


**B**



C

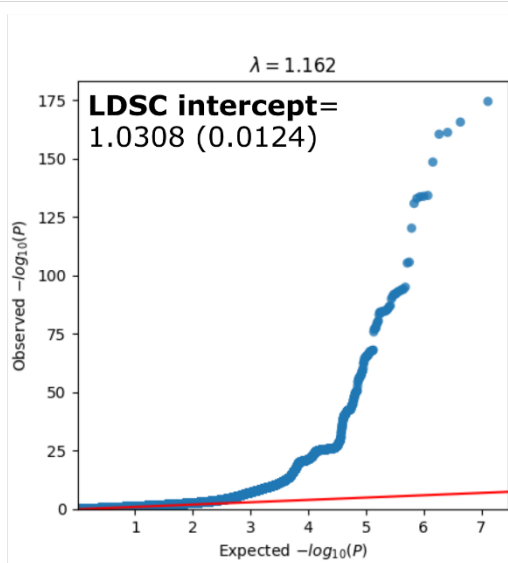
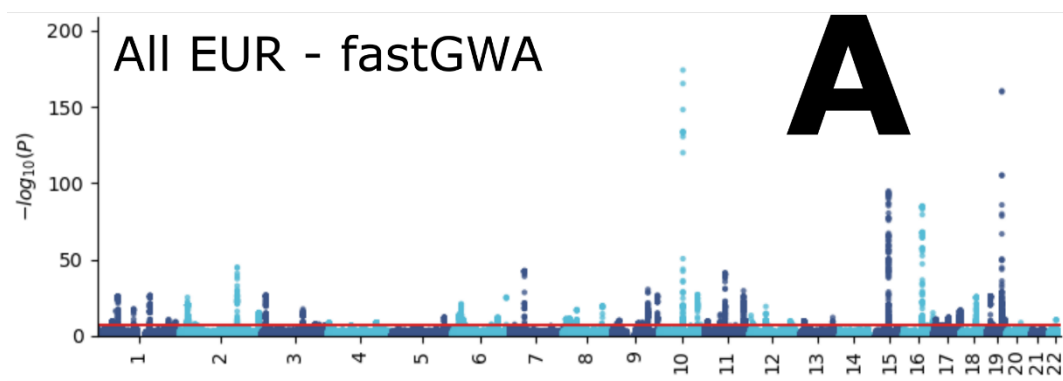
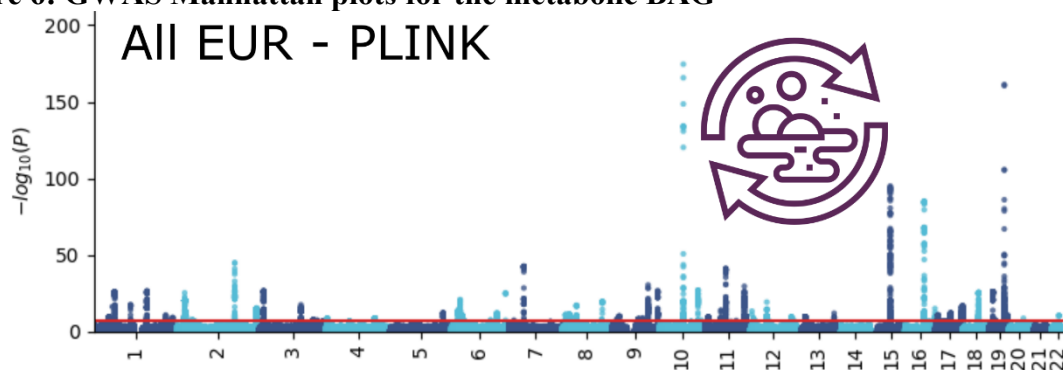




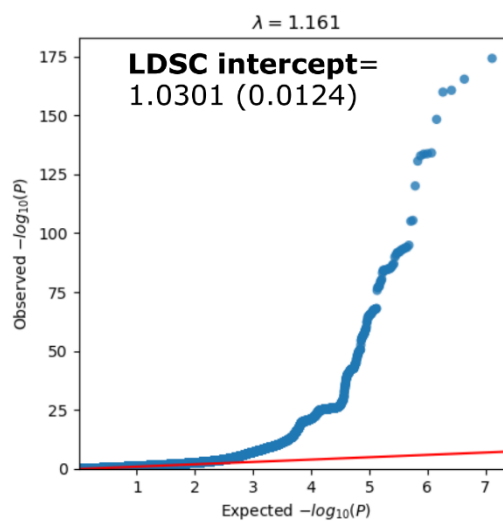
D

328
 329 Manhattan and QQ plots, along with genomic inflation factors and LDSC intercepts, are
 330 displayed for the primary GWAS conducted on individuals of European ancestry ($N=111,386$)
 331 using PLINK and fastGWA (**A**). Additionally, results are presented for split-sample GWAS
 332 (split1 and split2, **B**), sex-stratified GWAS (female and male, **C**), and GWAS involving non-
 333 European ancestry populations ($N=20,408$, **D**).

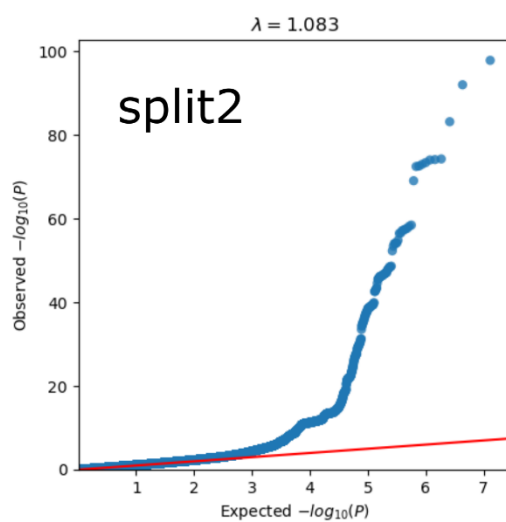
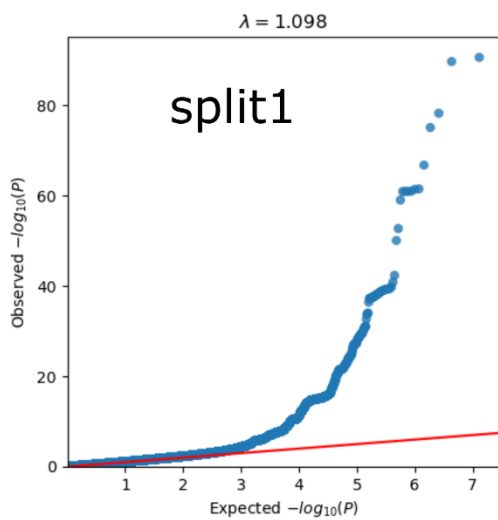
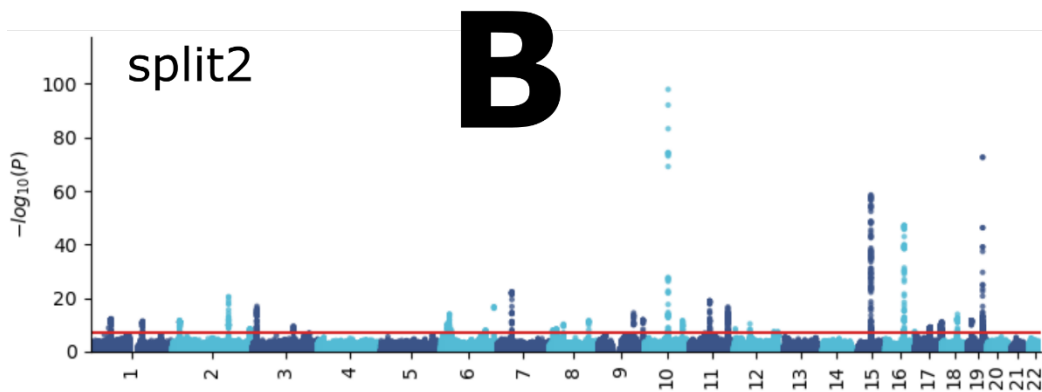
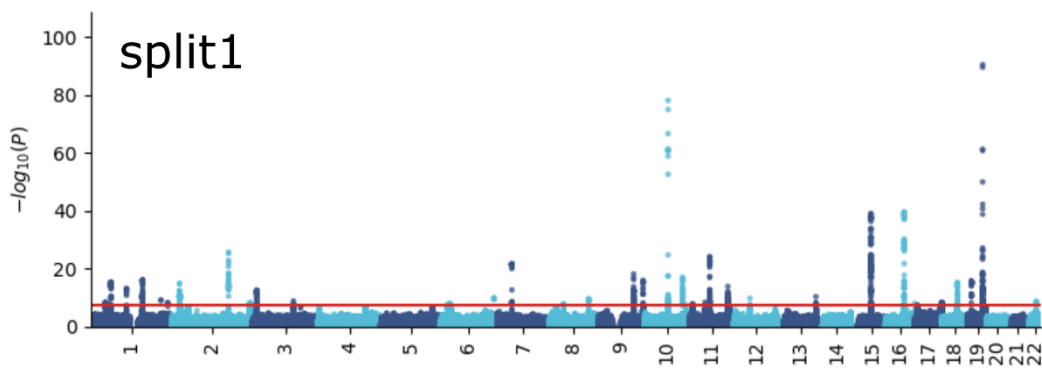
334 eFigure 6: GWAS Manhattan plots for the metabolic BAG

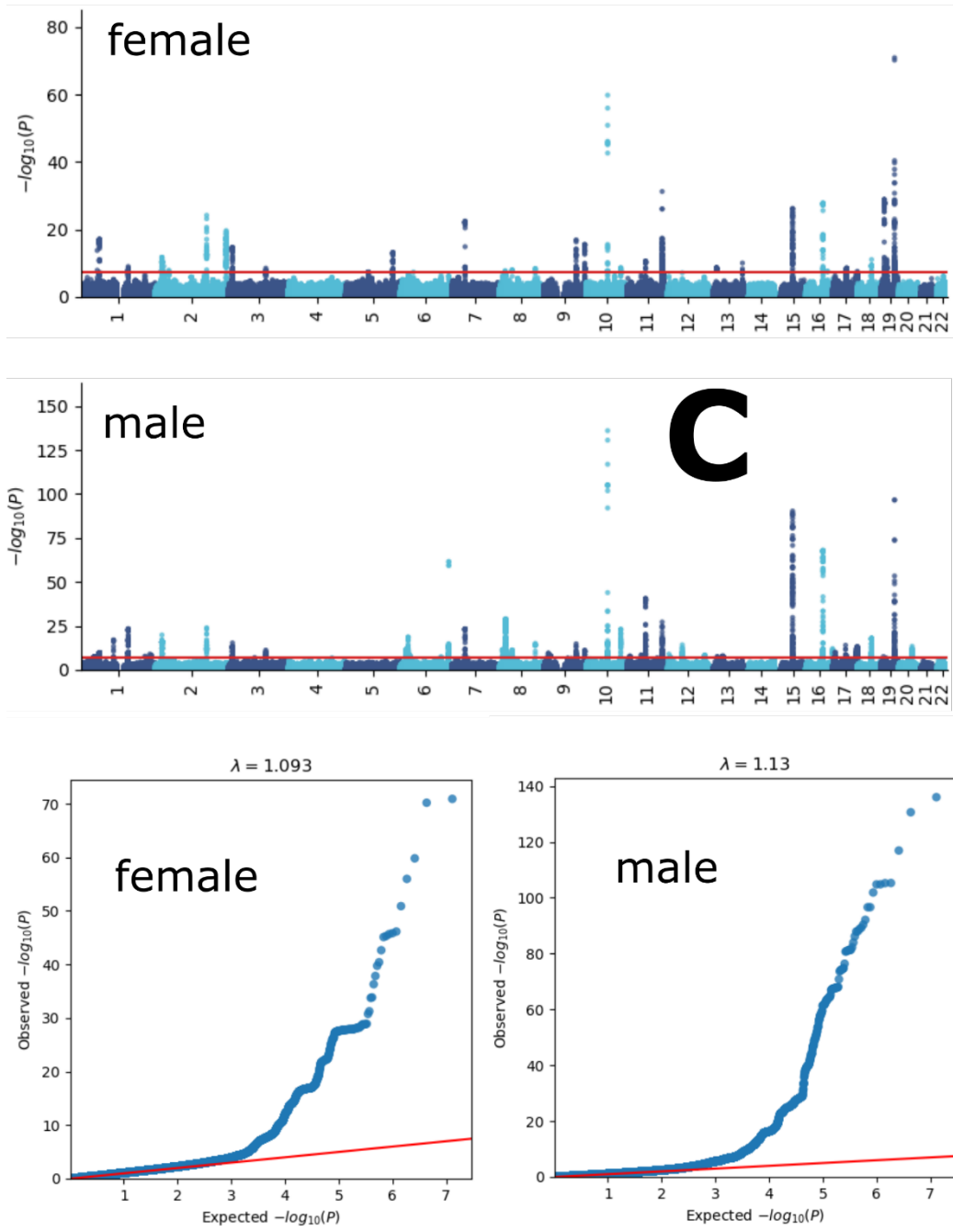


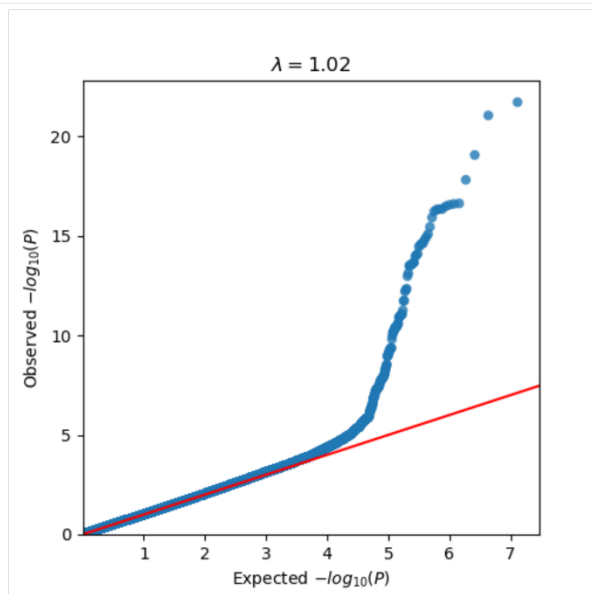
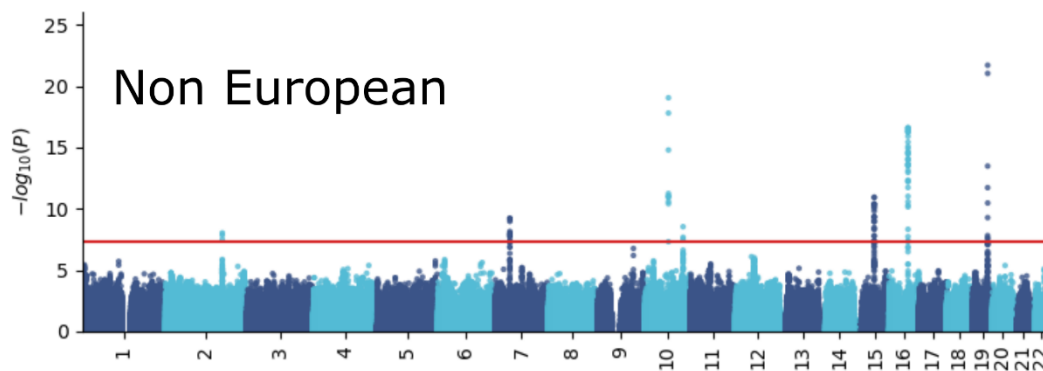
All EUR - PLINK



All EUR - fastGWA



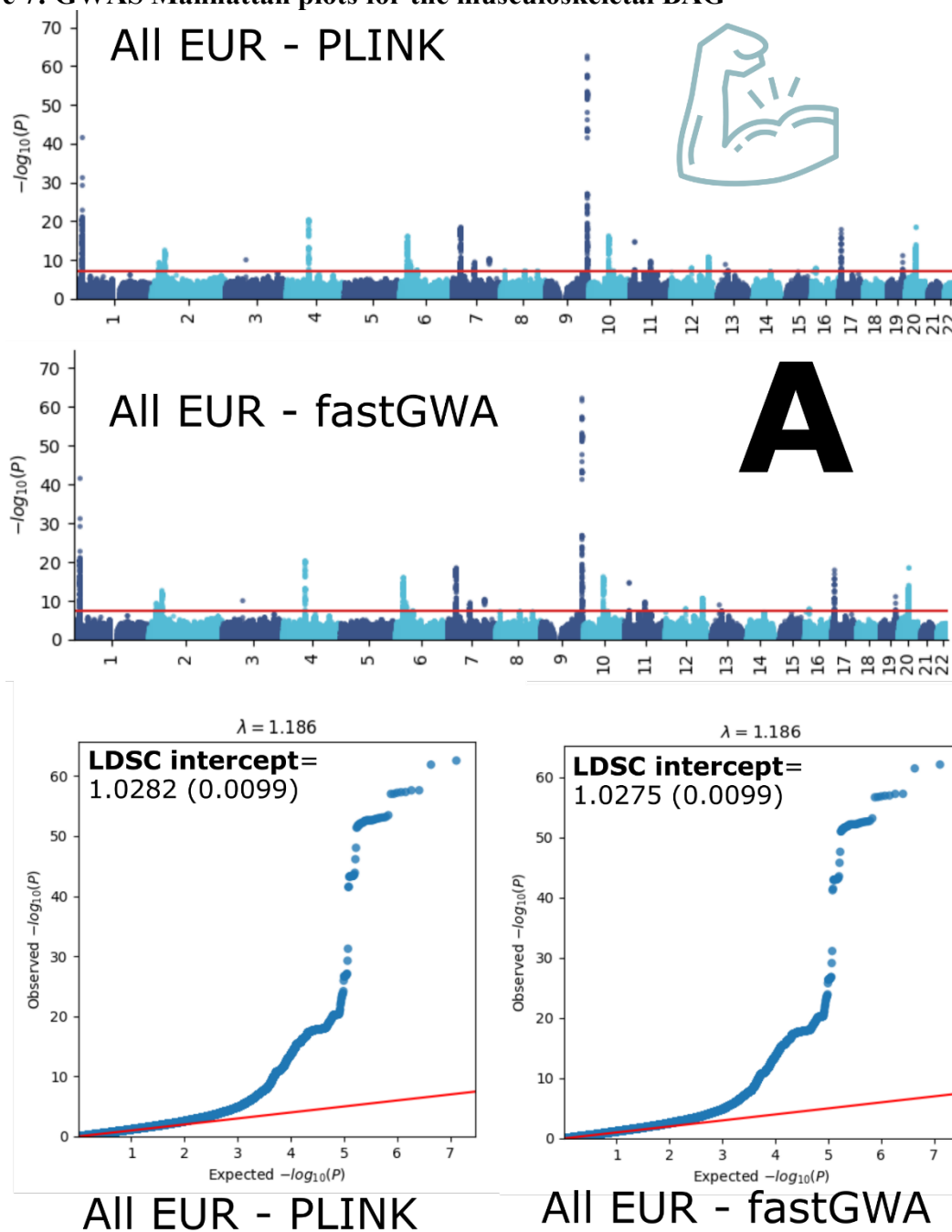




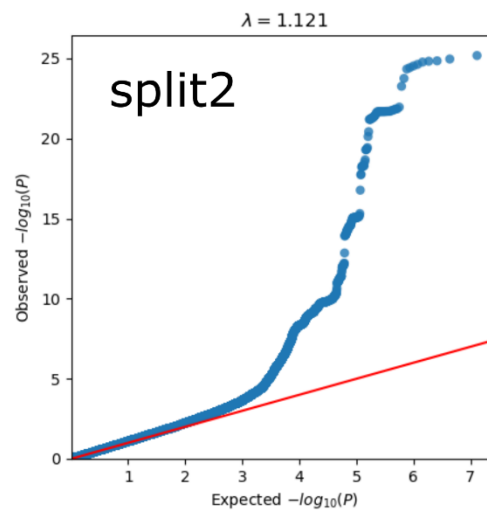
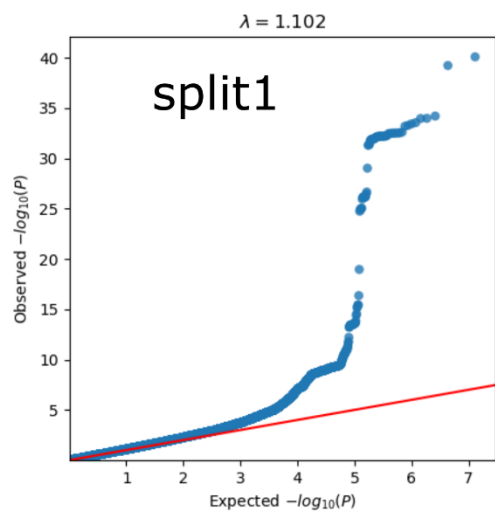
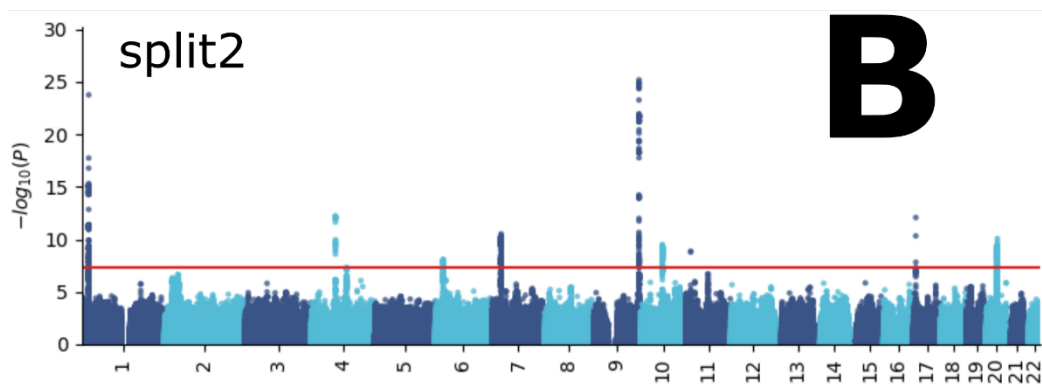
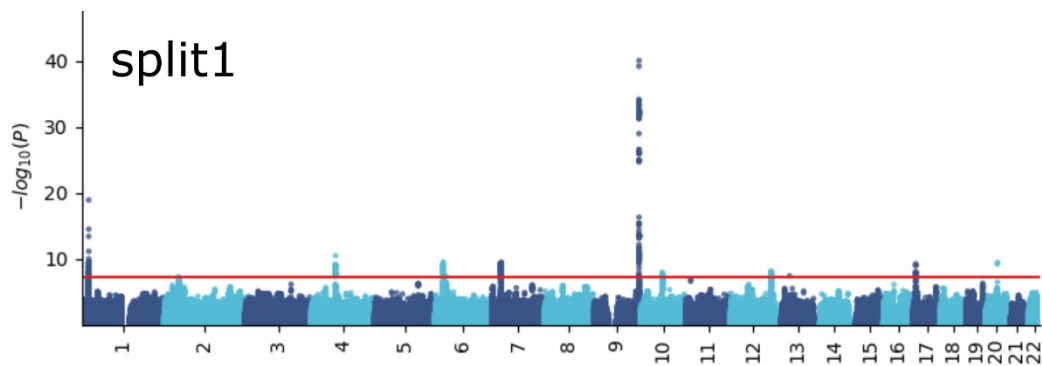
D

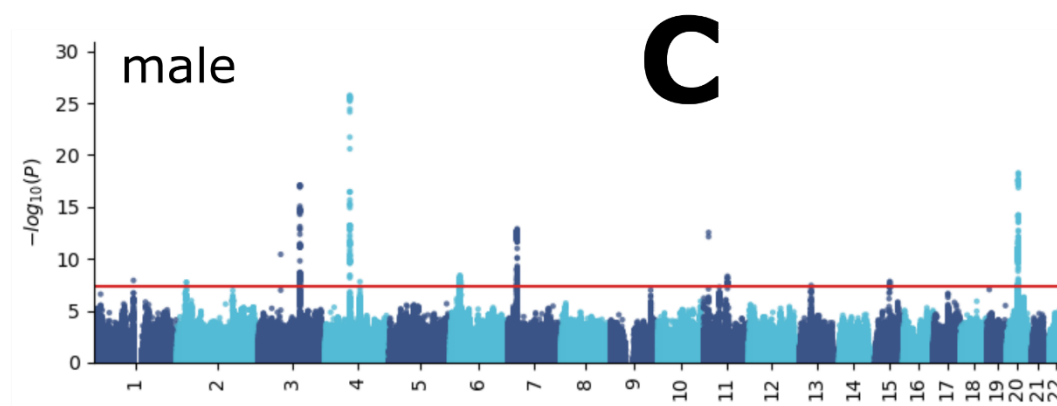
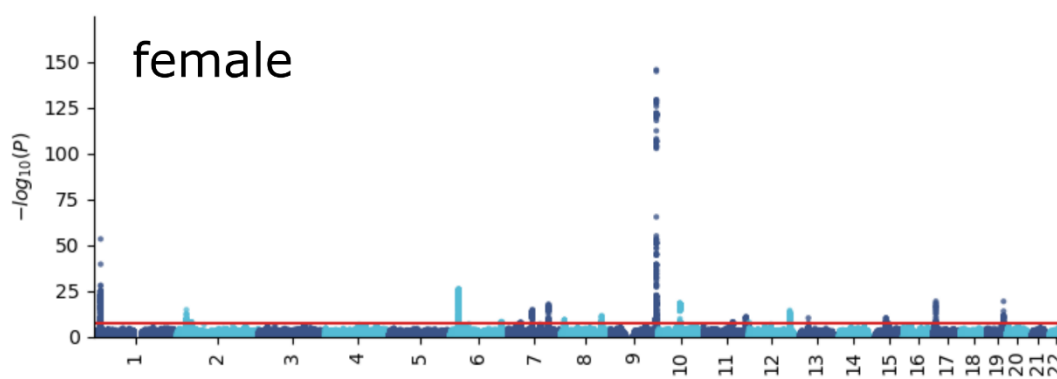
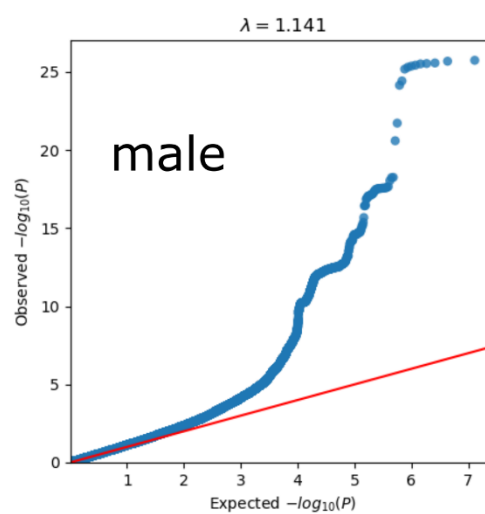
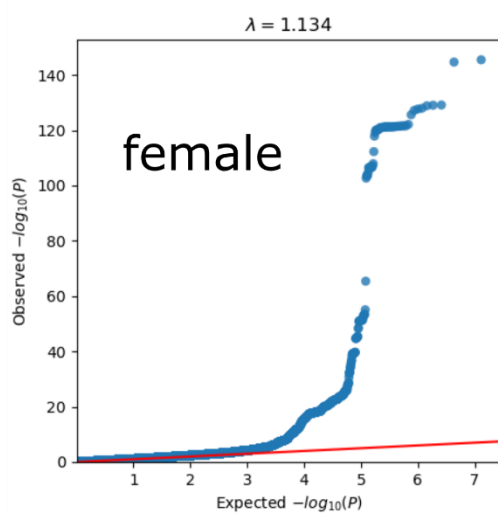
338
 339 Manhattan and QQ plots, along with genomic inflation factors and LDSC intercepts, are
 340 displayed for the primary GWAS conducted on individuals of European ancestry ($N=111,386$)
 341 using PLINK and fastGWA (**A**). Additionally, results are presented for split-sample GWAS
 342 (split1 and split2, **B**), sex-stratified GWAS (female and male, **C**), and GWAS involving non-
 343 European ancestry populations ($N=20,408$, **D**).

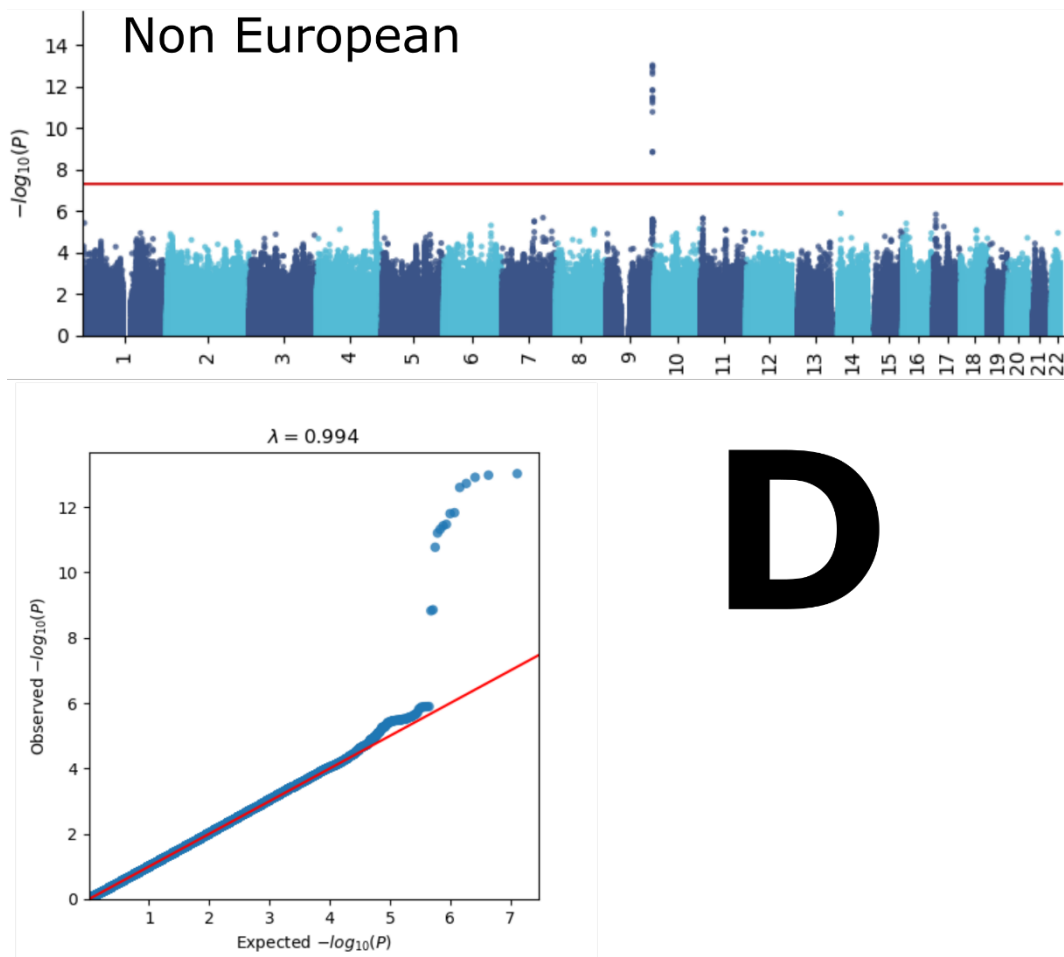
344 eFigure 7: GWAS Manhattan plots for the musculoskeletal BAG



345



**C**

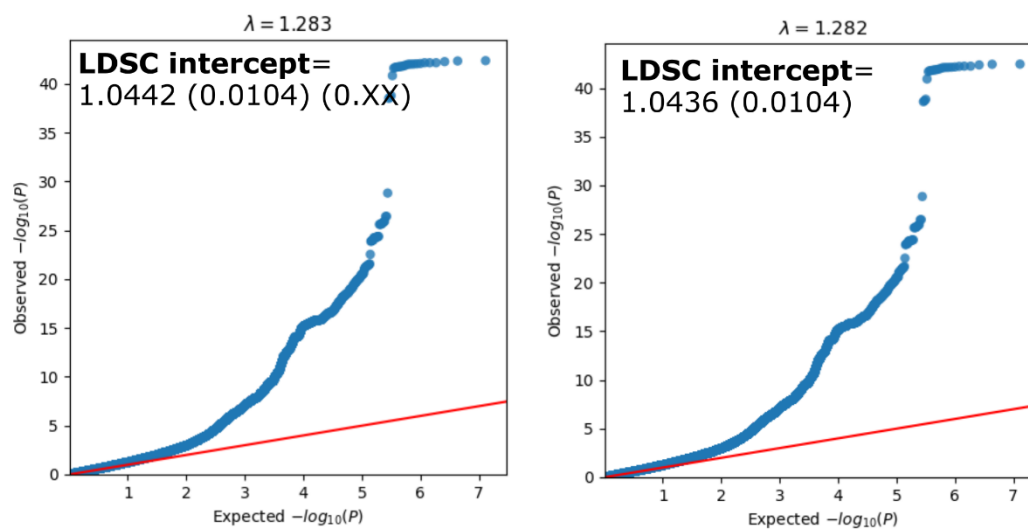
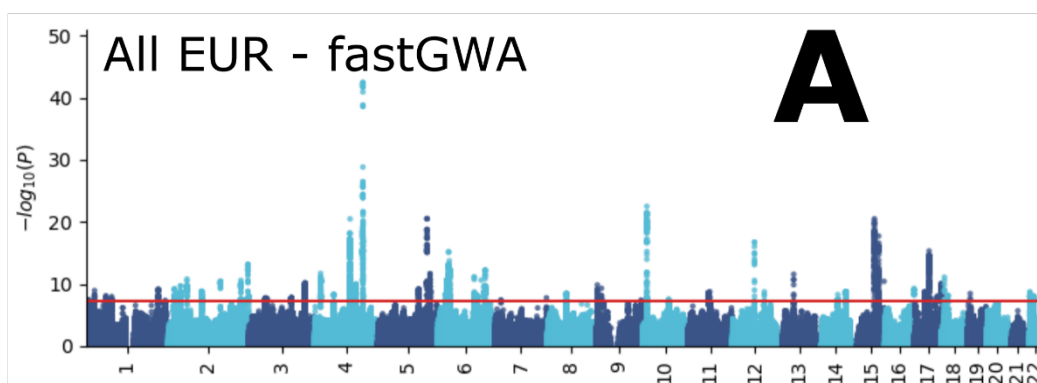
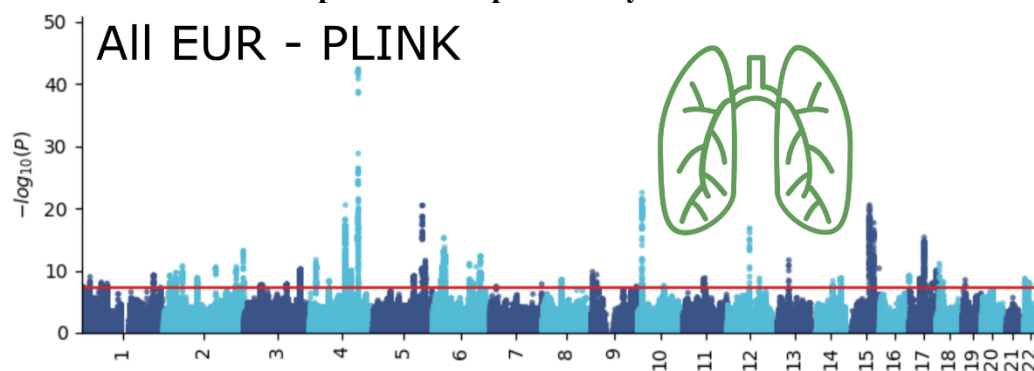


D

348
 349
 350
 351
 352
 353

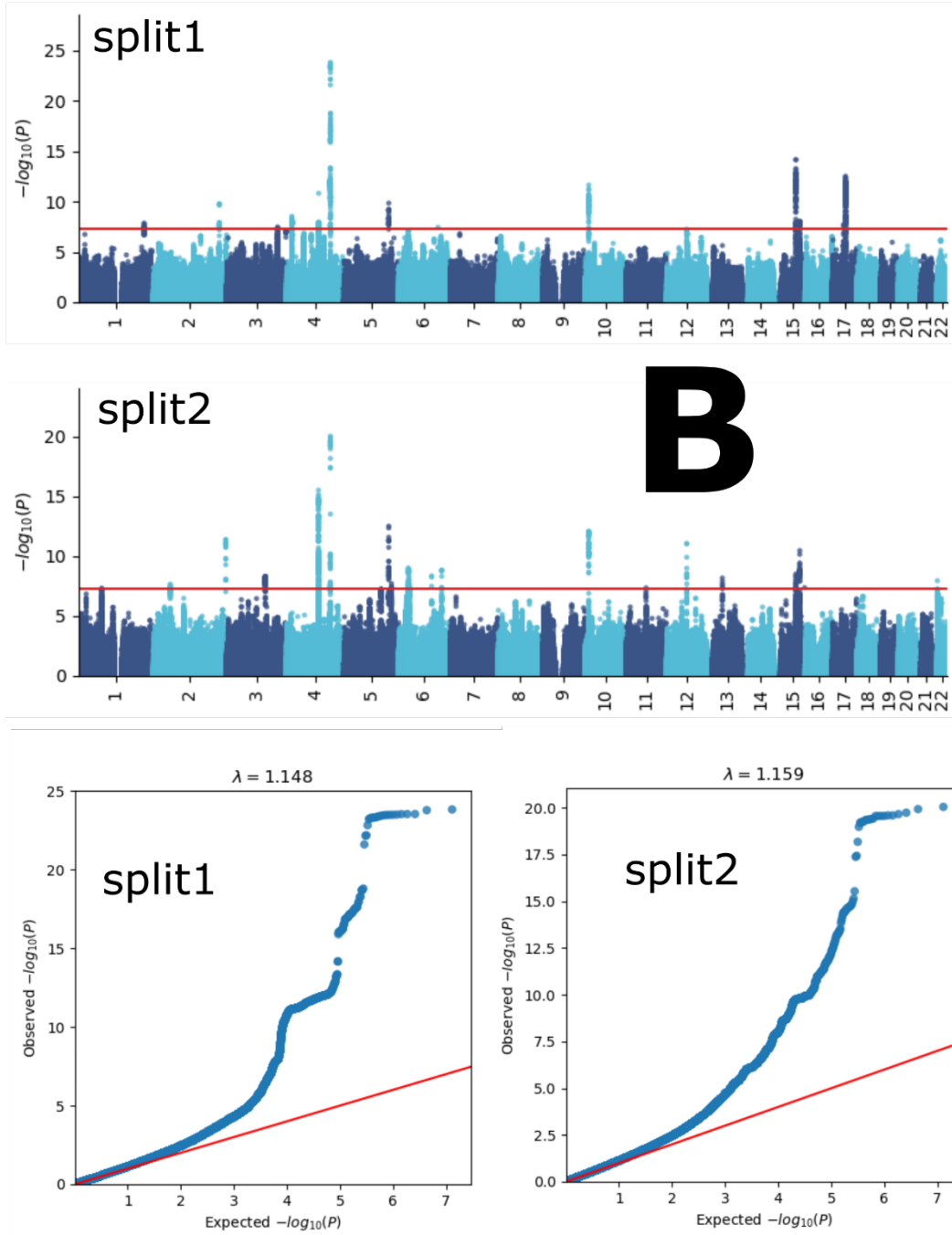
Manhattan and QQ plots, along with genomic inflation factors and LDSC intercepts, are displayed for the primary GWAS conducted on individuals of European ancestry ($N=111,386$) using PLINK and fastGWA (A). Additionally, results are presented for split-sample GWAS (split1 and split2, B), sex-stratified GWAS (female and male, C), and GWAS involving non-European ancestry populations ($N=20,408$, D).

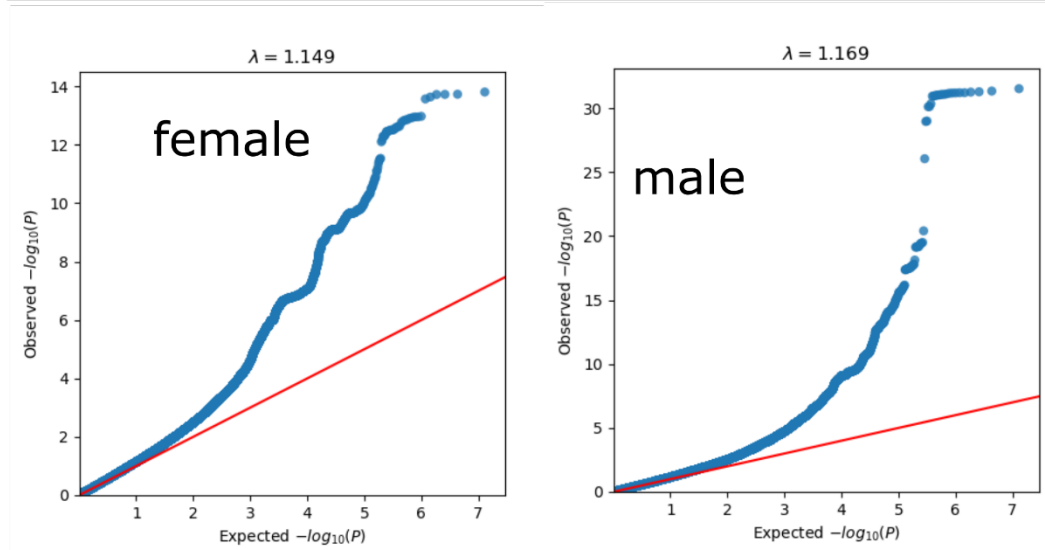
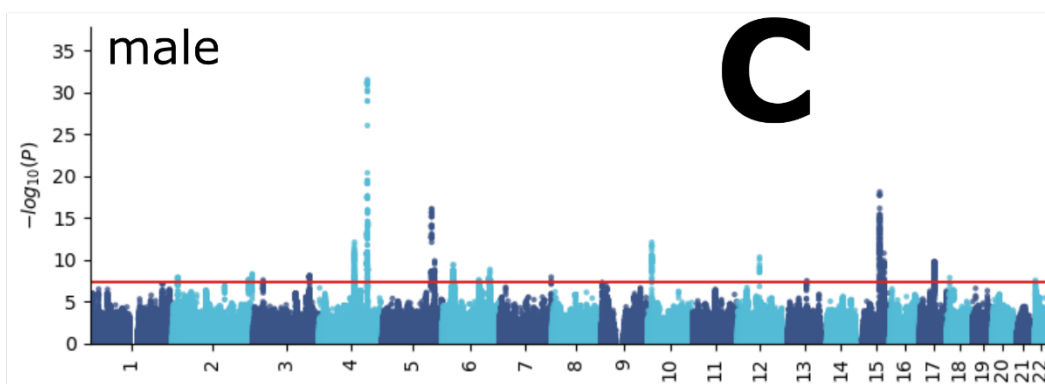
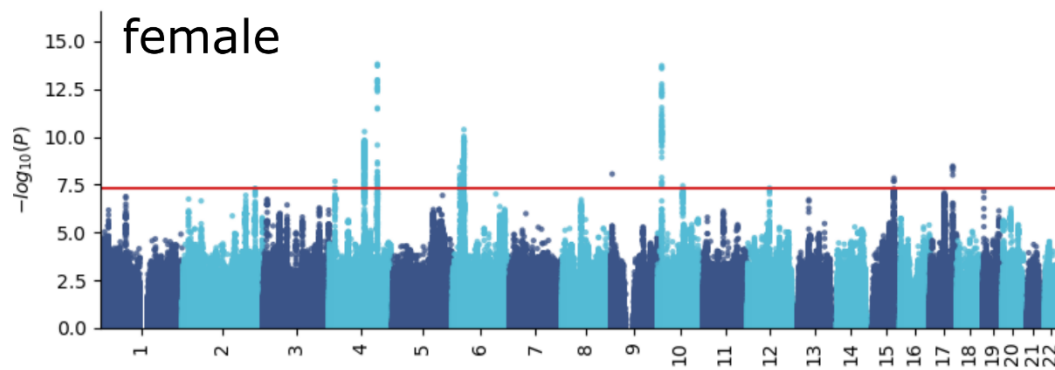
354 eFigure 8: GWAS Manhattan plots for the pulmonary BAG

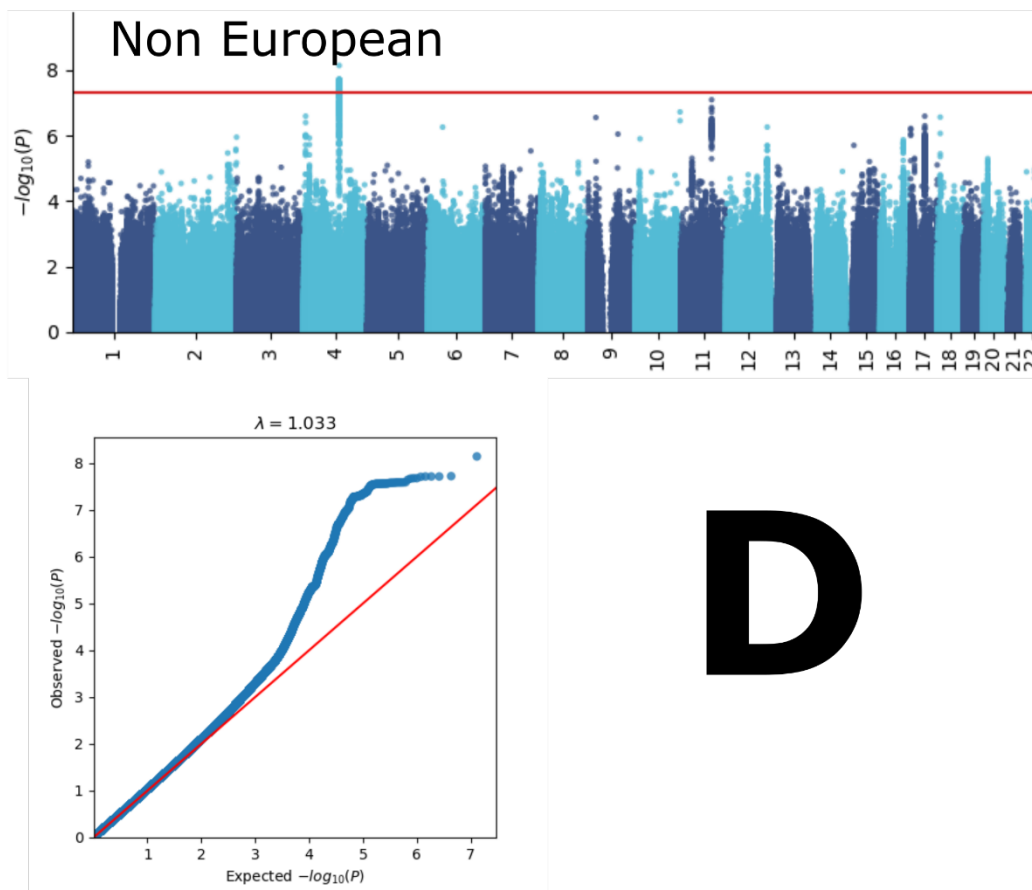


All EUR - PLINK

All EUR - fastGWA





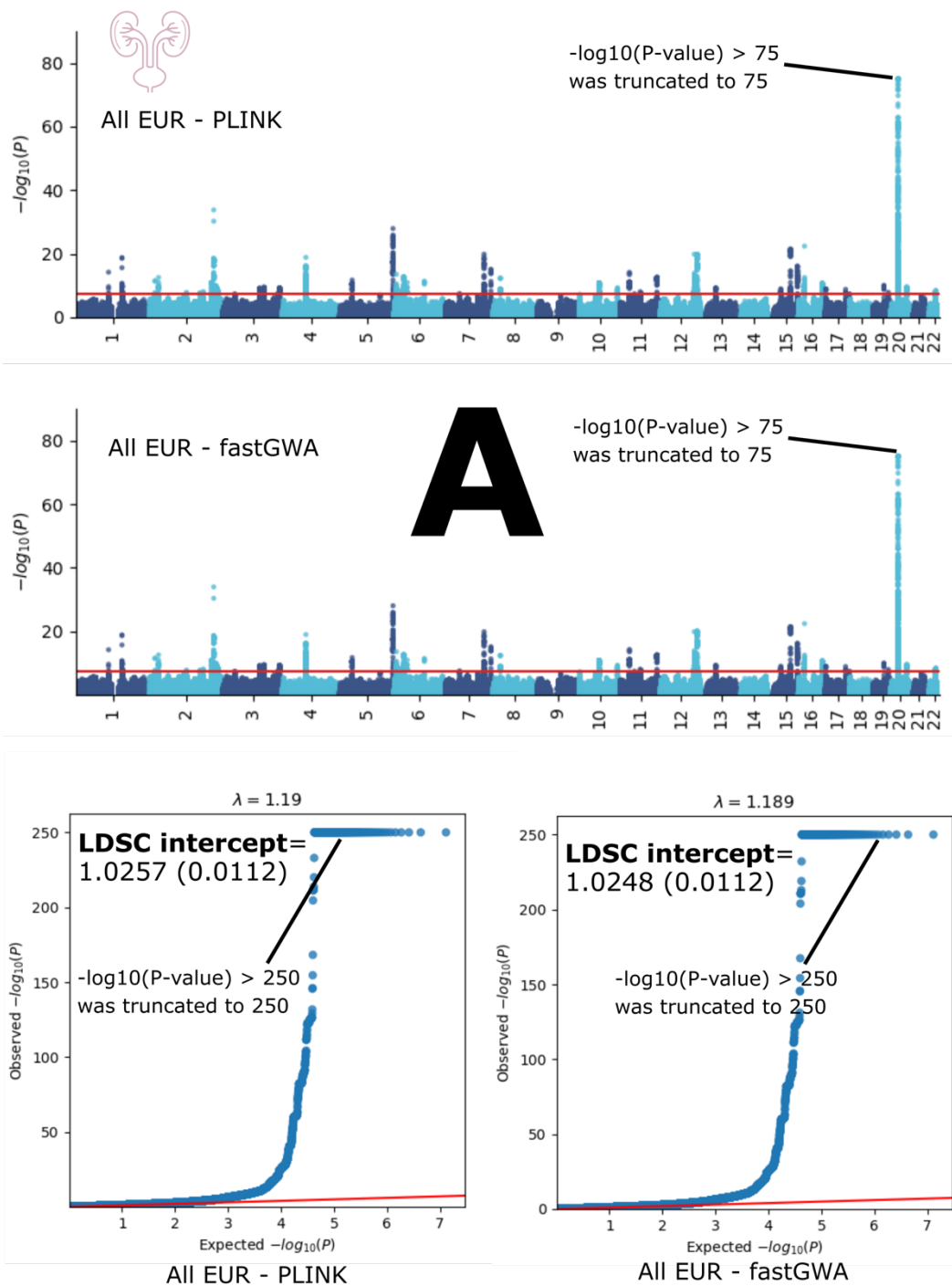


D

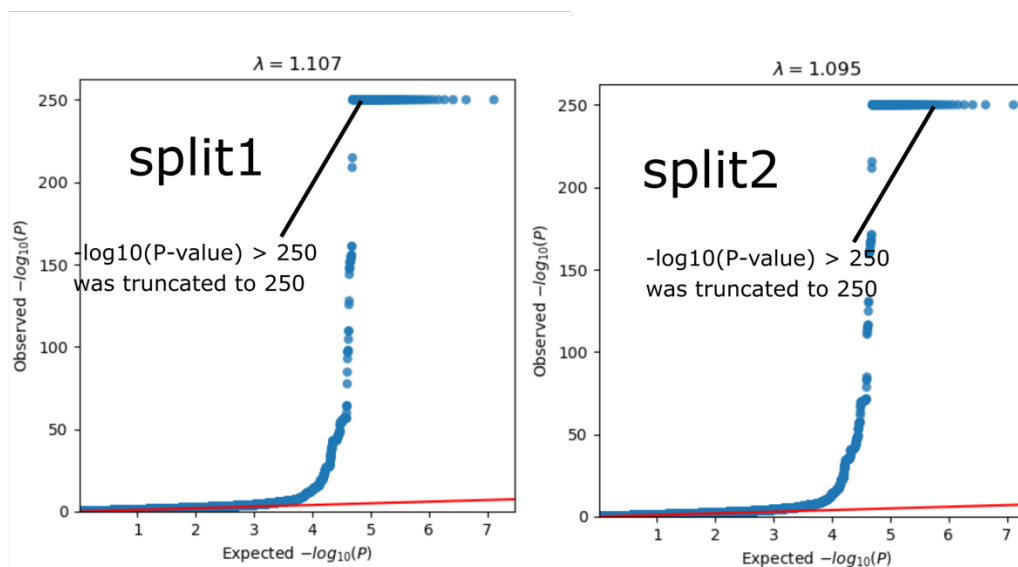
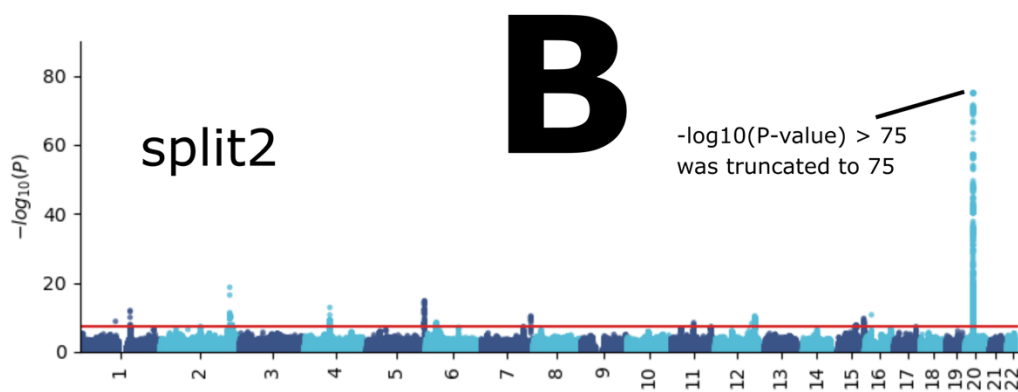
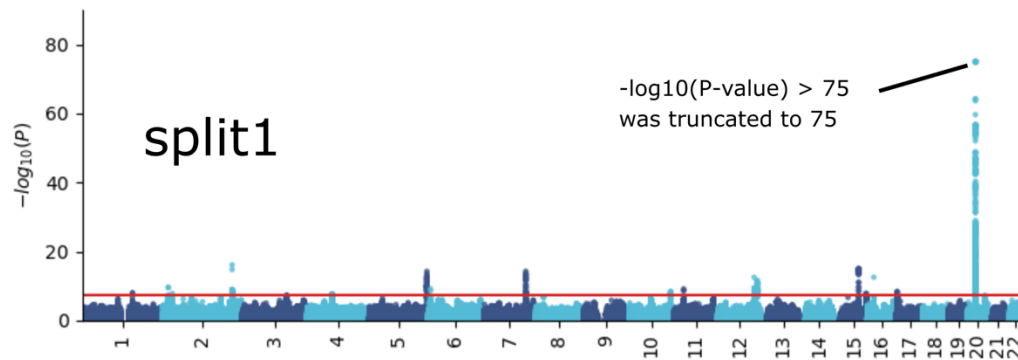
358
 359
 360
 361
 362
 363

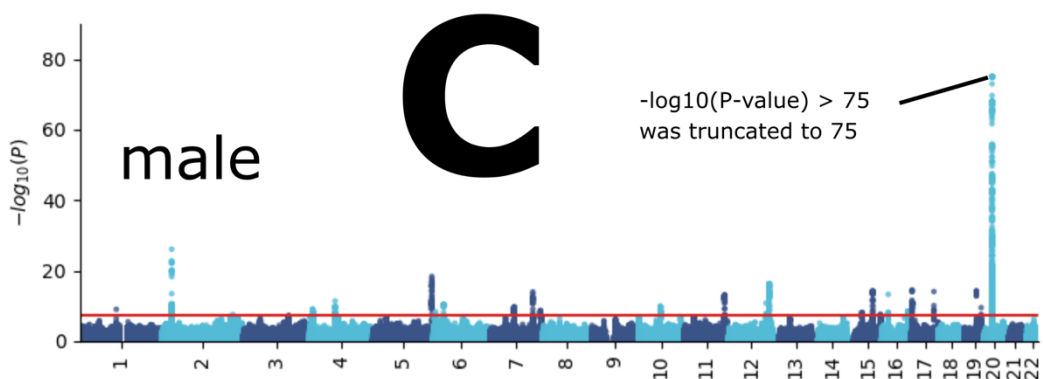
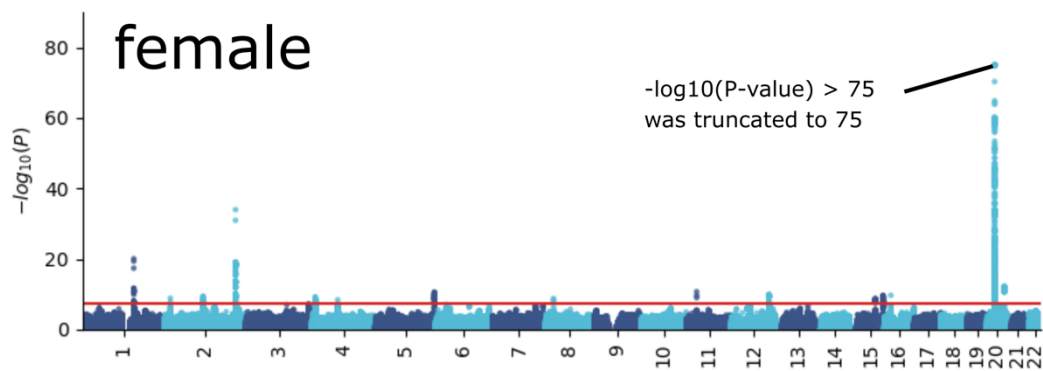
Manhattan and QQ plots, along with genomic inflation factors and LDSC intercepts, are displayed for the primary GWAS conducted on individuals of European ancestry ($N=111,386$) using PLINK and fastGWA (**A**). Additionally, results are presented for split-sample GWAS (split1 and split2, **B**), sex-stratified GWAS (female and male, **C**), and GWAS involving non-European ancestry populations ($N=20,408$, **D**).

364 eFigure 9: GWAS Manhattan plots for the renal BAG

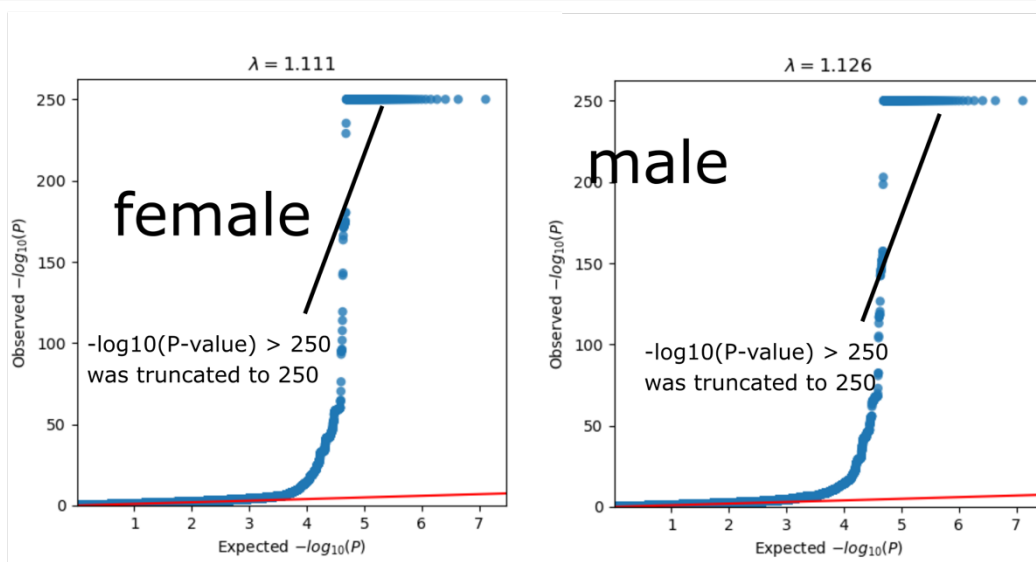


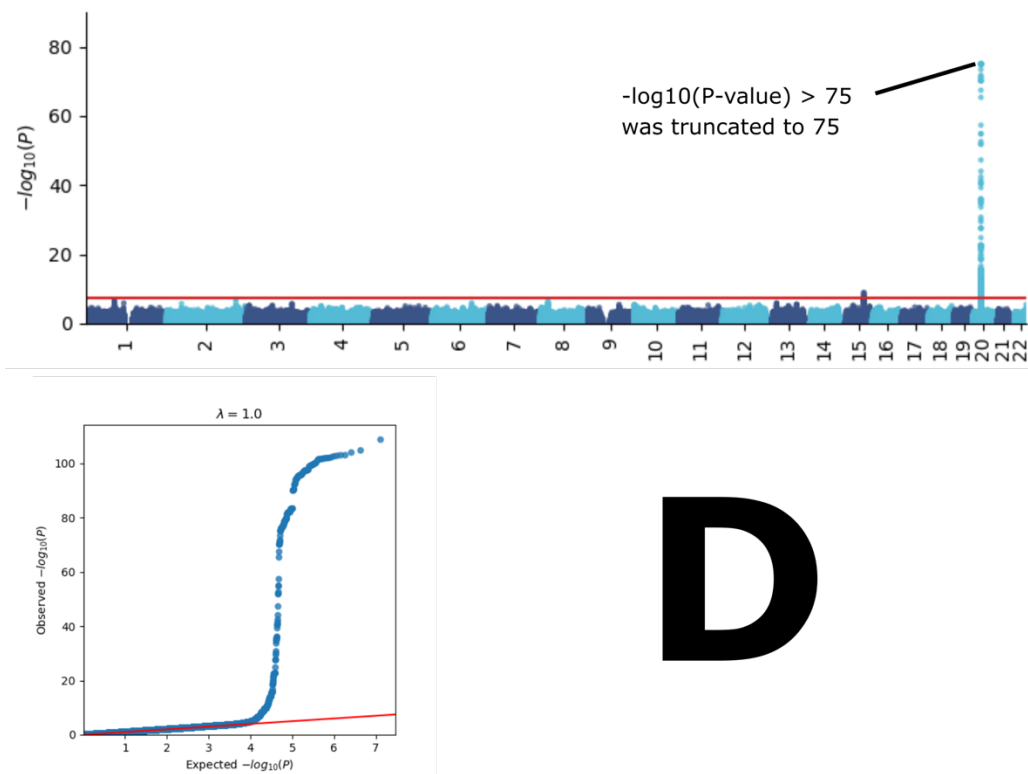
365





C



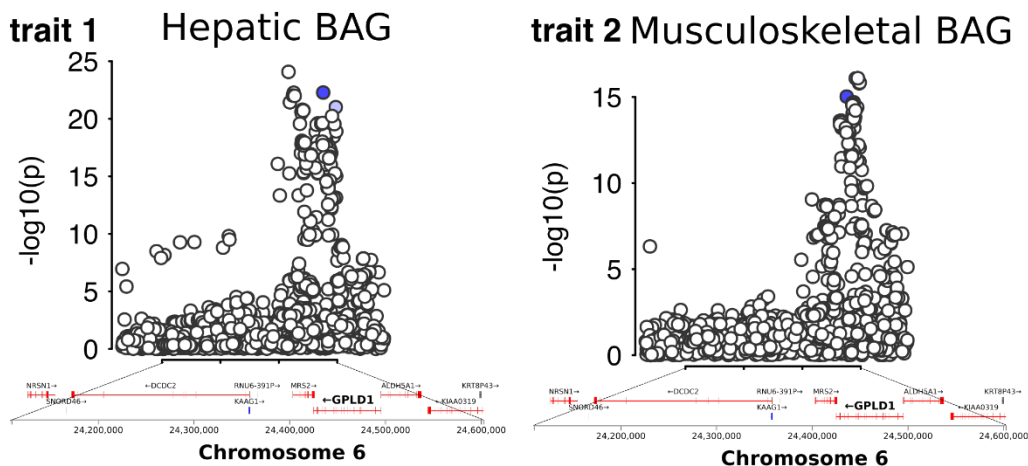


D

368
 369
 370
 371
 372
 373
 374
 375

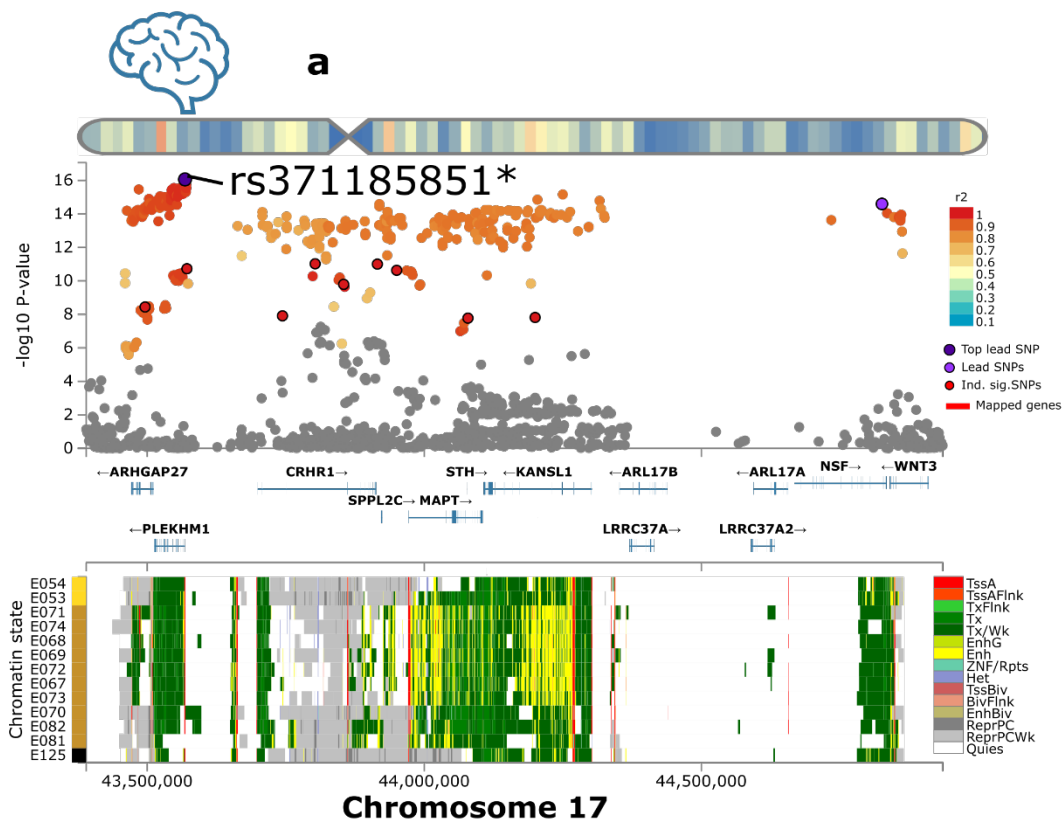
Manhattan and QQ plots, along with genomic inflation factors and LDSC intercepts, are displayed for the primary GWAS conducted on individuals of European ancestry ($N=111,386$) using PLINK and fastGWA (**A**). Additionally, results are presented for split-sample GWAS (split1 and split2, **B**), sex-stratified GWAS (female and male, **C**), and GWAS involving non-European ancestry populations ($N=20,408$, **D**). For visualization purposes, we chose to truncate the highly significant P-value ($P\text{-value} < 1 \times 10^{-300}$) to a lower P-value (1×10^{-75} for Manhattan plots and 1×10^{-250} for QQ plots).

376 **eFigure 10: Bayesian colocalization analysis for the locus on chromosome 6 between the**
 377 **hepatic and musculoskeletal BAGs**

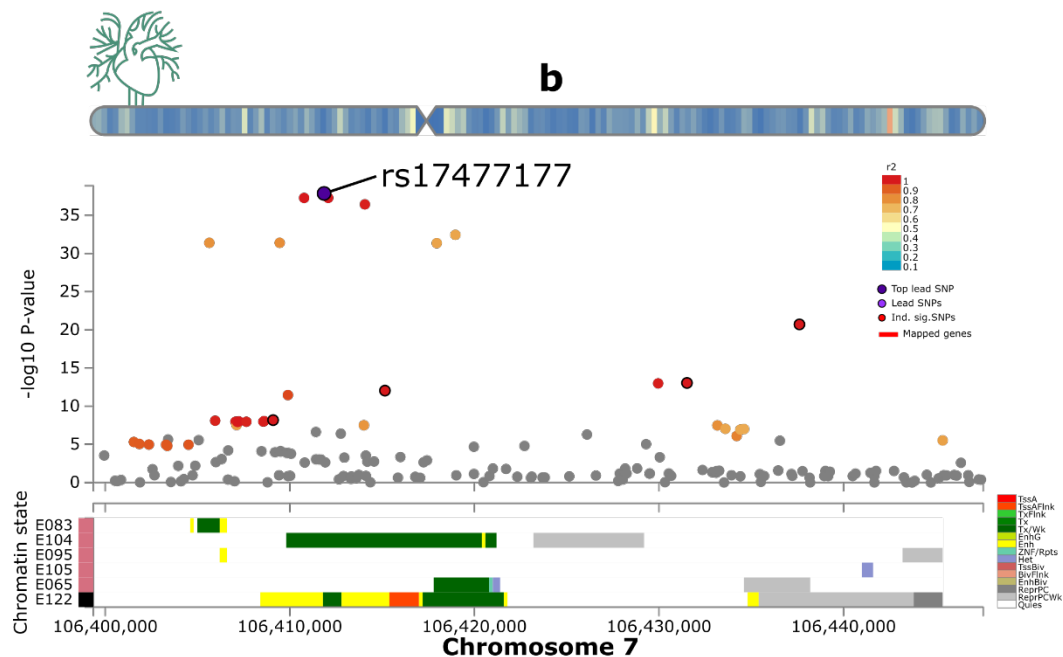


378 We conducted a Bayesian colocalization analysis using Bayes factors to investigate shared causal
 379 variants in a specific locus on chromosome 6 for the hepatic and musculoskeletal BAGs. The
 380 analysis tested five hypotheses, denoted by their posterior probabilities: H0 (no association with
 381 either trait), H1 (association with trait 1 but not trait 2), H2 (association with trait 2 but not trait
 382 1), H3 (association with both traits but with separate causal variants), and H4 (association with
 383 both traits with a shared causal variant). The potential causal variants for both traits are indicated
 384 by blue-colored SNPs, assuming each locus contains at most one causal variant. The gene
 385 mapped to this locus (*GPLD1*) is shown in bold based on physical positions.
 386
 387

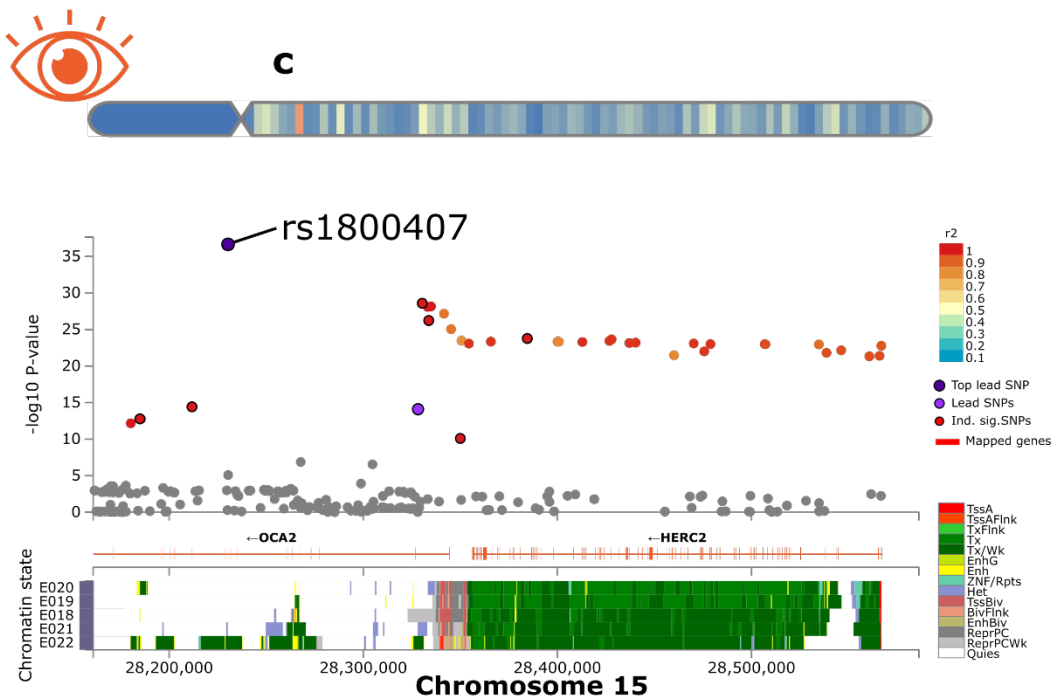
388 eFigure 11: Exemplary genomic locus for each BAG in the nine human organ systems



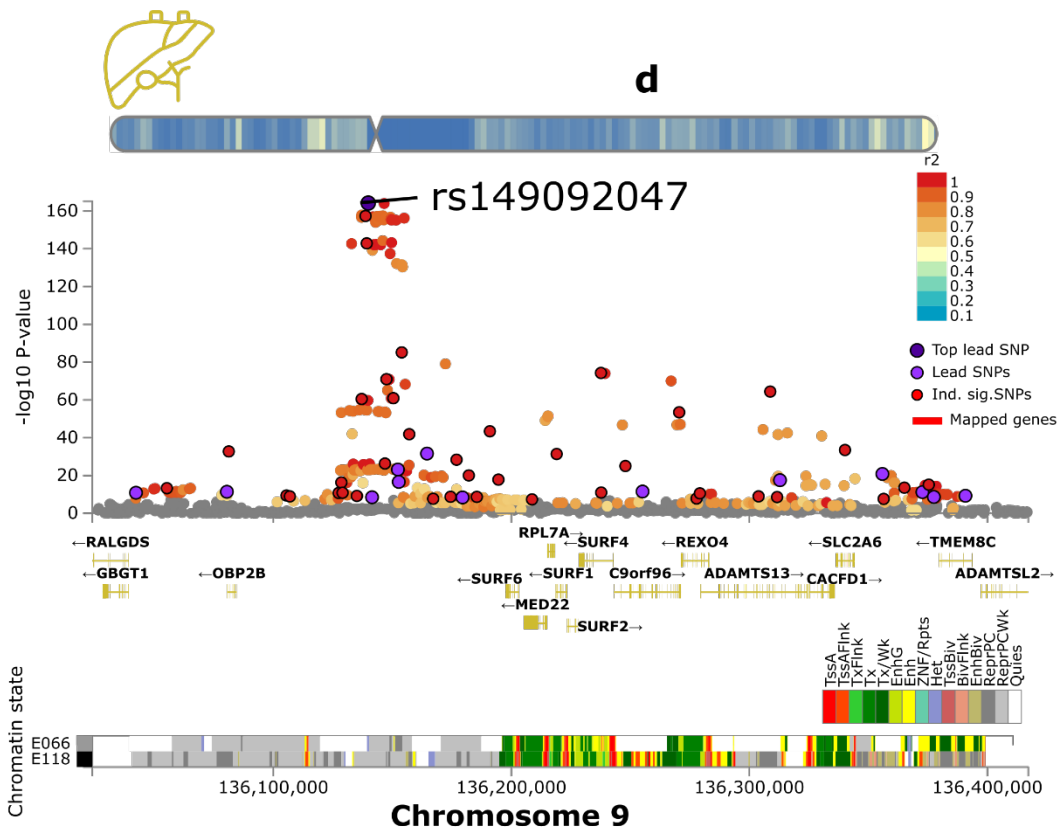
389



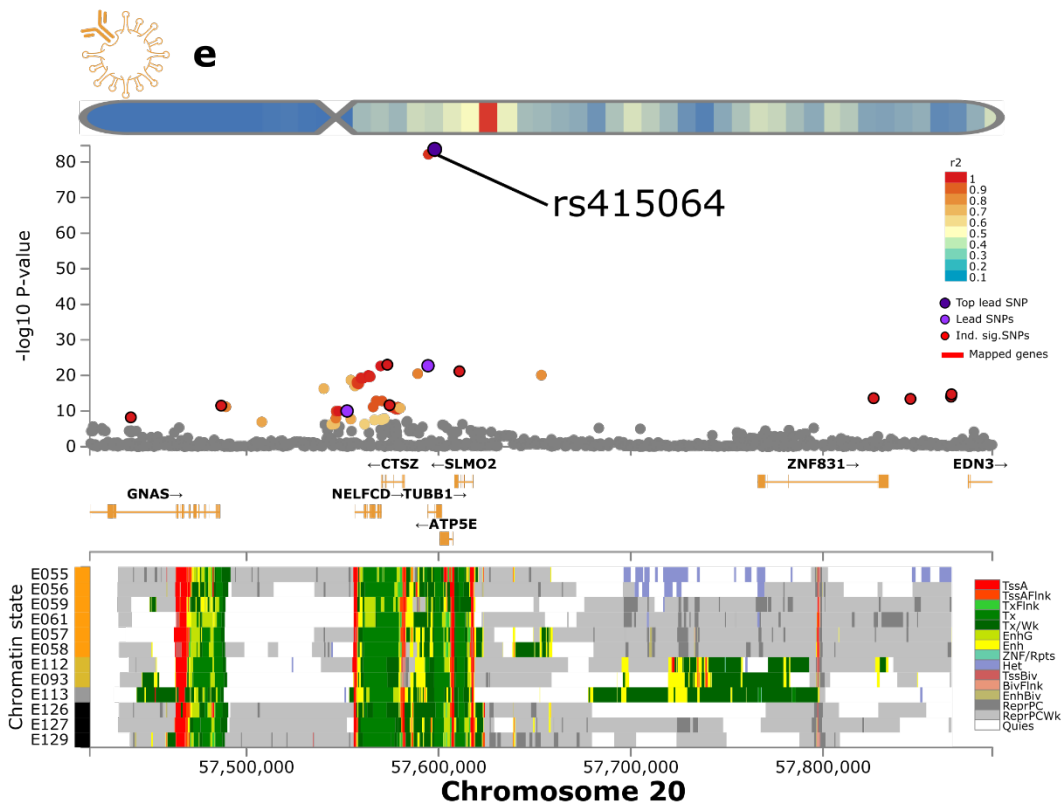
390



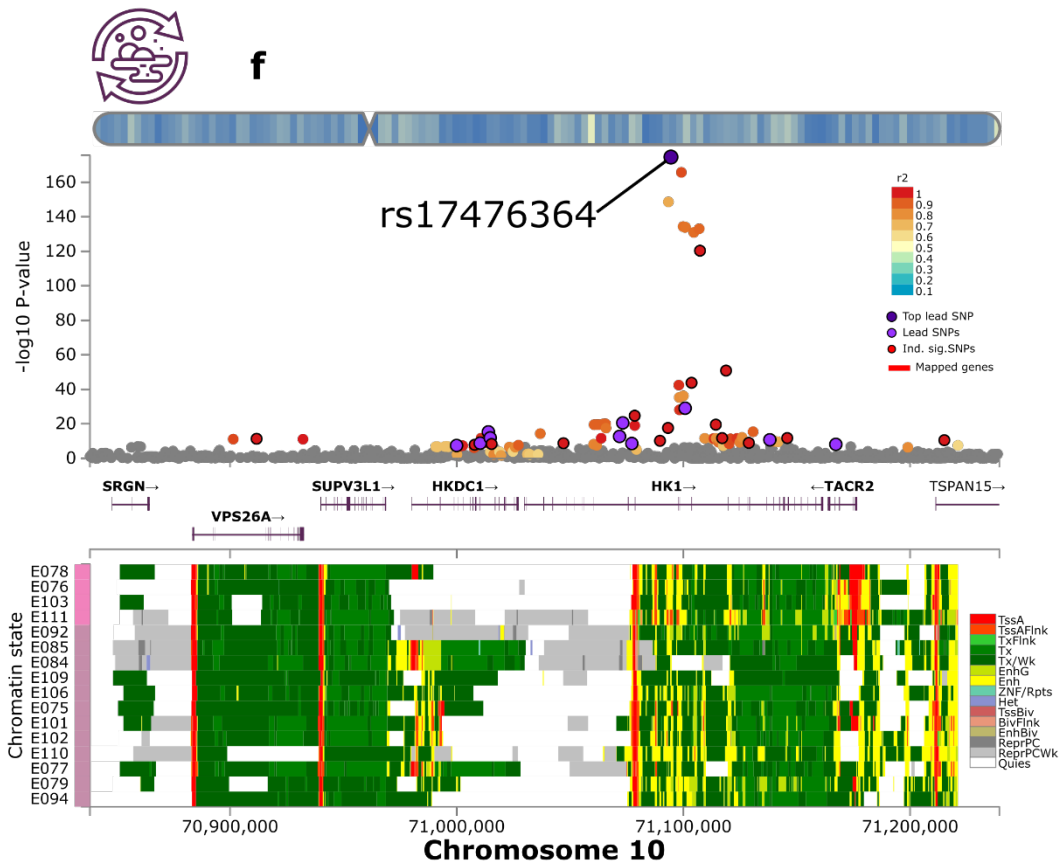
391



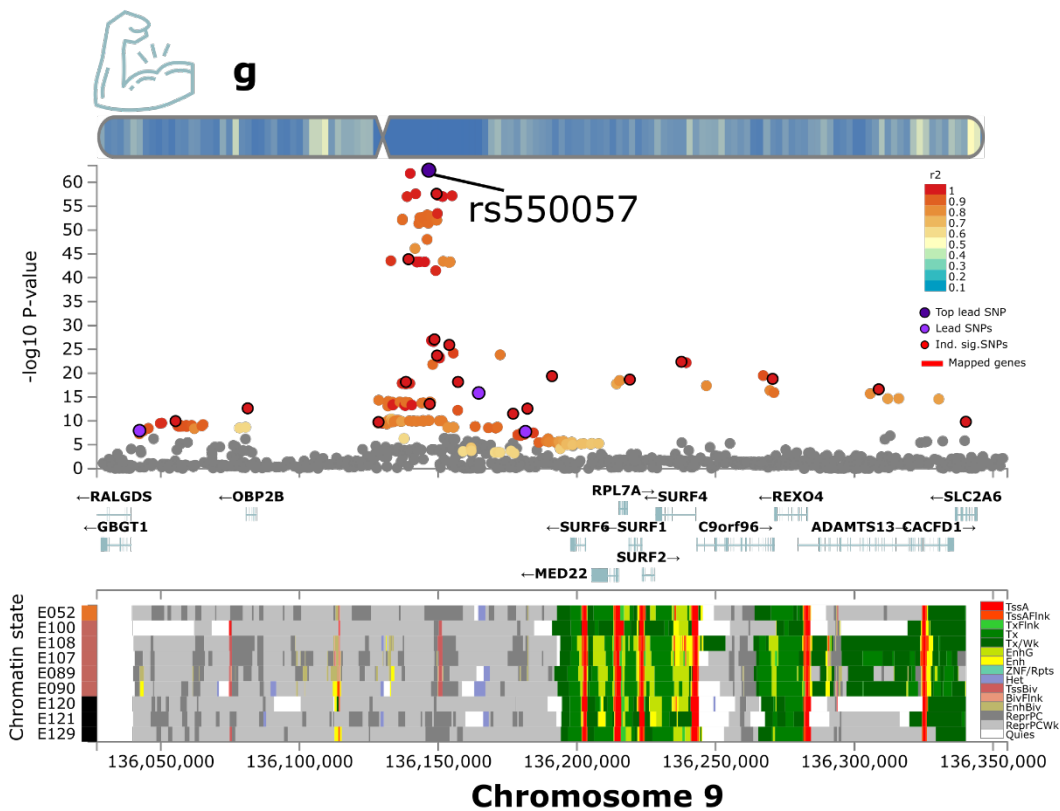
392



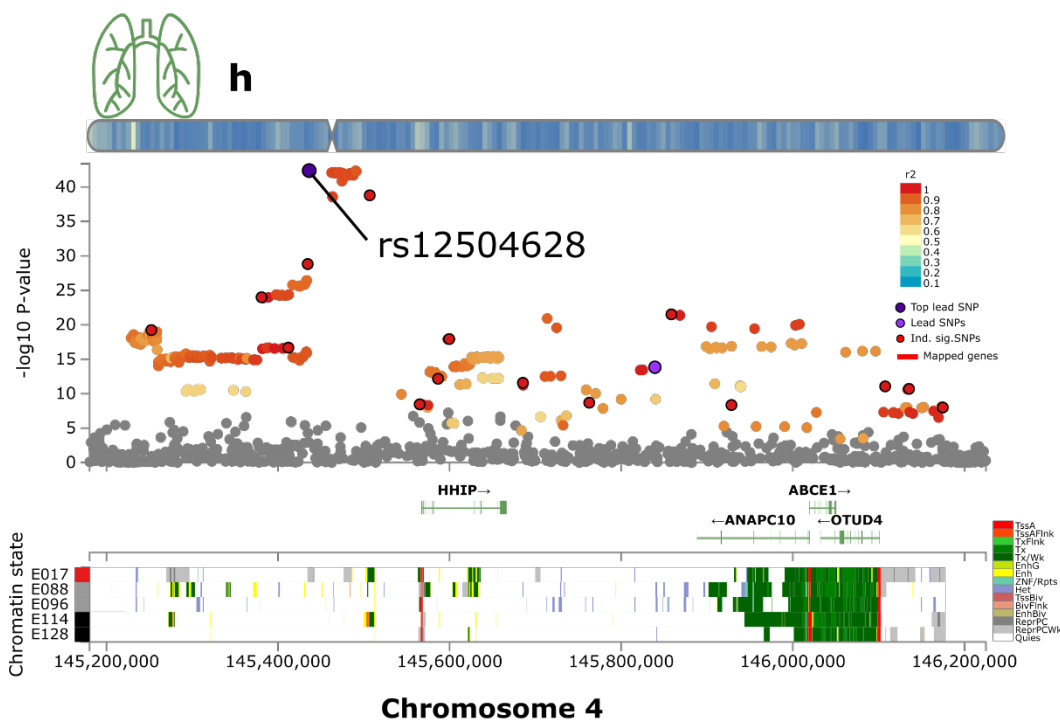
393



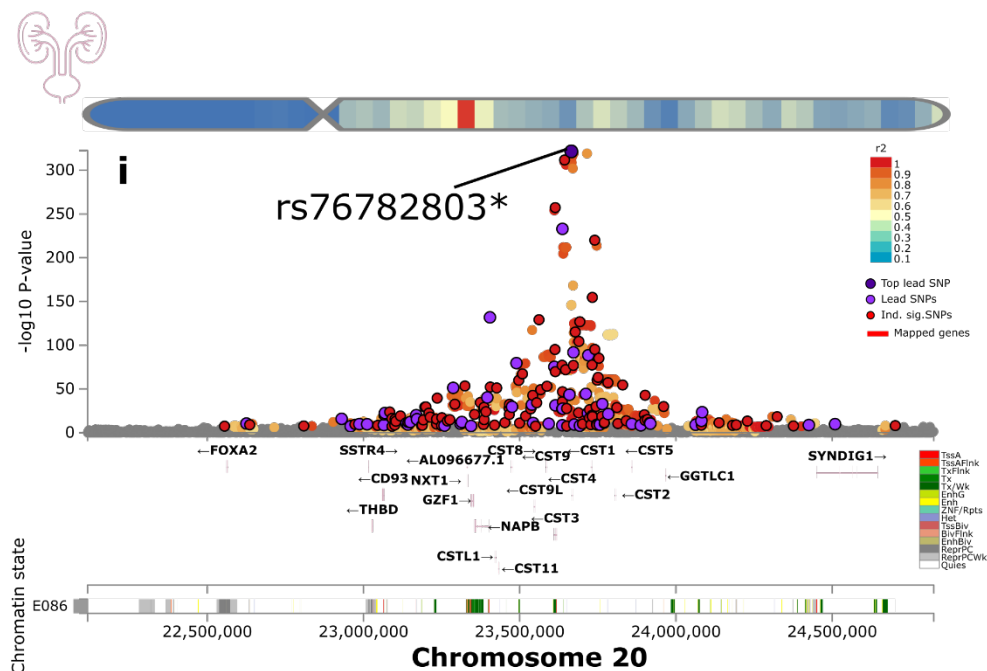
394



395

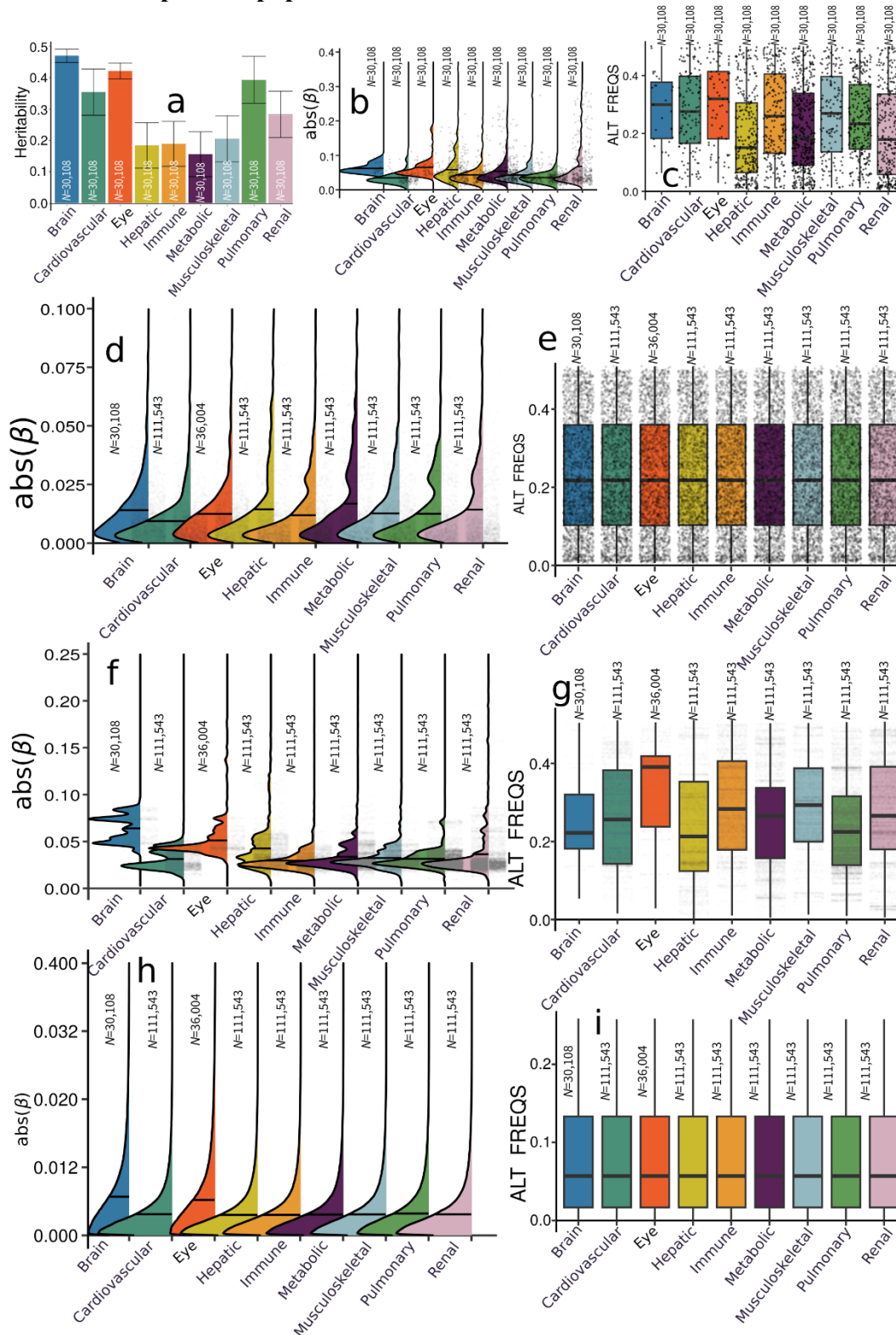


396



397
 398 **a-i)** The exemplary genomic locus with the most significant signals for the brain, cardiovascular,
 399 eye, hepatic, immune, metabolic, musculoskeletal, pulmonary, and renal BAGs. The top lead
 400 SNP, lead SNPs, and independent significant SNPs are annotated within each locus. We mapped
 401 the SNPs to the genes and predicted their chromatin states in specific tissues, including the brain
 402 for the brain BAG, the heart and vascular tissues for the cardiovascular BAG, the iPSC for the
 403 eye BAG, the liver for the hepatic BAG, the spleen, bone, skin, and thymus tissues for the
 404 immune BAG, the gastrointestinal tissue for the metabolic BAG, the muscle and bone tissues for
 405 the musculoskeletal BAG, the lung tissue for the pulmonary BAG, and the kidney for the renal
 406 BAG, respectively.
 407

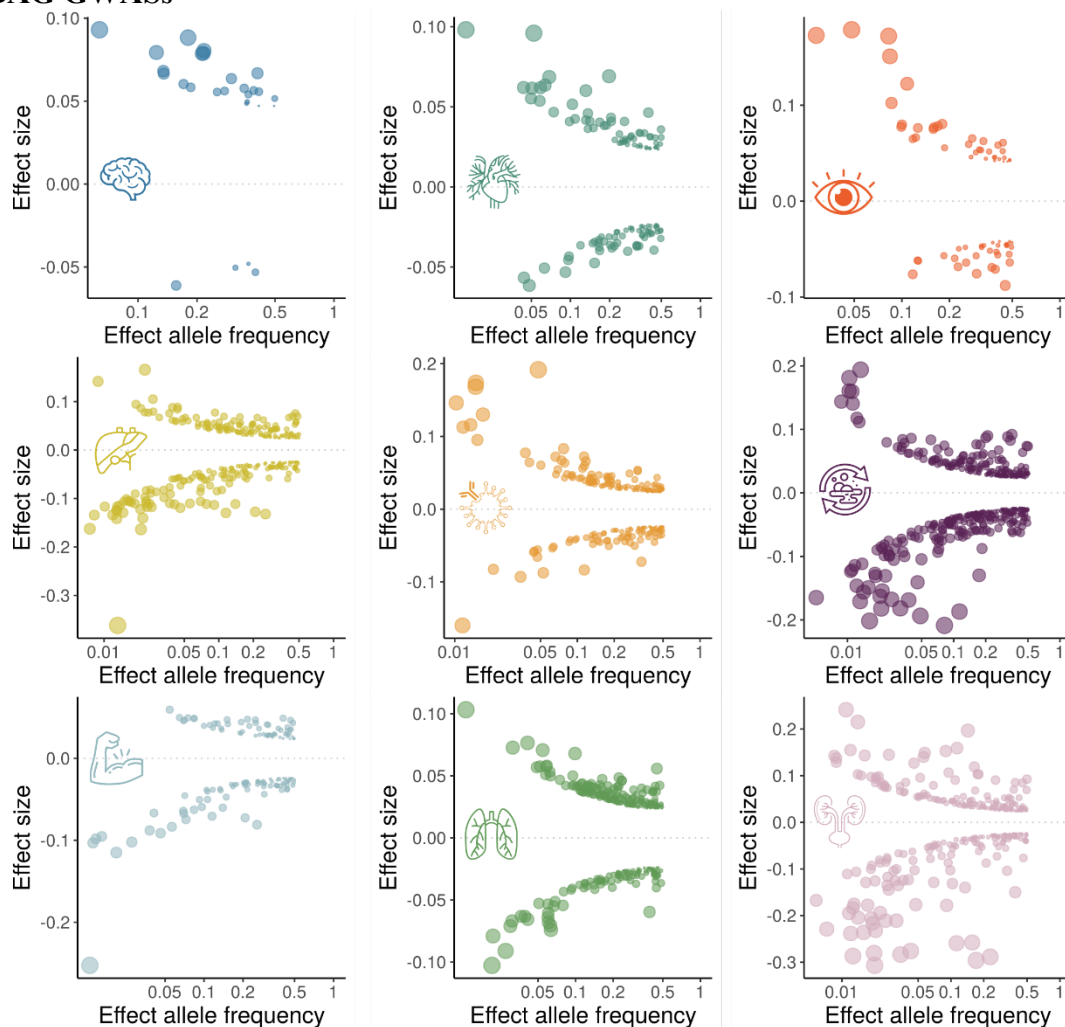
408 eFigure 12: SNP-based heritability, beta coefficients, and alternative allele frequency using
 409 the brain-BAG comparable populations and different inclusion criteria for the SNPs



410 **a)** The SNP-based heritability of the nine BAGs using populations from downsampling to the
 411 brain BAG population. **b)** The absolute value of the beta coefficients of the independent
 412

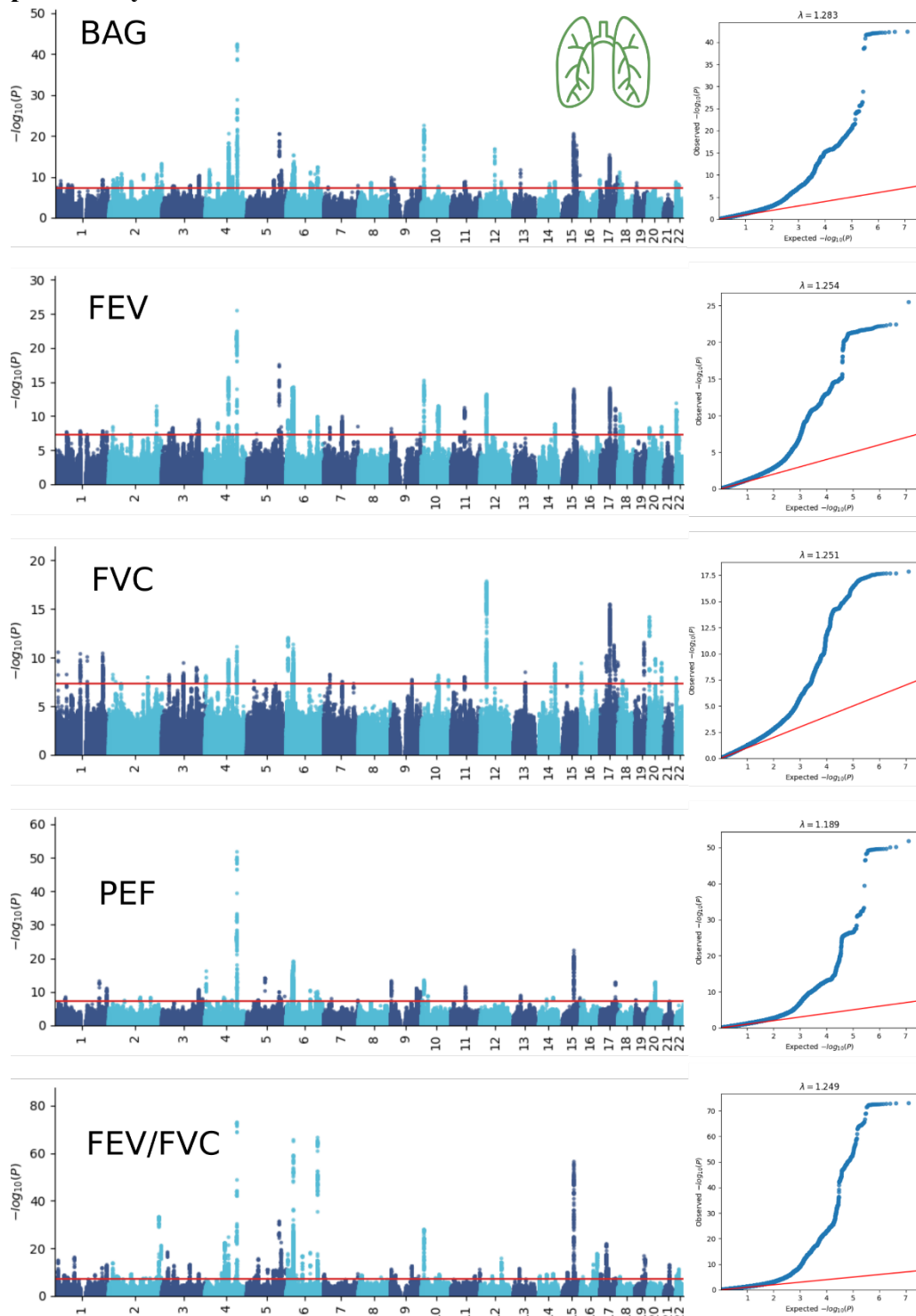
413 significant SNPs of the nine BAG GWASs using populations from downsampling to the brain
414 BAG population ($N=30,108$); the independent significant SNPs are shown separately for each
415 BAG. **c)** The alternative (effective) allele frequency of the independent significant SNPs from
416 the nine BAG GWASs using populations from downsampling to the brain BAG population
417 ($N=30,108$). **d)** The beta coefficients of the independent significant SNPs using the original full
418 samples but with all identified independent significant SNPs across the nine BAG GWASs (with
419 the same number of SNPs tested), where we see no difference regarding allele frequency in
420 Figure **e)**. **f)** The absolute value of the beta coefficients of the independent significant SNPs plus
421 the candidate SNPs in LD of the nine BAG GWASs using the original full samples; the SNPs are
422 shown separately for each BAG. **g)** The alternative allele frequency for the setting in Figure **f)**.
423 **h)** The absolute beta coefficients of the nine BAGs using all genome-wide SNPs (the y-axis was
424 truncated to 0.1 for visualization purposes). **i)** the alternative allele frequency did not differ for
425 Figure **h)** including all genome-wide SNPs.
426

427 **eFigure 13: Trumpet plots of the alternative allele frequency vs. the beta coefficient of the**
 428 **nine BAG GWASs**



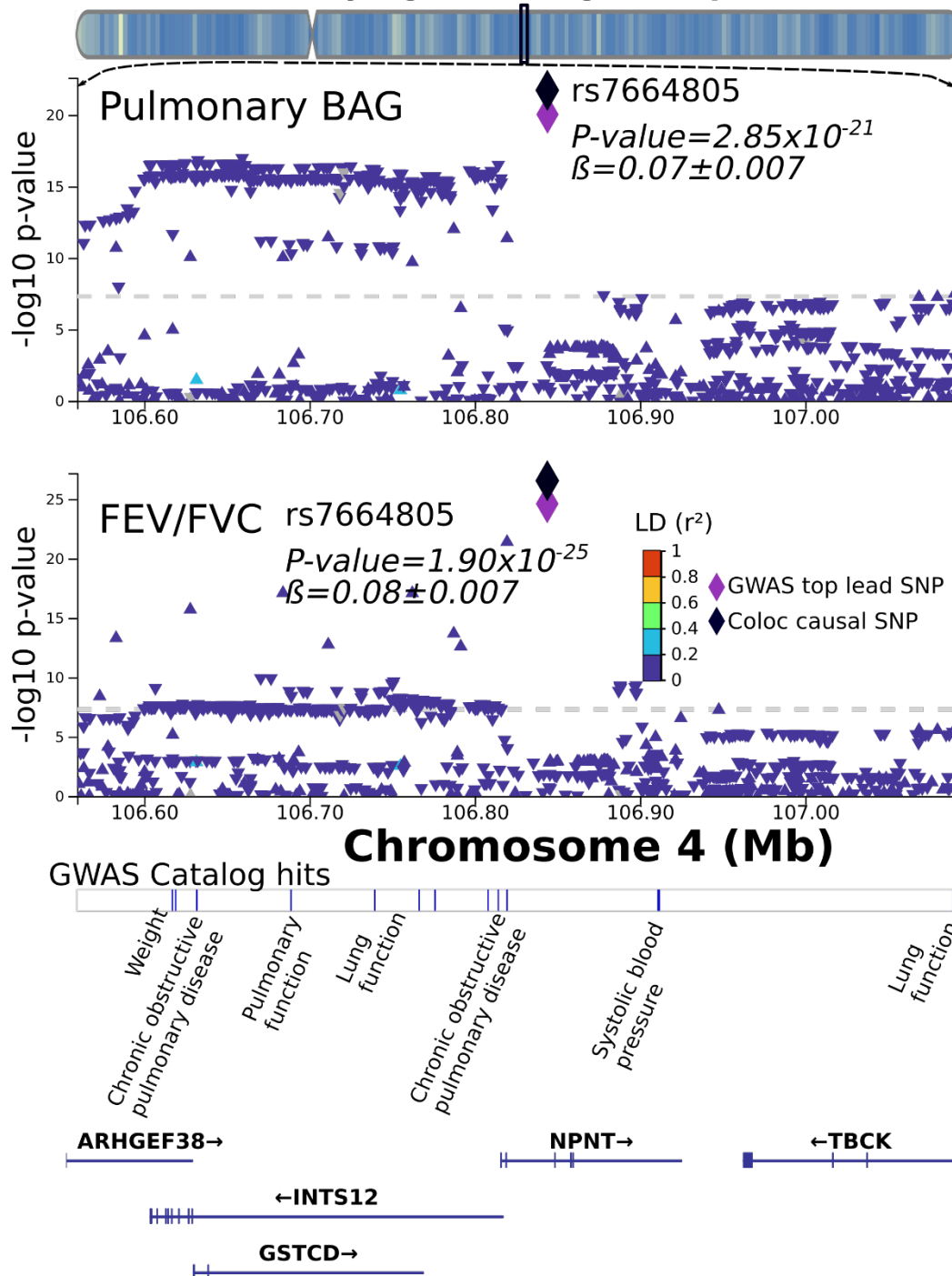
429 The trumpet plots display the inverse relationship between the alternative (effect) allele
 430 frequency and the effect size (beta coefficient) for the brain, cardiovascular, eye, hepatic,
 431 immune, metabolic, musculoskeletal, pulmonary, and renal BAGs. Only the independent
 432 significant SNPs were considered. The dot size corresponds to the effect size, while the
 433 transparency of the dot is proportional to its statistical significance.
 434
 435

436 **eFigure 14: Manhattan and QQ plots for the four pulmonary features used to compute the**
 437 **pulmonary BAG**



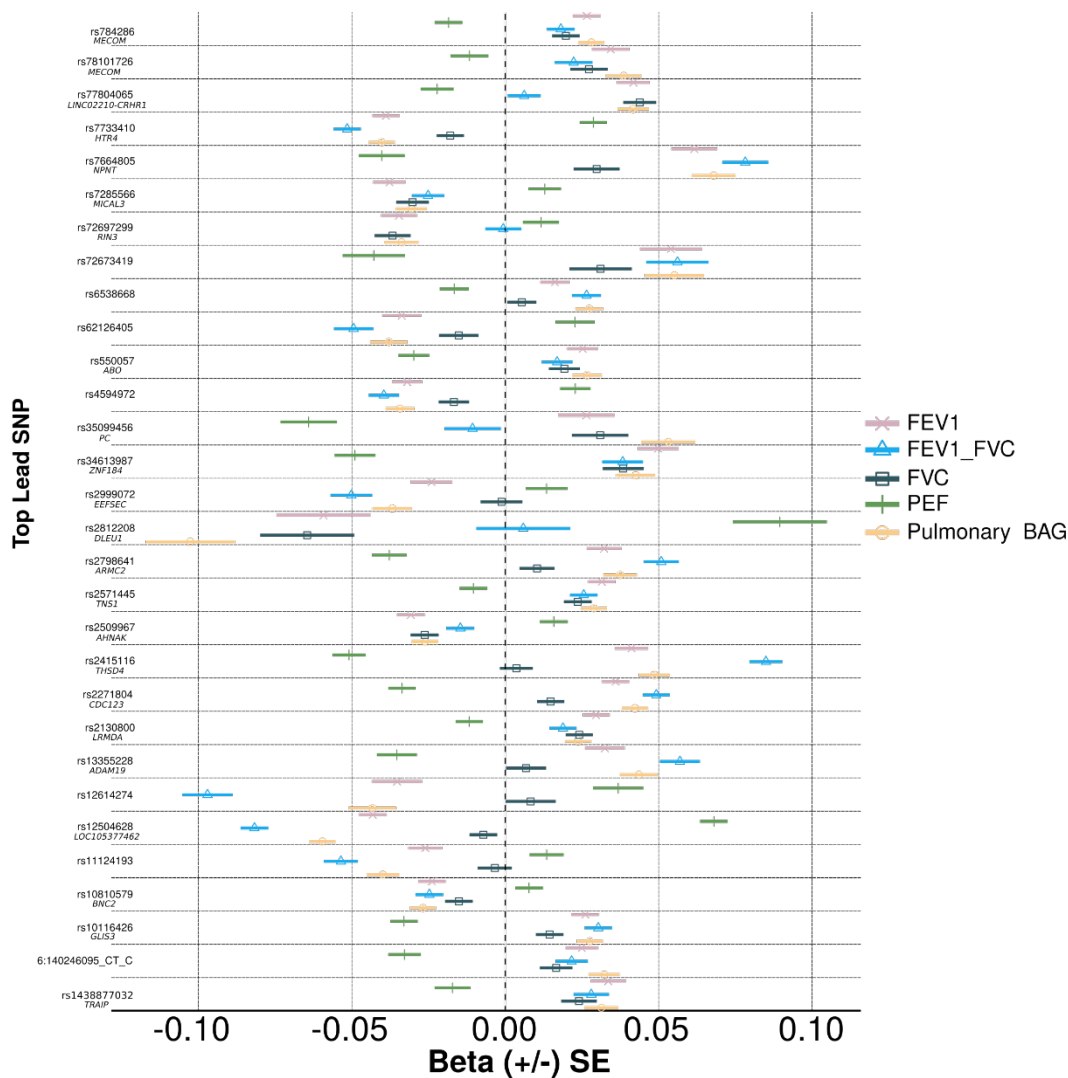
438 The Manhattan and QQ plots for the pulmonary BAG vs. its four features used to compute the
 439 BAG: forced vital capacity (FVC), forced expiratory volume (FEV), peak expiratory flow (PEF),
 440 and the ratio of forced expiratory volume to forced vital capacity (FEV/FVC).
 441
 442

443 **eFigure 15: Bayesian colocalization signal between the pulmonary BAG and FEV/FVC**
chr4; Cytogenetic region: 4q24



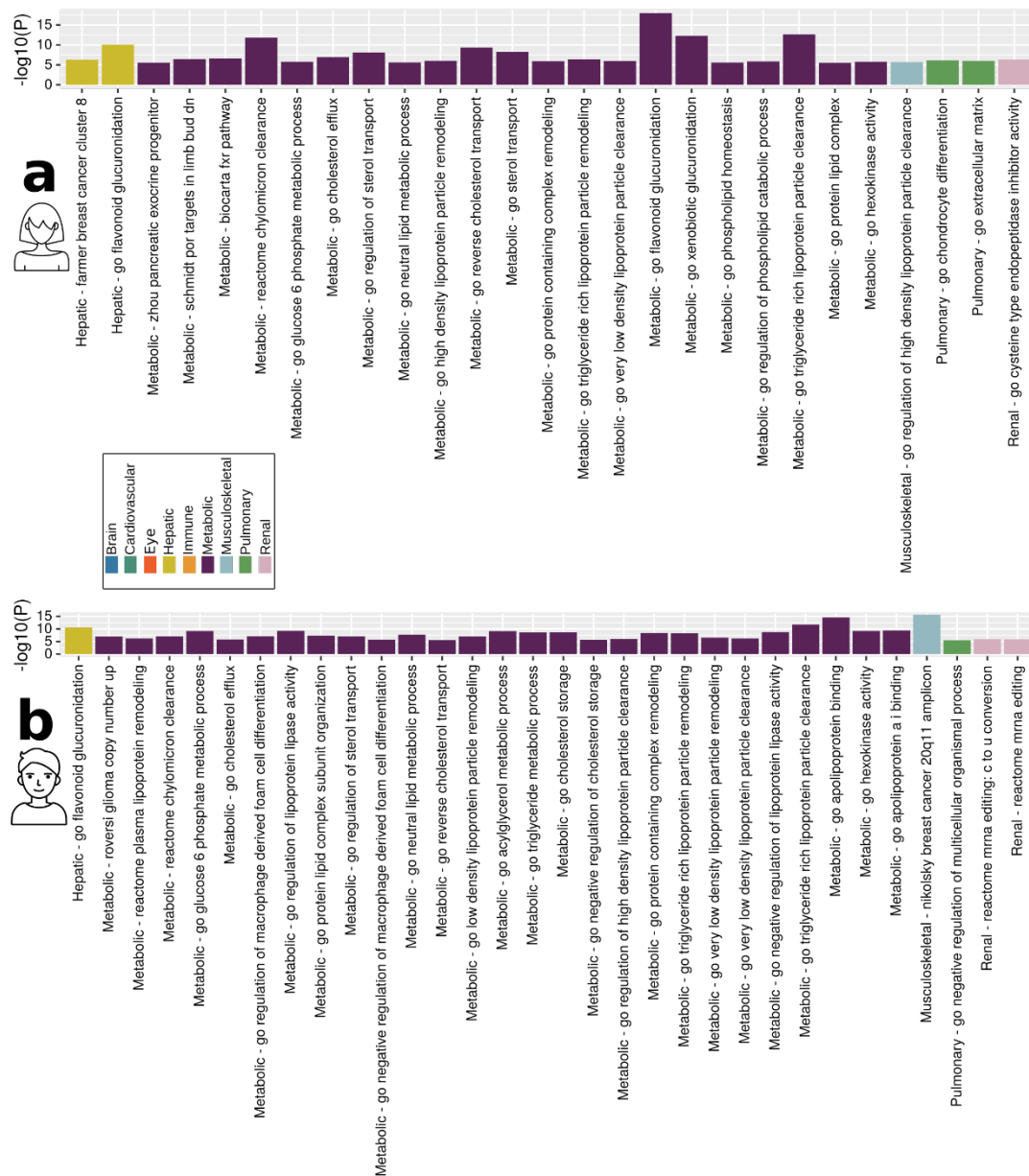
444 We illustrate here the colocalization signal between the pulmonary BAG and the FEV/FCV
 445 feature at the genomic locus: 4q24 with the top lead SNP (causal SNP: rs7664805). Genetic
 446 colocalization was evidenced at one locus (4q24) between the pulmonary BAG and the
 447 FEV/FCV feature. The signed PP.H4.ABF (0.99) denotes the posterior probability (PP) of
 448 hypothesis H4, which suggests that both traits share the same causal SNP (rs7664805).
 449
 450

451 **eFigure 16: Beta coefficients of the significant colocalization signal between the pulmonary**
 452 **BAG and the four pulmonary features**

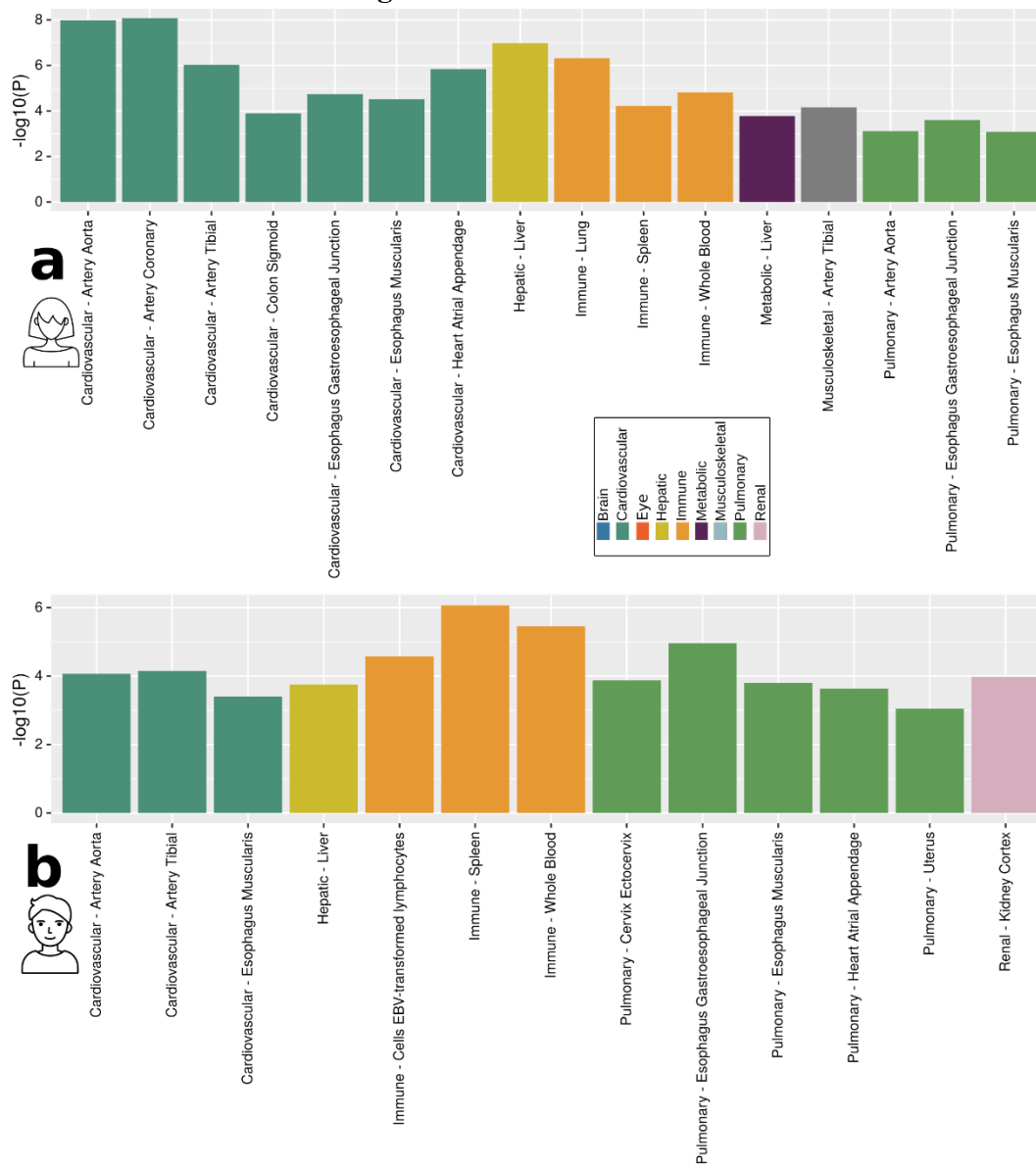


453 We show the beta coefficients of the significant colocalization signals between the pulmonary
 454 BAG and its underlying four pulmonary features. We ensured that at least one of the four
 455 pulmonary features achieved the genome-wide P-value threshold, totaling 48 loci (represented by
 456 its top lead SNP). We also showed the mapped gene when available.
 457
 458

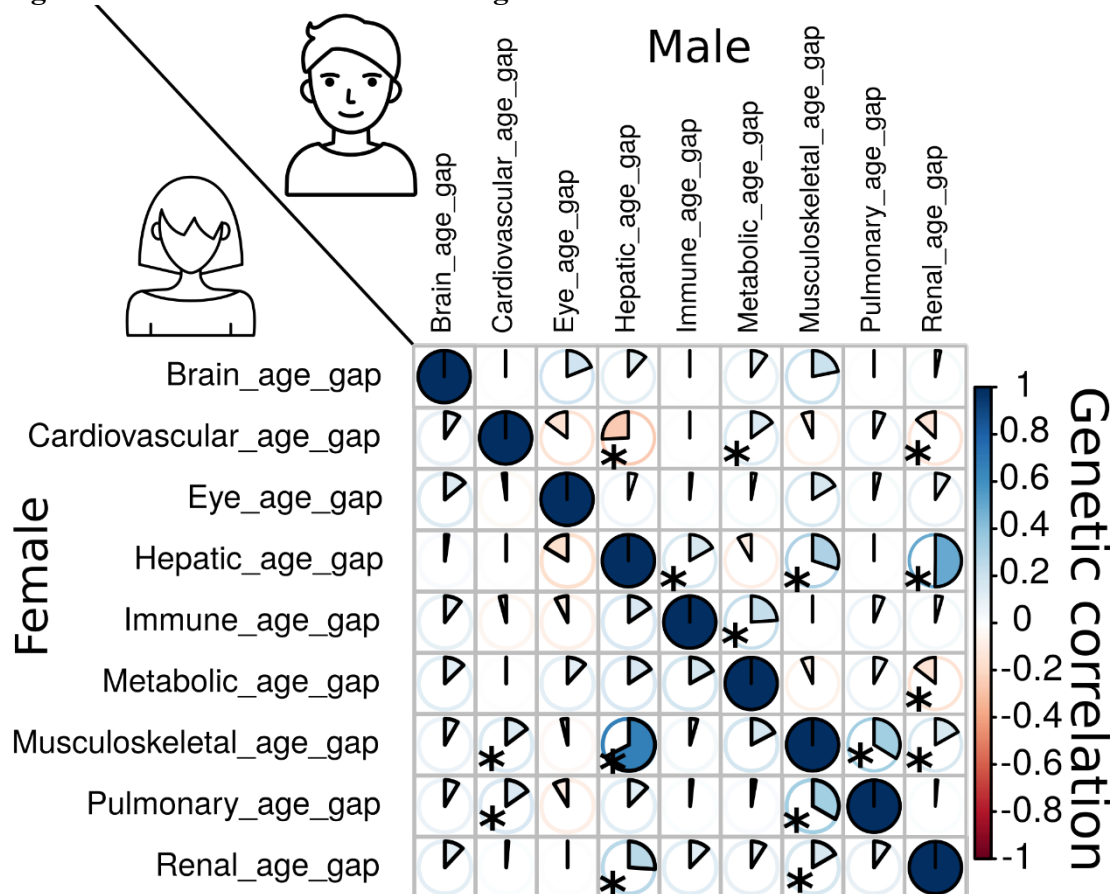
459 eFigure 17: GSEA using sex-stratified GWAS results



460
 461 Gene-set enrichment analysis was performed using the GWAS summary statistics specific to
 462 females (a) and males (b).
 463

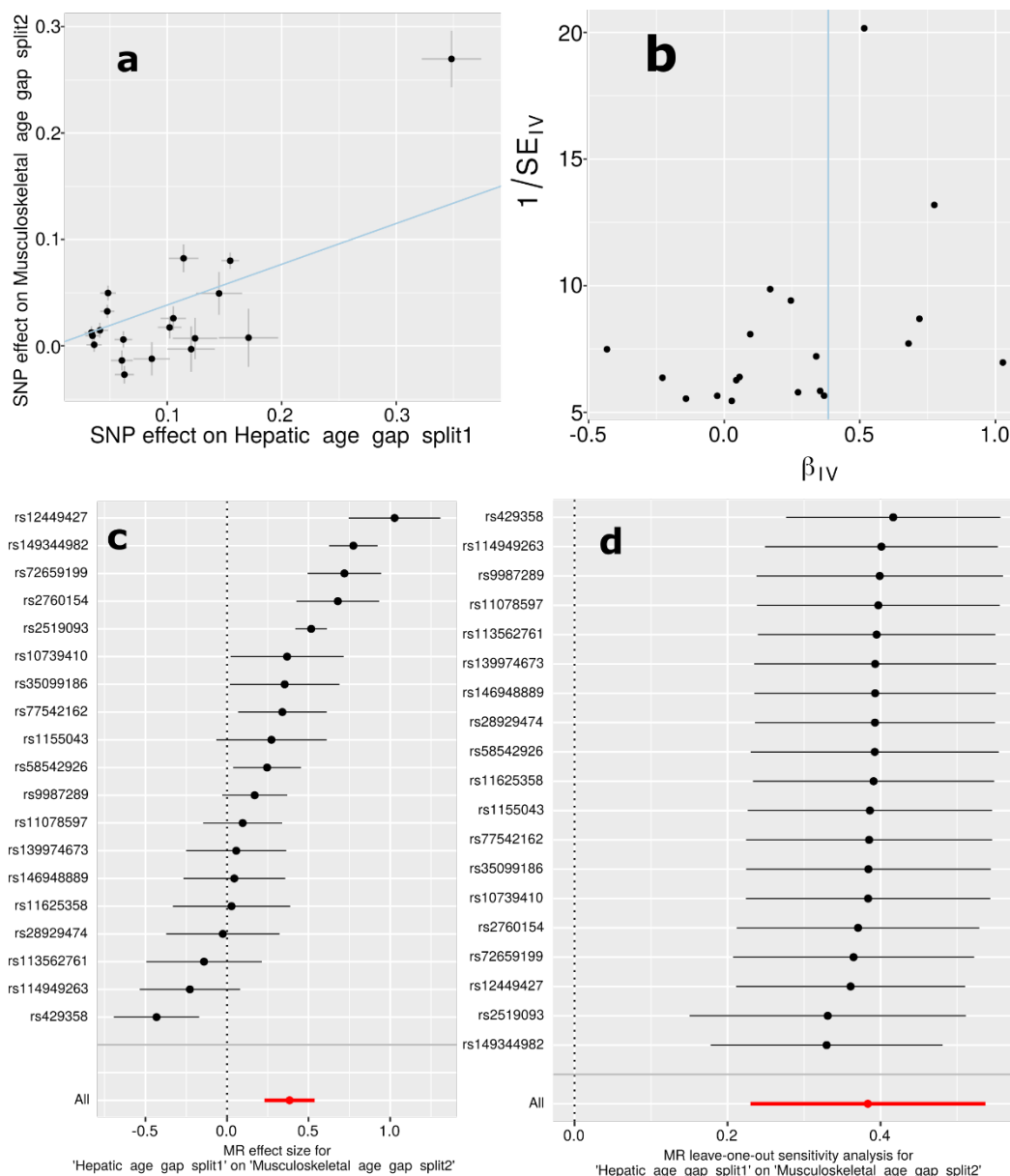
464 **eFigure 18: TEA correlations using sex-stratified GWAS results**

465
 466 Tissue-specific enrichment analysis was performed using the GWAS summary statistics specific
 467 to females (a) and males (b).
 468

469 **eFigure 19: Genetic correlations using sex-stratified GWAS results**

470 The
 471 Genetic correlation between each pair of BAGs using sex-stratified GWAS summary statistics
 472 from our analyses. Most of the genetic correlations showed consistency between females and
 473 males, albeit sex differences are evident in certain BAGs, particularly in the cardiovascular BAG
 474 results. Specifically, males exhibit dominant correlations between cardiovascular BAGs and
 475 hepatic and renal BAGs, while females demonstrate specific correlations with musculoskeletal
 476 and pulmonary BAGs.
 477

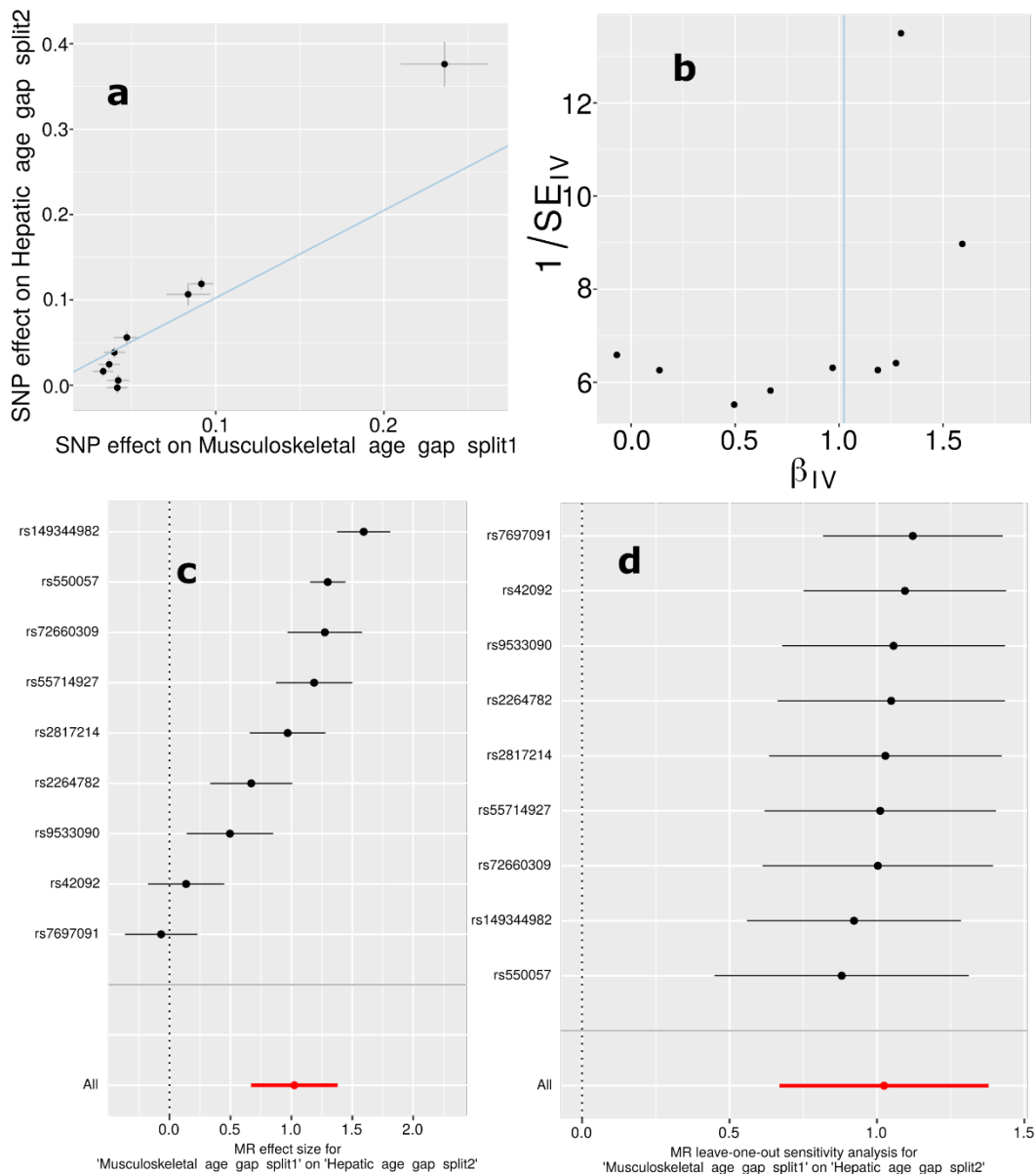
478 **eFigure 20: Mendelian randomization sensitivity check for the hepatic BAG on the**
 479 **musculoskeletal BAG**



480
 481 **a)** Scatter plot for the MR effect sizes of the exposure variable (hepatic BAG, x-axis, SD units)
 482 and the outcome variable (musculoskeletal BAG, y-axis, log OR) with standard error bars. The
 483 slopes of the regression line correspond to the causal effect sizes estimated by the IVW
 484 estimator. **b)** Funnel plot for the relationship between the causal effect of the exposure variable
 485 on the outcome variable. Each dot represents MR effect sizes estimated using each SNP as a
 486 separate instrument against the inverse of the standard error of the causal estimate. The vertical
 487 red line shows the MR estimates using all SNPs. **c)** Forest plot for the single-SNP MR results.
 488 Each line represents the MR effect (log OR) for the exposure variable on the outcome variable
 489 using only one SNP; the red line shows the MR effect using all SNPs together. **d)** Leave-one-out
 490 analysis of the exposure variable on the outcome variable. Each row represents the MR effect

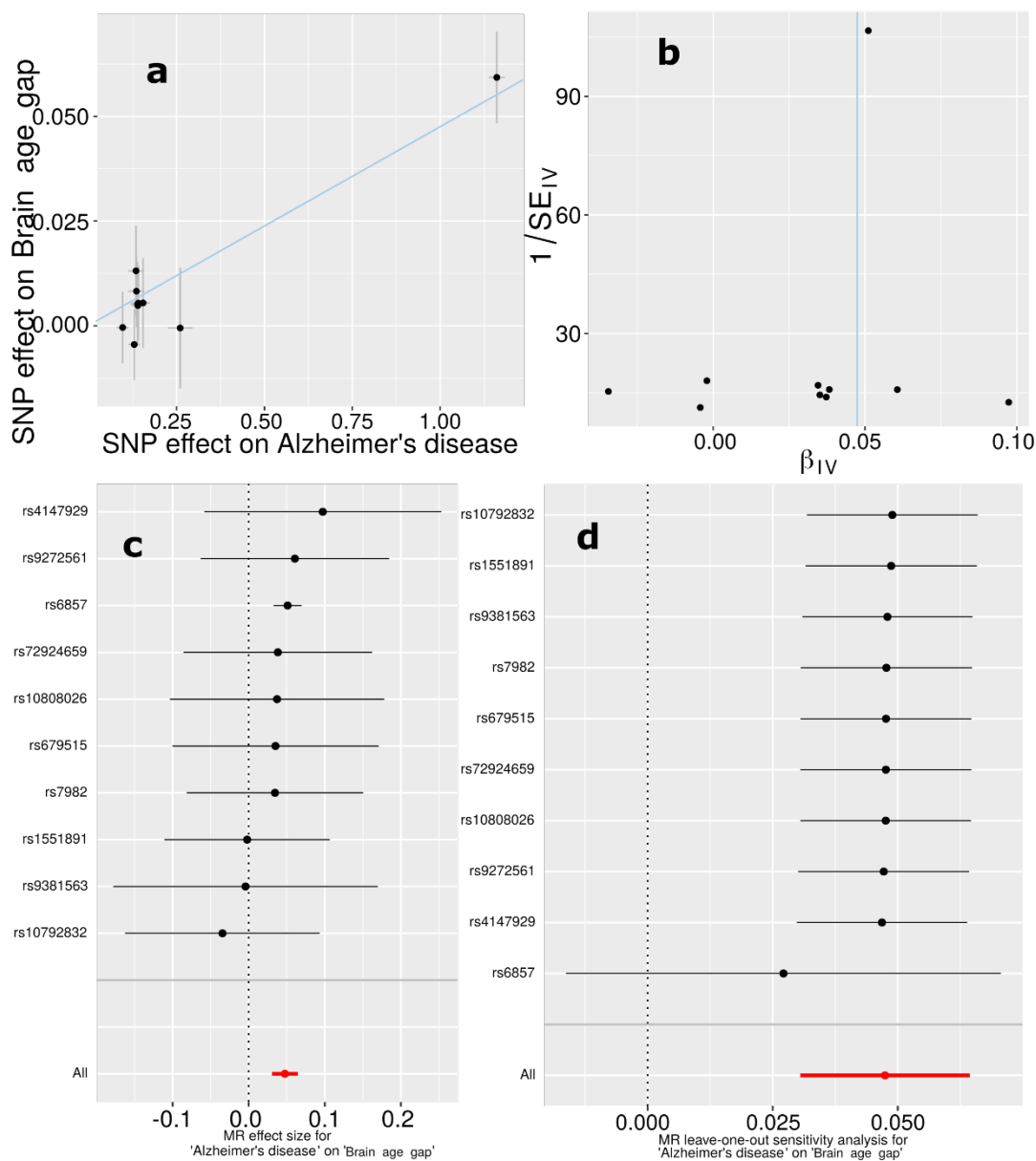
491 (log OR) and the 95% CI by excluding that SNP from the analysis. The red line depicts the IVW
492 estimator using all SNPs.
493

494 **eFigure 21: Mendelian randomization sensitivity check for the musculoskeletal BAG on the**
 495 **hepatic BAG**

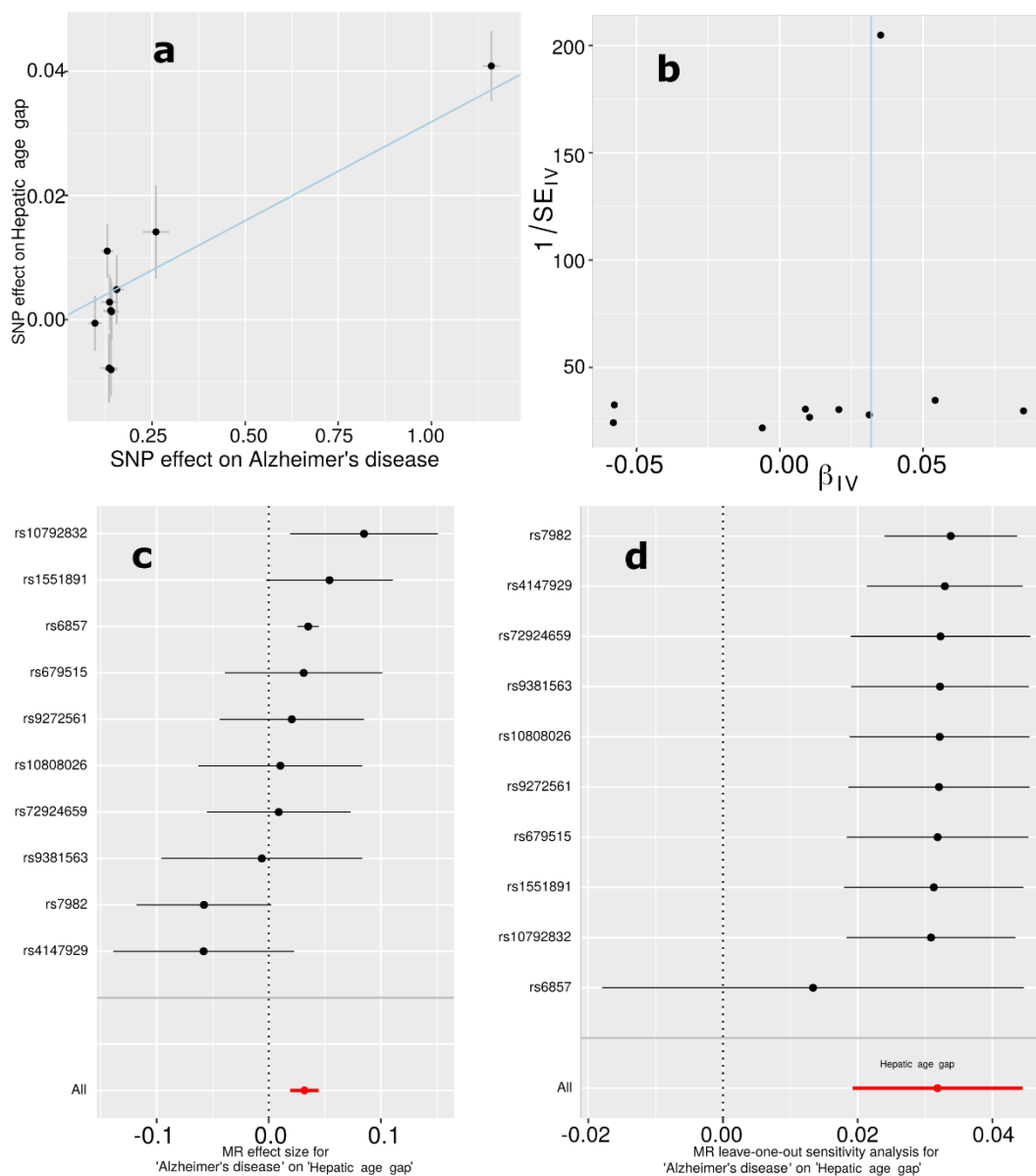


496 **a)** Scatter plot for the MR effect sizes of the exposure variable (musculoskeletal BAG, x-axis,
 497 SD units) and the outcome variable (hepatic BAG, y-axis, log OR) with standard error bars. The
 498 slopes of the regression line correspond to the causal effect sizes estimated by the IVW
 499 estimator. **b)** Funnel plot for the relationship between the causal effect of the exposure variable
 500 on the outcome variable. Each dot represents MR effect sizes estimated using each SNP as a
 501 separate instrument against the inverse of the standard error of the causal estimate. The vertical
 502 red line shows the MR estimates using all SNPs. **c)** Forest plot for the single-SNP MR results.
 503 Each line represents the MR effect (log OR) for the exposure variable on the outcome variable
 504 using only one SNP; the red line shows the MR effect using all SNPs together. **d)** Leave-one-out
 505 analysis of the exposure variable on the outcome variable. Each row represents the MR effect
 506

507 (log OR) and the 95% CI by excluding that SNP from the analysis. The red line depicts the IVW
508 estimator using all SNPs.
509

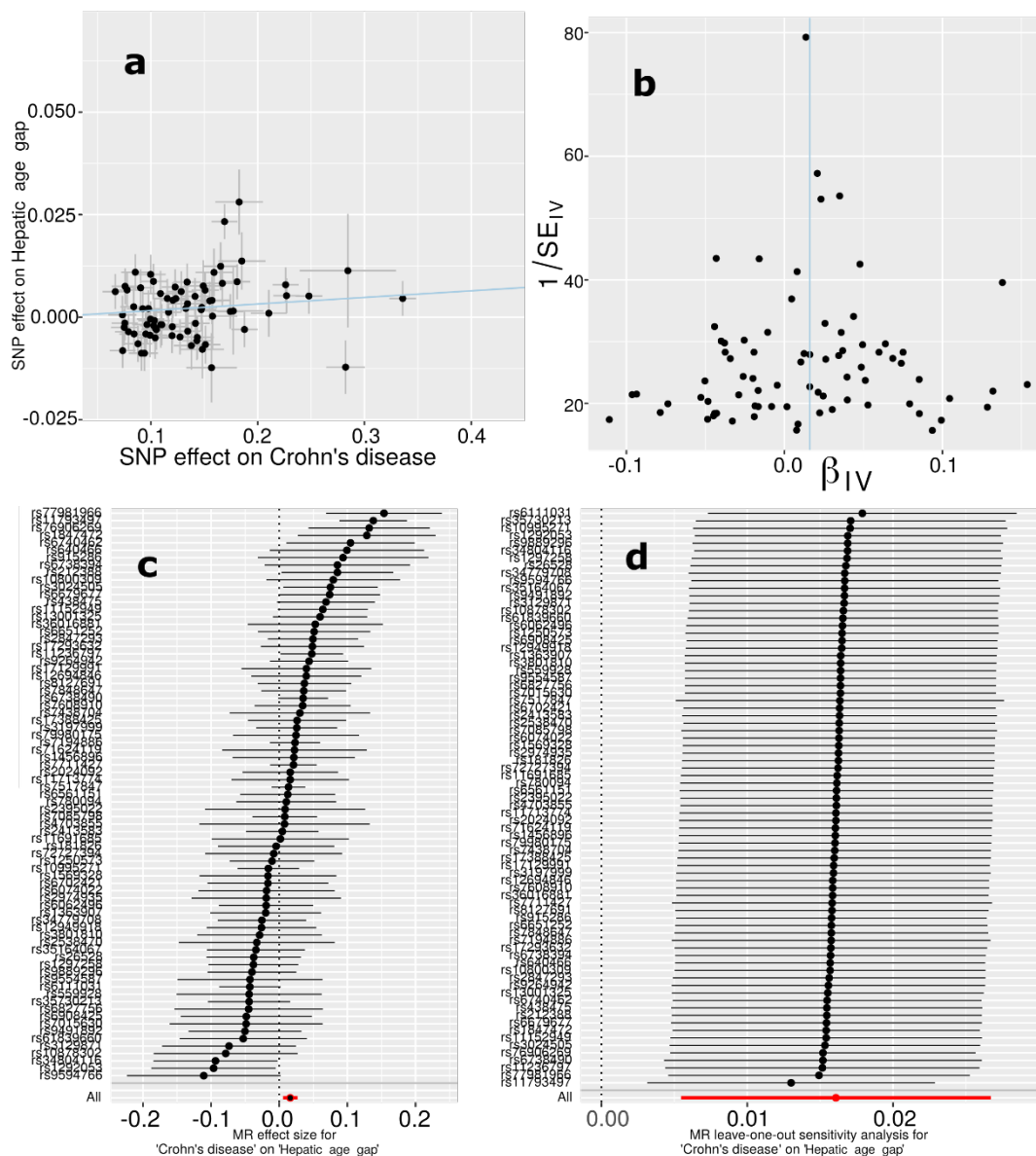
510 **eFigure 22: Mendelian randomization sensitivity check for AD on the brain BAG**

511
 512 **a)** Scatter plot for the MR effect sizes of the exposure variable (AD, x -axis, SD units) and the
 513 outcome variable (brain BAG, y -axis, log OR) with standard error bars. The slopes of the
 514 regression line correspond to the causal effect sizes estimated by the IVW estimator. **b)** Funnel
 515 plot for the relationship between the causal effect of the exposure variable on the outcome
 516 variable. Each dot represents MR effect sizes estimated using each SNP as a separate instrument
 517 against the inverse of the standard error of the causal estimate. The vertical red line shows the
 518 MR estimates using all SNPs. **c)** Forest plot for the single-SNP MR results. Each line represents
 519 the MR effect (log OR) for the exposure variable on the outcome variable using only one SNP;
 520 the red line shows the MR effect using all SNPs together. **d)** Leave-one-out analysis of the
 521 exposure variable on the outcome variable. Each row represents the MR effect (log OR) and the
 522 95% CI by excluding that SNP from the analysis. The red line depicts the IVW estimator using
 523 all SNPs.

524 **eFigure 23: Mendelian randomization sensitivity check for AD on the hepatic BAG**

525
 526 **a)** Scatter plot for the MR effect sizes of the exposure variable (AD, x -axis, SD units) and the
 527 outcome variable (hepatic BAG, y -axis, log OR) with standard error bars. The slopes of the
 528 regression line correspond to the causal effect sizes estimated by the IVW estimator. **b)** Funnel
 529 plot for the relationship between the causal effect of the exposure variable on the outcome
 530 variable. Each dot represents MR effect sizes estimated using each SNP as a separate instrument
 531 against the inverse of the standard error of the causal estimate. The vertical red line shows the
 532 MR estimates using all SNPs. **c)** Forest plot for the single-SNP MR results. Each line represents
 533 the MR effect (log OR) for the exposure variable on the outcome variable using only one SNP;
 534 the red line shows the MR effect using all SNPs together. **d)** Leave-one-out analysis of the
 535 exposure variable on the outcome variable. Each row represents the MR effect (log OR) and the
 536 95% CI by excluding that SNP from the analysis. The red line depicts the IVW estimator using
 537 all SNPs.

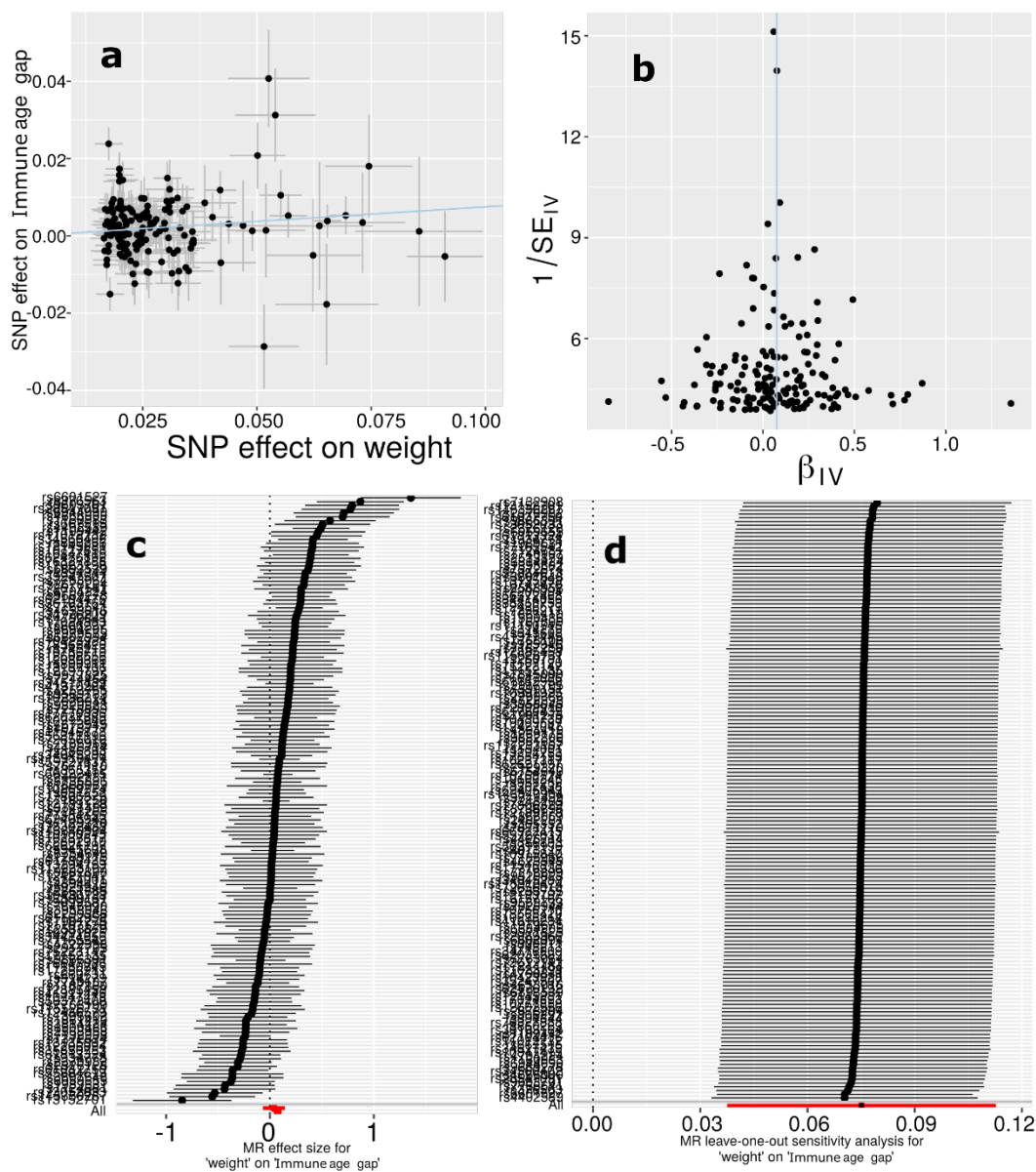
539 **eFigure 24: Mendelian randomization sensitivity check for Crohn's disease on the hepatic**
 540 **BAG**



541 **a)** Scatter plot for the MR effect sizes of the exposure variable (Crohn's disease, x-axis, SD units)
 542 and the outcome variable (hepatic BAG, y-axis, log OR) with standard error bars. The slopes of
 543 the regression line correspond to the causal effect sizes estimated by the IVW estimator. **b)**
 544 Funnel plot for the relationship between the causal effect of the exposure variable on the
 545 outcome variable. Each dot represents MR effect sizes estimated using each SNP as a separate
 546 instrument against the inverse of the standard error of the causal estimate. The vertical red line
 547 shows the MR estimates using all SNPs. **c)** Forest plot for the single-SNP MR results. Each line
 548 represents the MR effect (log OR) for the exposure variable on the outcome variable using only
 549 one SNP; the red line shows the MR effect using all SNPs together. **d)** Leave-one-out analysis of
 550 the exposure variable on the outcome variable. Each row represents the MR effect (log OR) and
 551

552 the 95% CI by excluding that SNP from the analysis. The red line depicts the IVW estimator
553 using all SNPs.
554

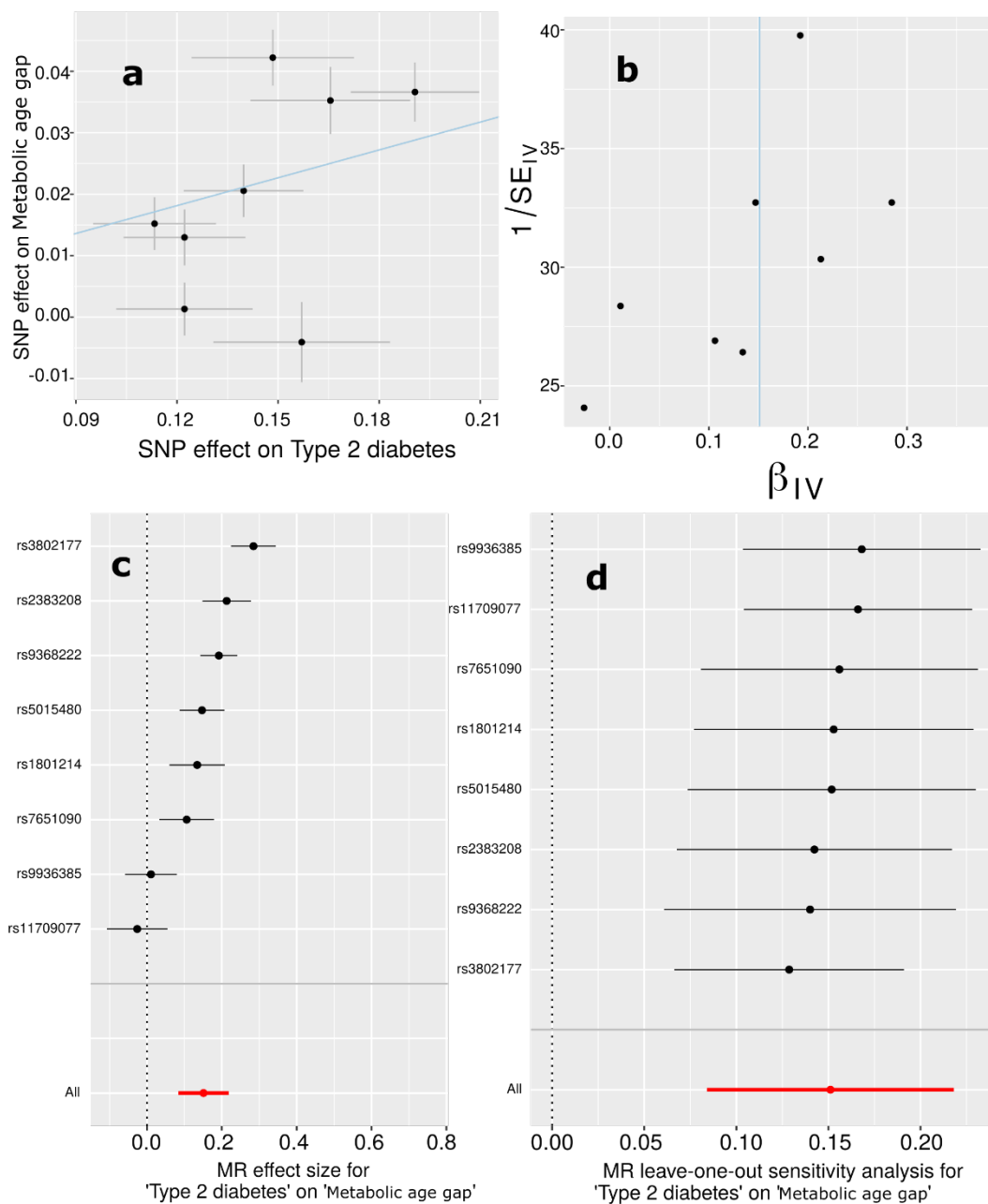
555 **eFigure 25: Mendelian randomization sensitivity check for body weight on the immune**
 556 **BAG**



557
 558 **a)** Scatter plot for the MR effect sizes of the exposure variable (body weight, x -axis, SD units)
 559 and the outcome variable (immune BAG, y -axis, log OR) with standard error bars. The slopes of
 560 the regression line correspond to the causal effect sizes estimated by the IVW estimator. **b)**
 561 Funnel plot for the relationship between the causal effect of the exposure variable on the
 562 outcome variable. Each dot represents MR effect sizes estimated using each SNP as a separate
 563 instrument against the inverse of the standard error of the causal estimate. The vertical red line
 564 shows the MR estimates using all SNPs. **c)** Forest plot for the single-SNP MR results. Each line
 565 represents the MR effect (log OR) for the exposure variable on the outcome variable using only
 566 one SNP; the red line shows the MR effect using all SNPs together. **d)** Leave-one-out analysis of
 567 the exposure variable on the outcome variable. Each row represents the MR effect (log OR) and

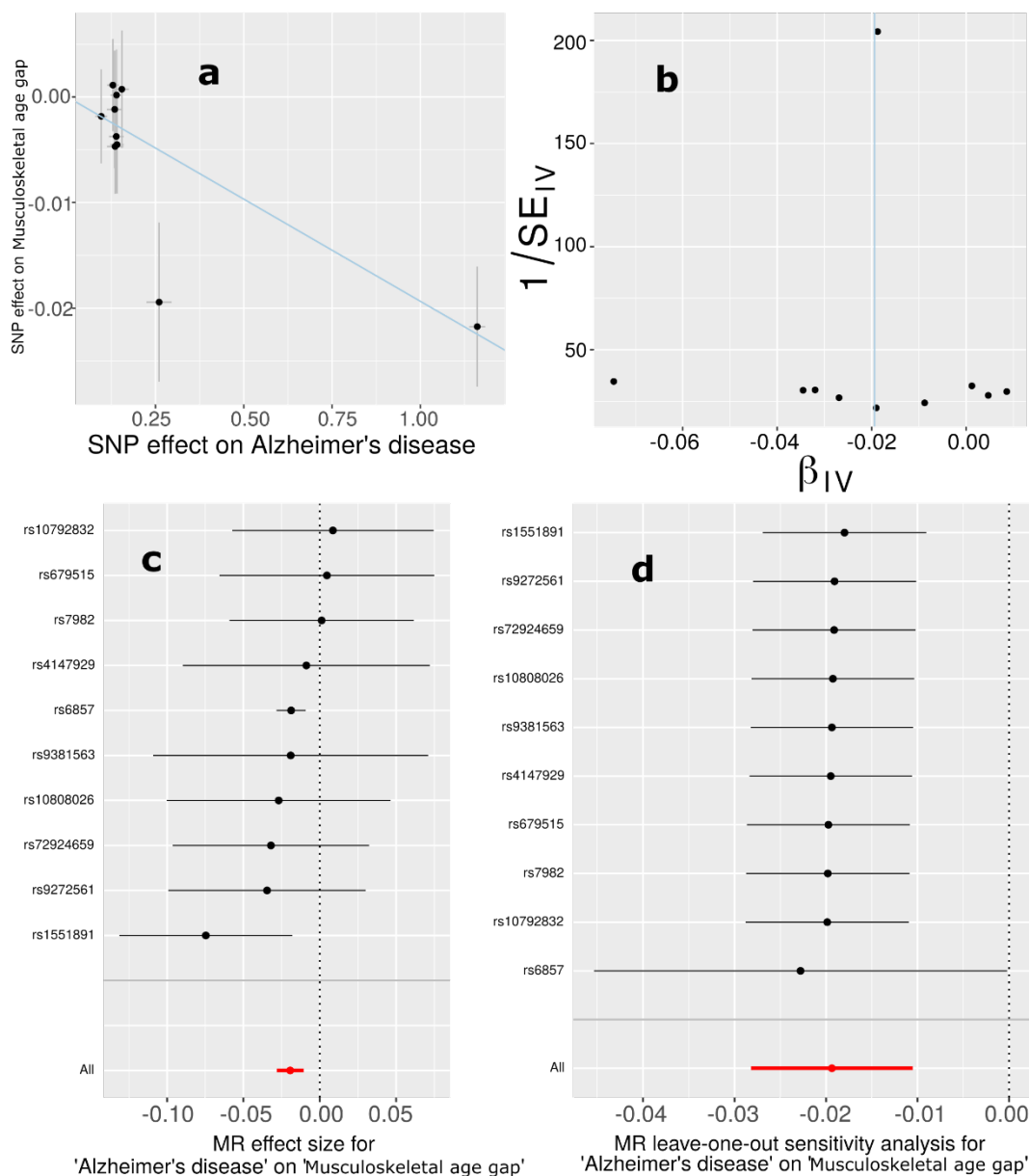
568 the 95% CI by excluding that SNP from the analysis. The red line depicts the IVW estimator
569 using all SNPs.
570

571 **eFigure 26: Mendelian randomization sensitivity check for type 2 diabetes on the metabolic**
 572 **BAG**



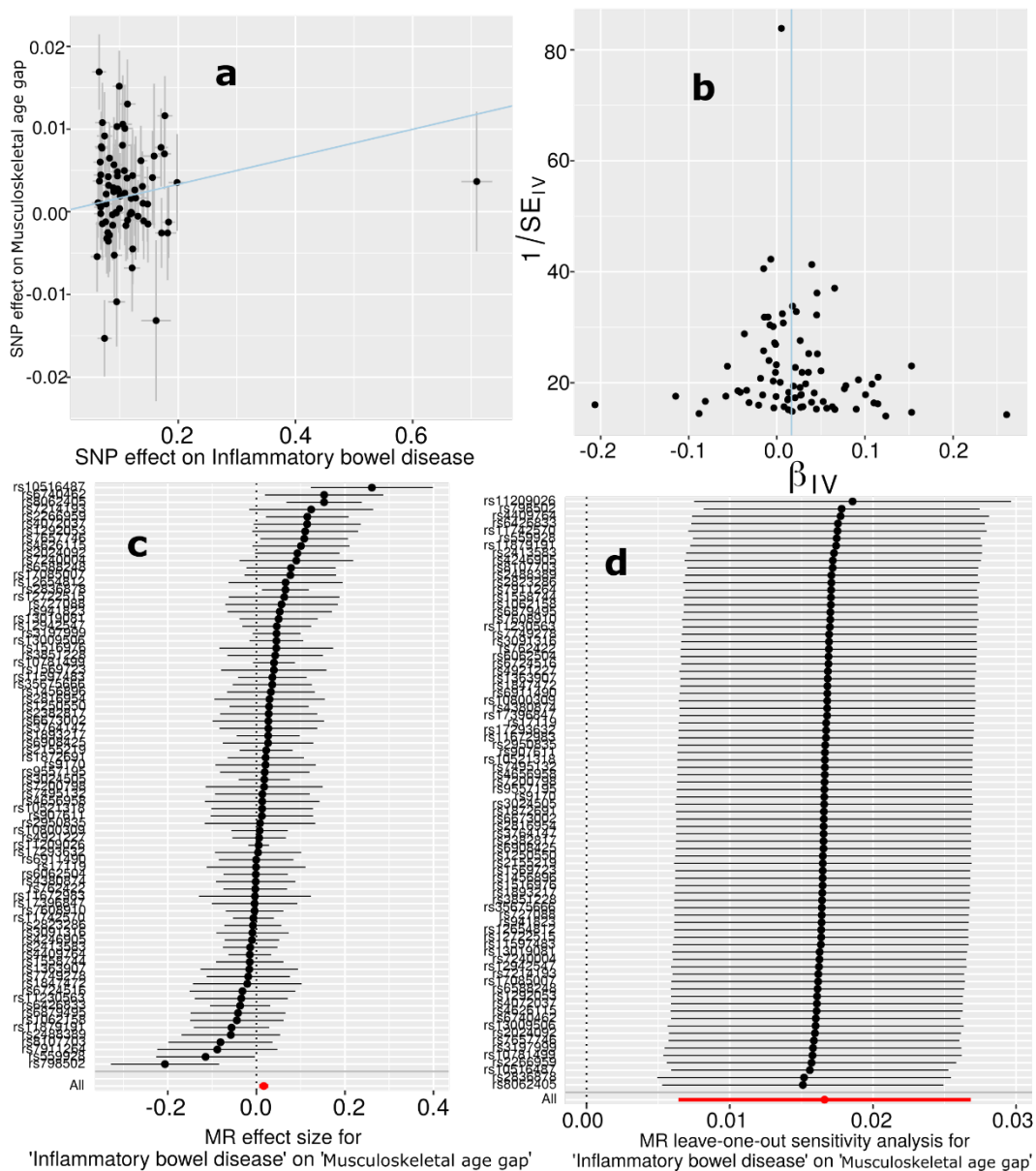
573 **a)** Scatter plot for the MR effect sizes of the exposure variable (type 2 diabetes, x -axis, SD units)
 574 and the outcome variable (metabolic BAG, y -axis, log OR) with standard error bars. The slopes
 575 of the regression line correspond to the causal effect sizes estimated by the IVW estimator. **b)**
 576 Funnel plot for the relationship between the causal effect of the exposure variable on the
 577 outcome variable. Each dot represents MR effect sizes estimated using each SNP as a separate
 578 instrument against the inverse of the standard error of the causal estimate. The vertical red line
 579 shows the MR estimates using all SNPs. **c)** Forest plot for the single-SNP MR results. Each line
 580 represents the MR effect (log OR) for the exposure variable on the outcome variable using only
 581

582 one SNP; the red line shows the MR effect using all SNPs together. **d)** Leave-one-out analysis of
583 the exposure variable on the outcome variable. Each row represents the MR effect (log OR) and
584 the 95% CI by excluding that SNP from the analysis. The red line depicts the IVW estimator
585 using all SNPs.
586

587 **eFigure 27: Mendelian randomization sensitivity check for AD on the musculoskeletal BAG**

588
 589 **a)** Scatter plot for the MR effect sizes of the exposure variable (AD, x -axis, SD units) and the
 590 outcome variable (musculoskeletal BAG, y -axis, log OR) with standard error bars. The slopes of
 591 the regression line correspond to the causal effect sizes estimated by the IVW estimator. **b)**
 592 Funnel plot for the relationship between the causal effect of the exposure variable on the
 593 outcome variable. Each dot represents MR effect sizes estimated using each SNP as a separate
 594 instrument against the inverse of the standard error of the causal estimate. The vertical red line
 595 shows the MR estimates using all SNPs. **c)** Forest plot for the single-SNP MR results. Each line
 596 represents the MR effect (log OR) for the exposure variable on the outcome variable using only
 597 one SNP; the red line shows the MR effect using all SNPs together. **d)** Leave-one-out analysis of
 598 the exposure variable on the outcome variable. Each row represents the MR effect (log OR) and
 599 the 95% CI by excluding that SNP from the analysis. The red line depicts the IVW estimator
 600 using all SNPs.

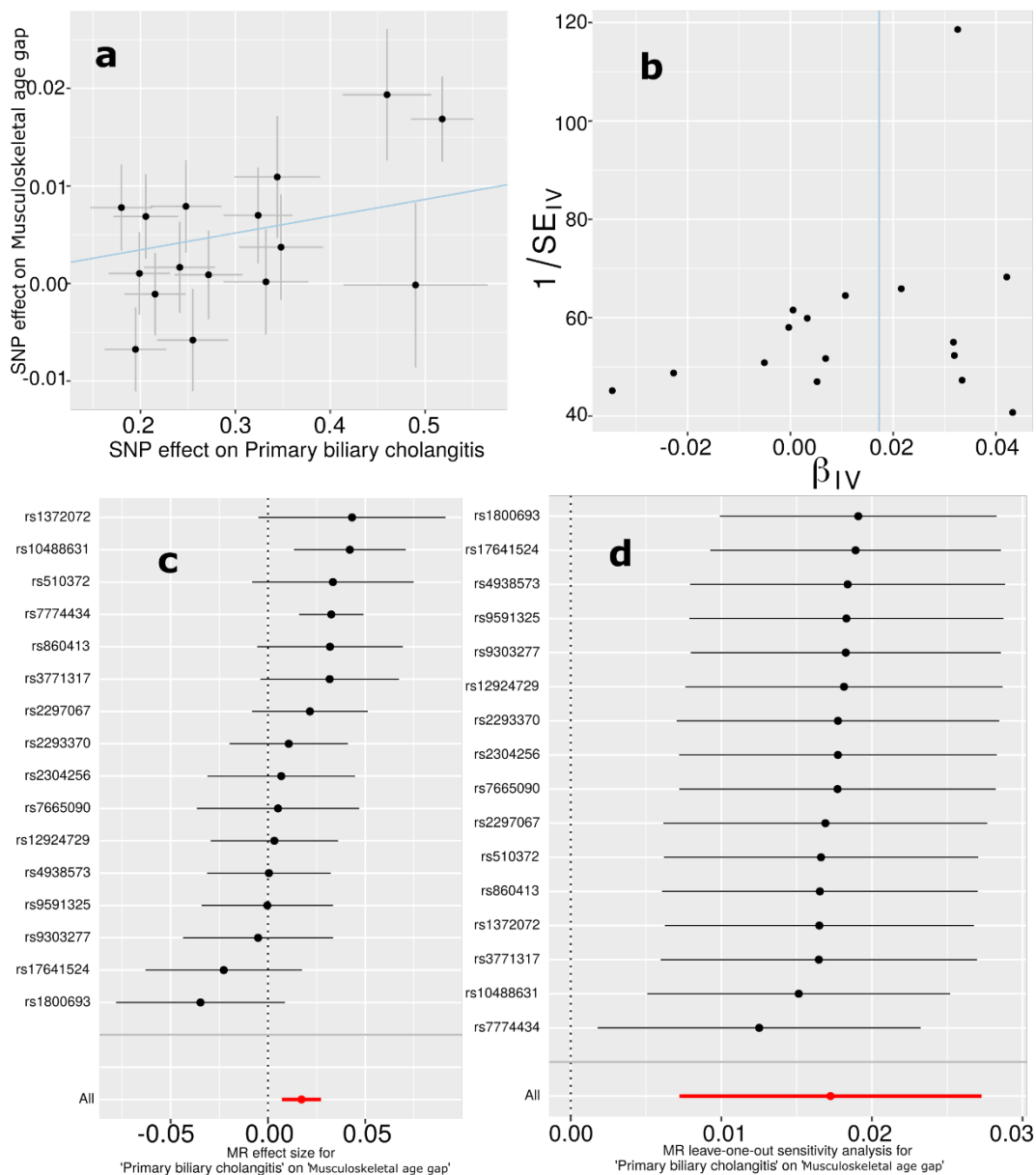
602 **eFigure 28: Mendelian randomization sensitivity check for IBD on the musculoskeletal**
 603 **BAG**



604 **a)** Scatter plot for the MR effect sizes of the exposure variable (IBD, x-axis, SD units) and the
 605 outcome variable (musculoskeletal BAG, y-axis, log OR) with standard error bars. The slopes of
 606 the regression line correspond to the causal effect sizes estimated by the IVW estimator. **b)**
 607 Funnel plot for the relationship between the causal effect of the exposure variable on the
 608 outcome variable. Each dot represents MR effect sizes estimated using each SNP as a separate
 609 instrument against the inverse of the standard error of the causal estimate. The vertical red line
 610 shows the MR estimates using all SNPs. **c)** Forest plot for the single-SNP MR results. Each line
 611 represents the MR effect (log OR) for the exposure variable on the outcome variable using only
 612 one SNP; the red line shows the MR effect using all SNPs together. **d)** Leave-one-out analysis of
 613 the exposure variable on the outcome variable. Each row represents the MR effect (log OR) and
 614

615 the 95% CI by excluding that SNP from the analysis. The red line depicts the IVW estimator
616 using all SNPs.
617

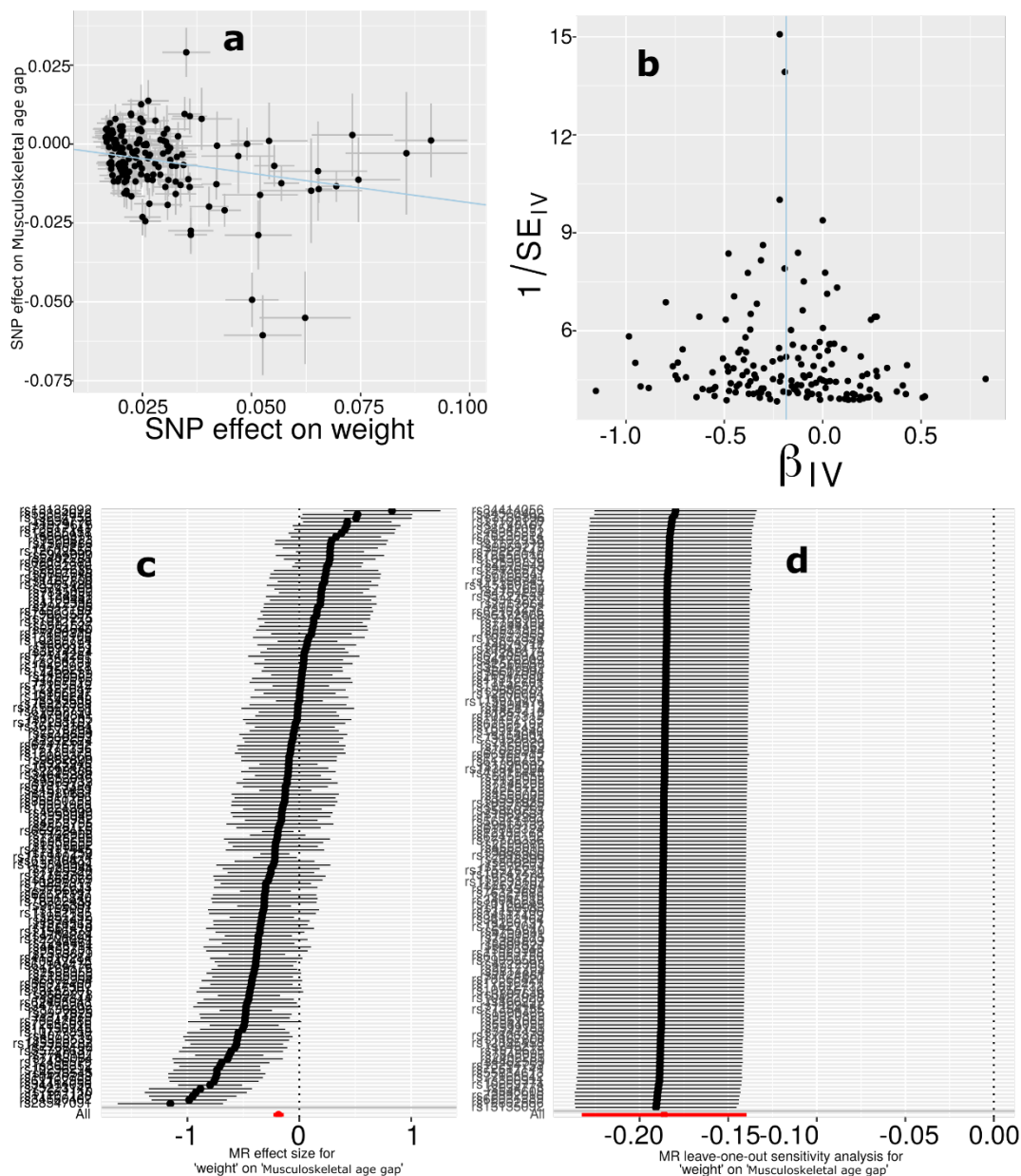
618 **eFigure 29: Mendelian randomization sensitivity check for PBC on the musculoskeletal**
 619 **BAG**



620
 621 **a)** Scatter plot for the MR effect sizes of the exposure variable (PBC, x -axis, SD units) and the
 622 outcome variable (musculoskeletal BAG, y -axis, log OR) with standard error bars. The slopes of
 623 the regression line correspond to the causal effect sizes estimated by the IVW estimator. **b)**
 624 Funnel plot for the relationship between the causal effect of the exposure variable on the
 625 outcome variable. Each dot represents MR effect sizes estimated using each SNP as a separate
 626 instrument against the inverse of the standard error of the causal estimate. The vertical red line
 627 shows the MR estimates using all SNPs. **c)** Forest plot for the single-SNP MR results. Each line
 628 represents the MR effect (log OR) for the exposure variable on the outcome variable using only
 629 one SNP; the red line shows the MR effect using all SNPs together. **d)** Leave-one-out analysis of
 630 the exposure variable on the outcome variable. Each row represents the MR effect (log OR) and

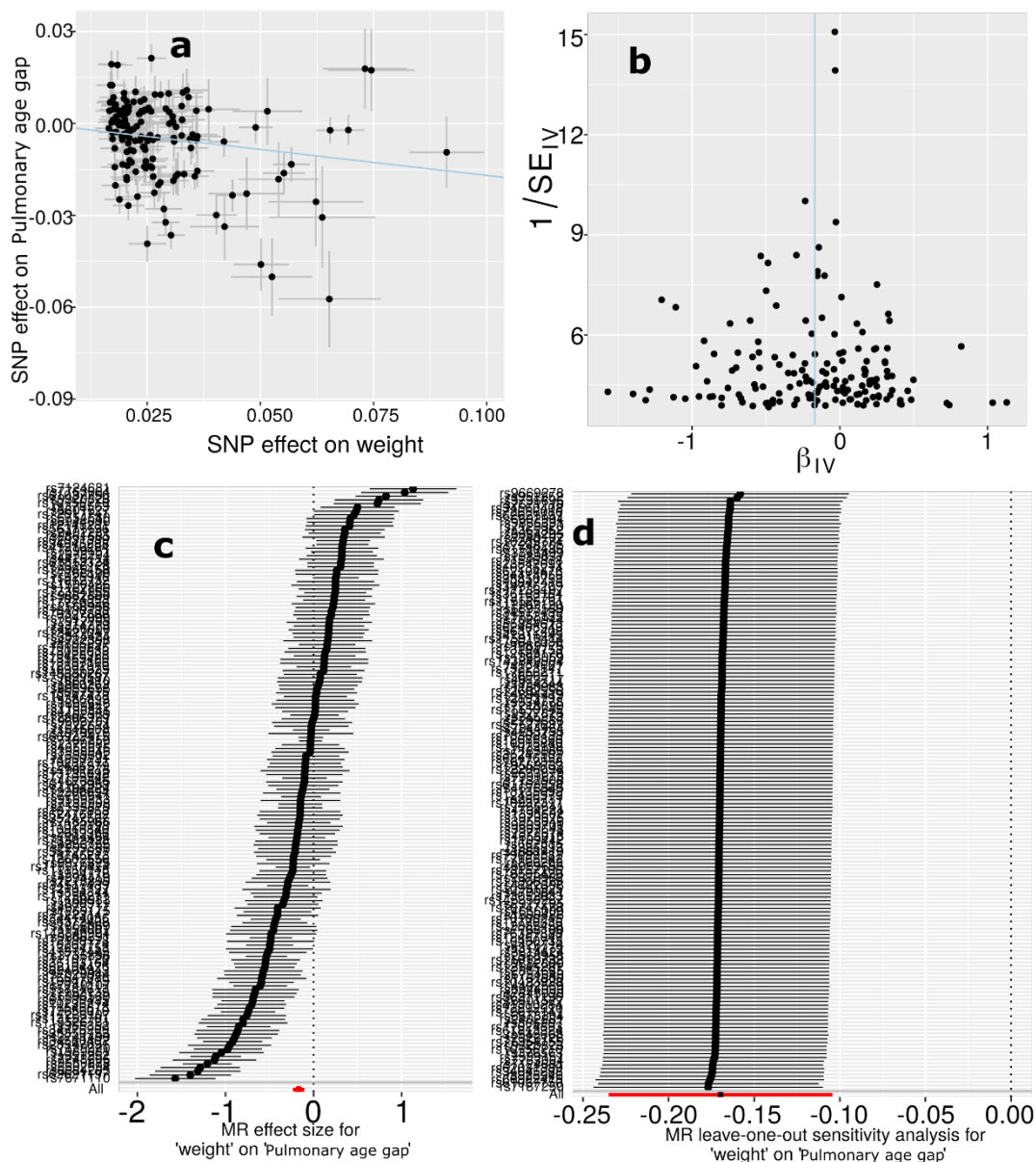
631 the 95% CI by excluding that SNP from the analysis. The red line depicts the IVW estimator
632 using all SNPs.
633

634 **eFigure 30: Mendelian randomization sensitivity check for weight on the musculoskeletal**
 635 **BAG**

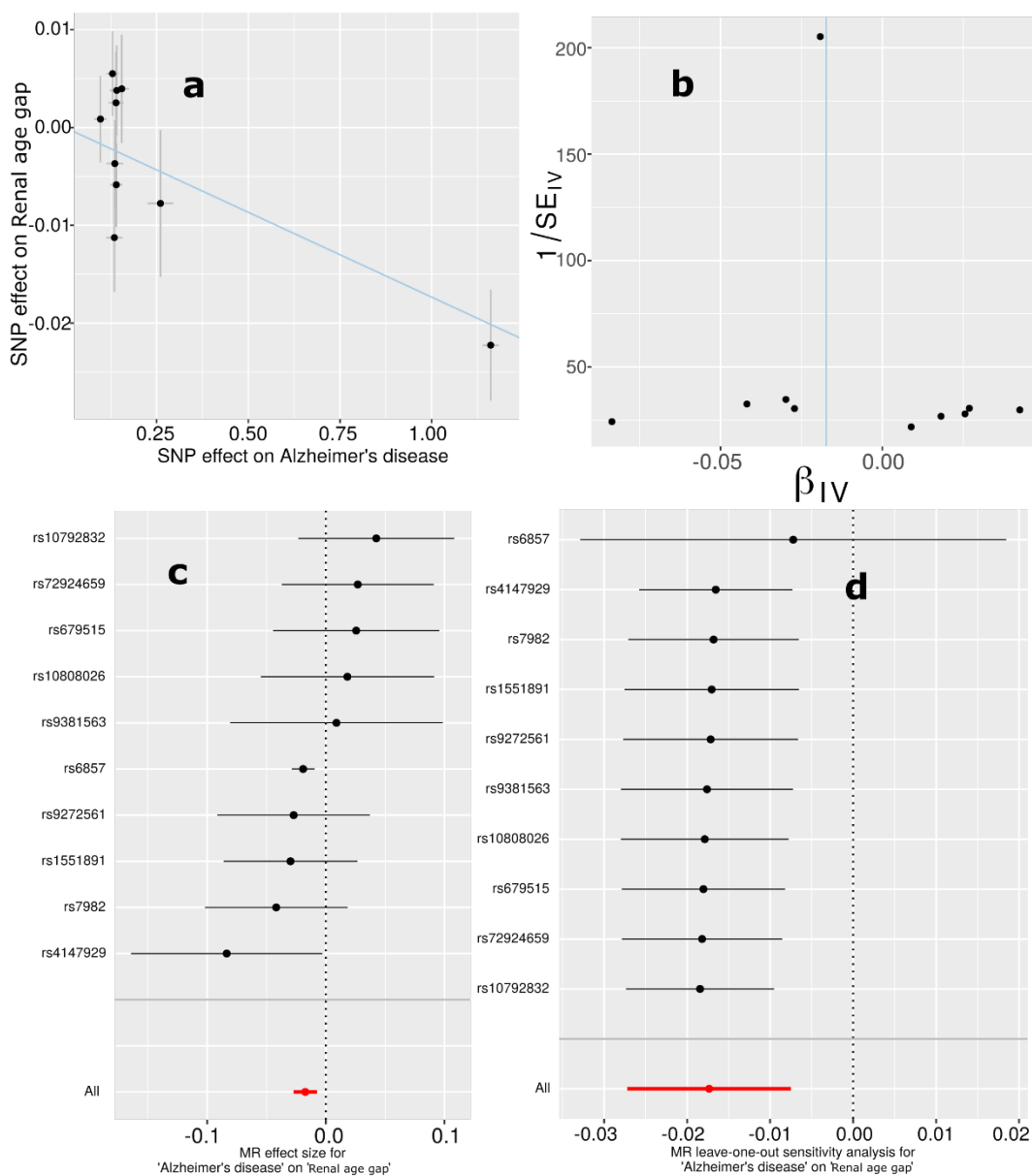


636
 637 **a)** Scatter plot for the MR effect sizes of the exposure variable (body weight, x -axis, SD units)
 638 and the outcome variable (musculoskeletal BAG, y -axis, log OR) with standard error bars. The
 639 slopes of the regression line correspond to the causal effect sizes estimated by the IVW
 640 estimator. **b)** Funnel plot for the relationship between the causal effect of the exposure variable
 641 on the outcome variable. Each dot represents MR effect sizes estimated using each SNP as a
 642 separate instrument against the inverse of the standard error of the causal estimate. The vertical
 643 red line shows the MR estimates using all SNPs. **c)** Forest plot for the single-SNP MR results.
 644 Each line represents the MR effect (log OR) for the exposure variable on the outcome variable
 645 using only one SNP; the red line shows the MR effect using all SNPs together. **d)** Leave-one-out
 646 analysis of the exposure variable on the outcome variable. Each row represents the MR effect

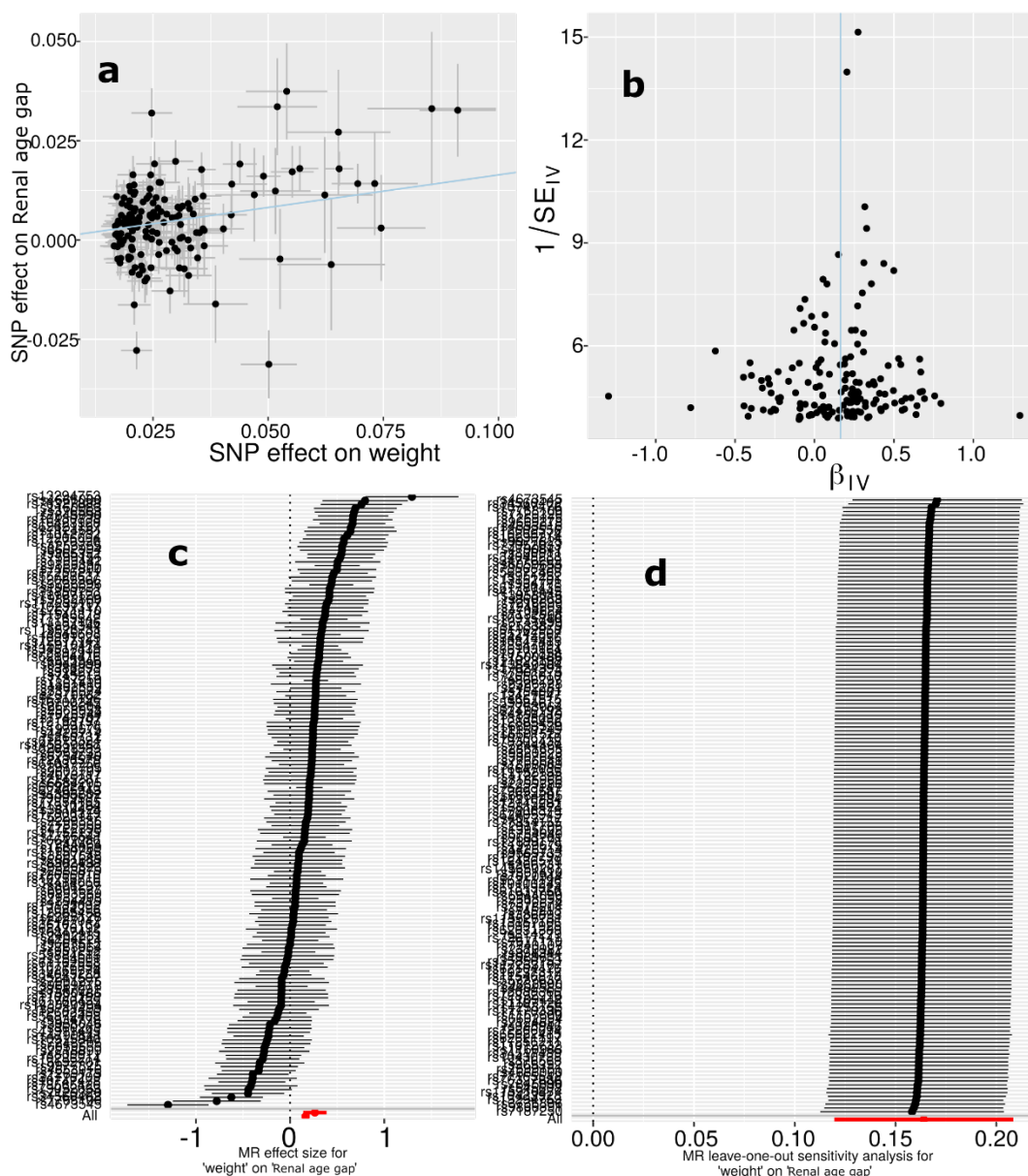
647 (log OR) and the 95% CI by excluding that SNP from the analysis. The red line depicts the IVW
648 estimator using all SNPs.
649

650 **eFigure 31: Mendelian randomization sensitivity check for weight on the pulmonary BAG**

651
 652 **a)** Scatter plot for the MR effect sizes of the exposure variable (body weight, x -axis, SD units)
 653 and the outcome variable (pulmonary BAG, y -axis, log OR) with standard error bars. The slopes
 654 of the regression line correspond to the causal effect sizes estimated by the IVW estimator. **b)**
 655 Funnel plot for the relationship between the causal effect of the exposure variable on the
 656 outcome variable. Each dot represents MR effect sizes estimated using each SNP as a separate
 657 instrument against the inverse of the standard error of the causal estimate. The vertical red line
 658 shows the MR estimates using all SNPs. **c)** Forest plot for the single-SNP MR results. Each line
 659 represents the MR effect (log OR) for the exposure variable on the outcome variable using only
 660 one SNP; the red line shows the MR effect using all SNPs together. **d)** Leave-one-out analysis of
 661 the exposure variable on the outcome variable. Each row represents the MR effect (log OR) and
 662 the 95% CI by excluding that SNP from the analysis. The red line depicts the IVW estimator
 663 using all SNPs.

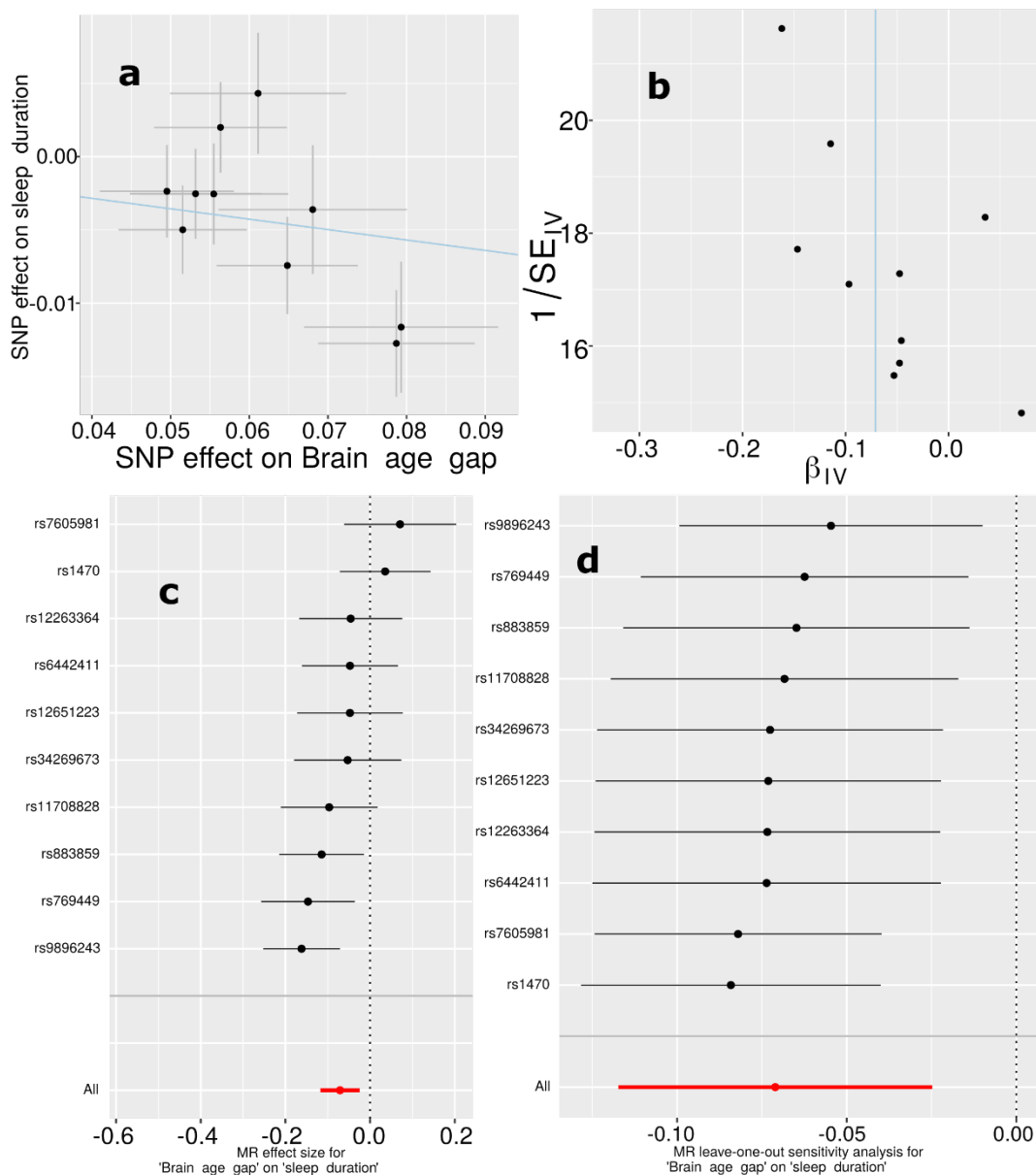
664 **eFigure 32: Mendelian randomization sensitivity check for AD on the renal BAG**

665
 666 **a)** Scatter plot for the MR effect sizes of the exposure variable (AD, x -axis, SD units) and the
 667 outcome variable (renal BAG, y -axis, log OR) with standard error bars. The slopes of the
 668 regression line correspond to the causal effect sizes estimated by the IVW estimator. **b)** Funnel
 669 plot for the relationship between the causal effect of the exposure variable on the outcome
 670 variable. Each dot represents MR effect sizes estimated using each SNP as a separate instrument
 671 against the inverse of the standard error of the causal estimate. The vertical red line shows the
 672 MR estimates using all SNPs. **c)** Forest plot for the single-SNP MR results. Each line represents
 673 the MR effect (log OR) for the exposure variable on the outcome variable using only one SNP;
 674 the red line shows the MR effect using all SNPs together. **d)** Leave-one-out analysis of the
 675 exposure variable on the outcome variable. Each row represents the MR effect (log OR) and the
 676 95% CI by excluding that SNP from the analysis. The red line depicts the IVW estimator using
 677 all SNPs.

678 **eFigure 33: Mendelian randomization sensitivity check for weight on the renal BAG**

679
 680 **a)** Scatter plot for the MR effect sizes of the exposure variable (body weight, x -axis, SD units)
 681 and the outcome variable (renal BAG, y -axis, log OR) with standard error bars. The slopes of the
 682 regression line correspond to the causal effect sizes estimated by the IVW estimator. **b)** Funnel
 683 plot for the relationship between the causal effect of the exposure variable on the outcome
 684 variable. Each dot represents MR effect sizes estimated using each SNP as a separate instrument
 685 against the inverse of the standard error of the causal estimate. The vertical red line shows the
 686 MR estimates using all SNPs. **c)** Forest plot for the single-SNP MR results. Each line represents
 687 the MR effect (log OR) for the exposure variable on the outcome variable using only one SNP;
 688 the red line shows the MR effect using all SNPs together. **d)** Leave-one-out analysis of the
 689 exposure variable on the outcome variable. Each row represents the MR effect (log OR) and the
 690 95% CI by excluding that SNP from the analysis. The red line depicts the IVW estimator using
 691 all SNPs.

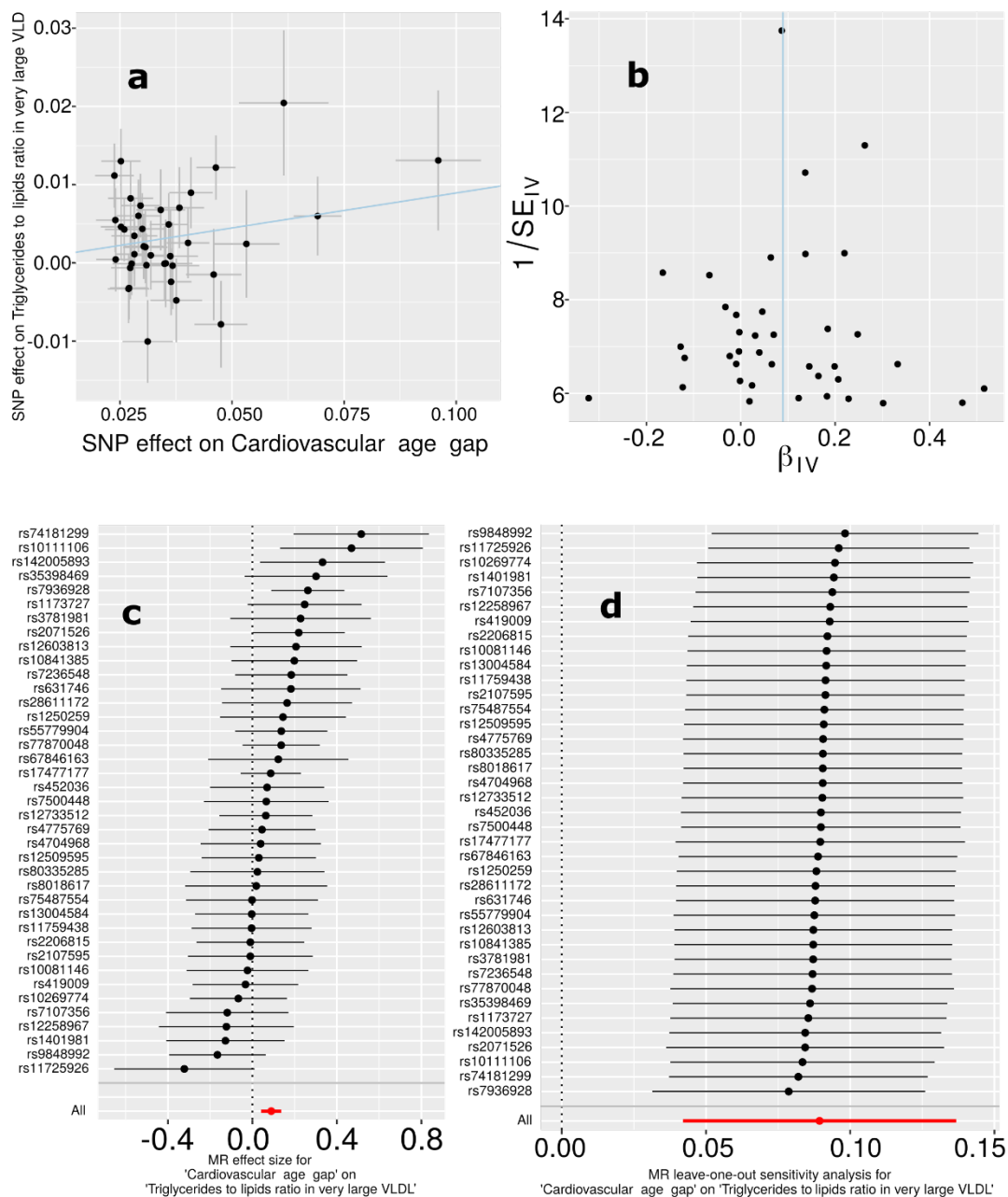
692 **eFigure 34: Mendelian randomization sensitivity check for the brain BAG on sleep**
 693 **duration**



694
 695 **a)** Scatter plot for the MR effect sizes of the exposure variable (brain BAG, x-axis, SD units) and
 696 the outcome variable (sleep duration, y-axis, log OR) with standard error bars. The slopes of the
 697 regression line correspond to the causal effect sizes estimated by the IVW estimator. **b)** Funnel
 698 plot for the relationship between the causal effect of the exposure variable on the outcome
 699 variable. Each dot represents MR effect sizes estimated using each SNP as a separate instrument
 700 against the inverse of the standard error of the causal estimate. The vertical red line shows the
 701 MR estimates using all SNPs. **c)** Forest plot for the single-SNP MR results. Each line represents
 702 the MR effect (log OR) for the exposure variable on the outcome variable using only one SNP;
 703 the red line shows the MR effect using all SNPs together. **d)** Leave-one-out analysis of the
 704 exposure variable on the outcome variable. Each row represents the MR effect (log OR) and the

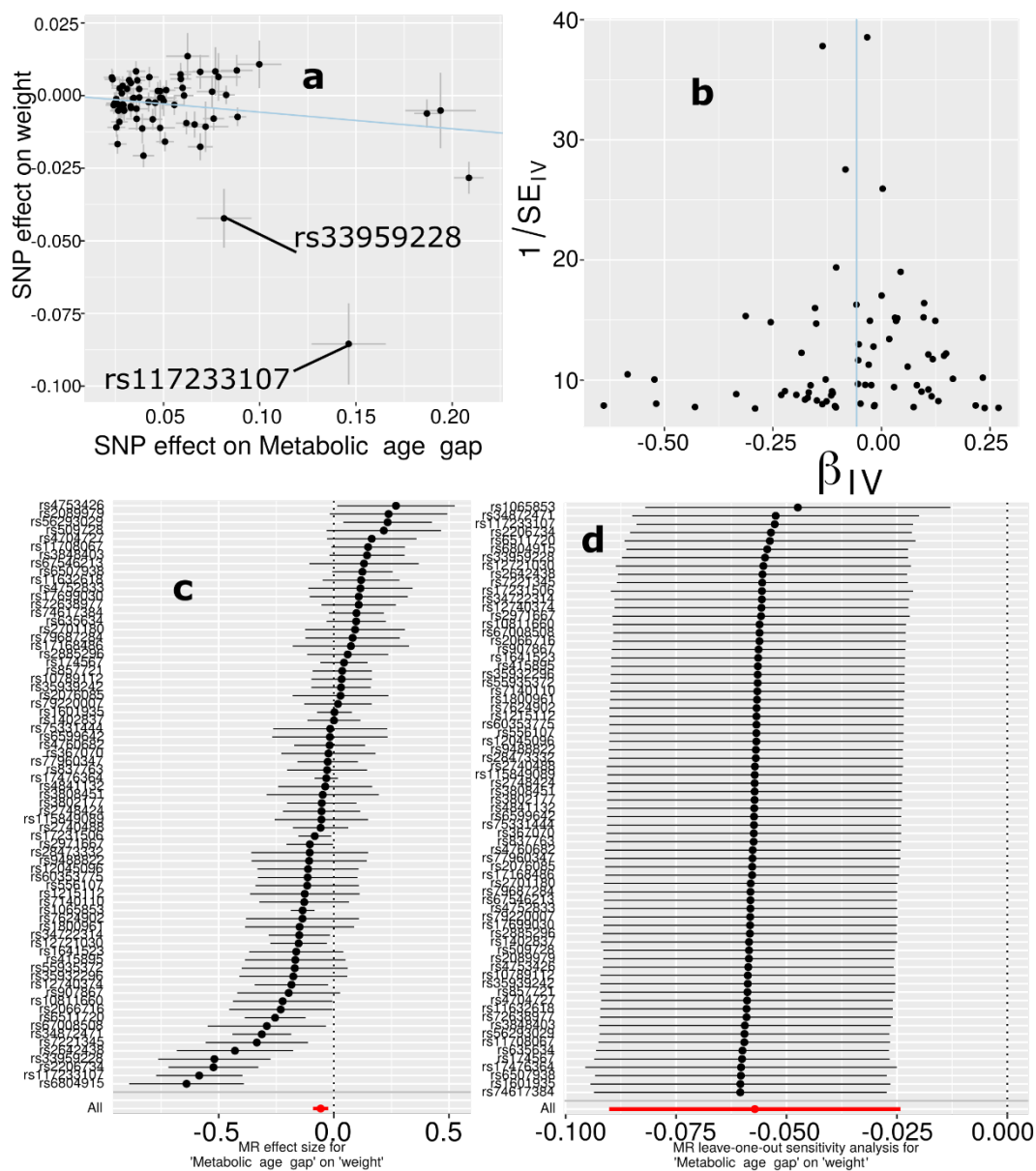
705 95% CI by excluding that SNP from the analysis. The red line depicts the IVW estimator using
706 all SNPs.
707

708 **eFigure 35: Mendelian randomization sensitivity check for the cardiovascular BAG on**
 709 **triglycerides to lipids ratio in very large VLDL**

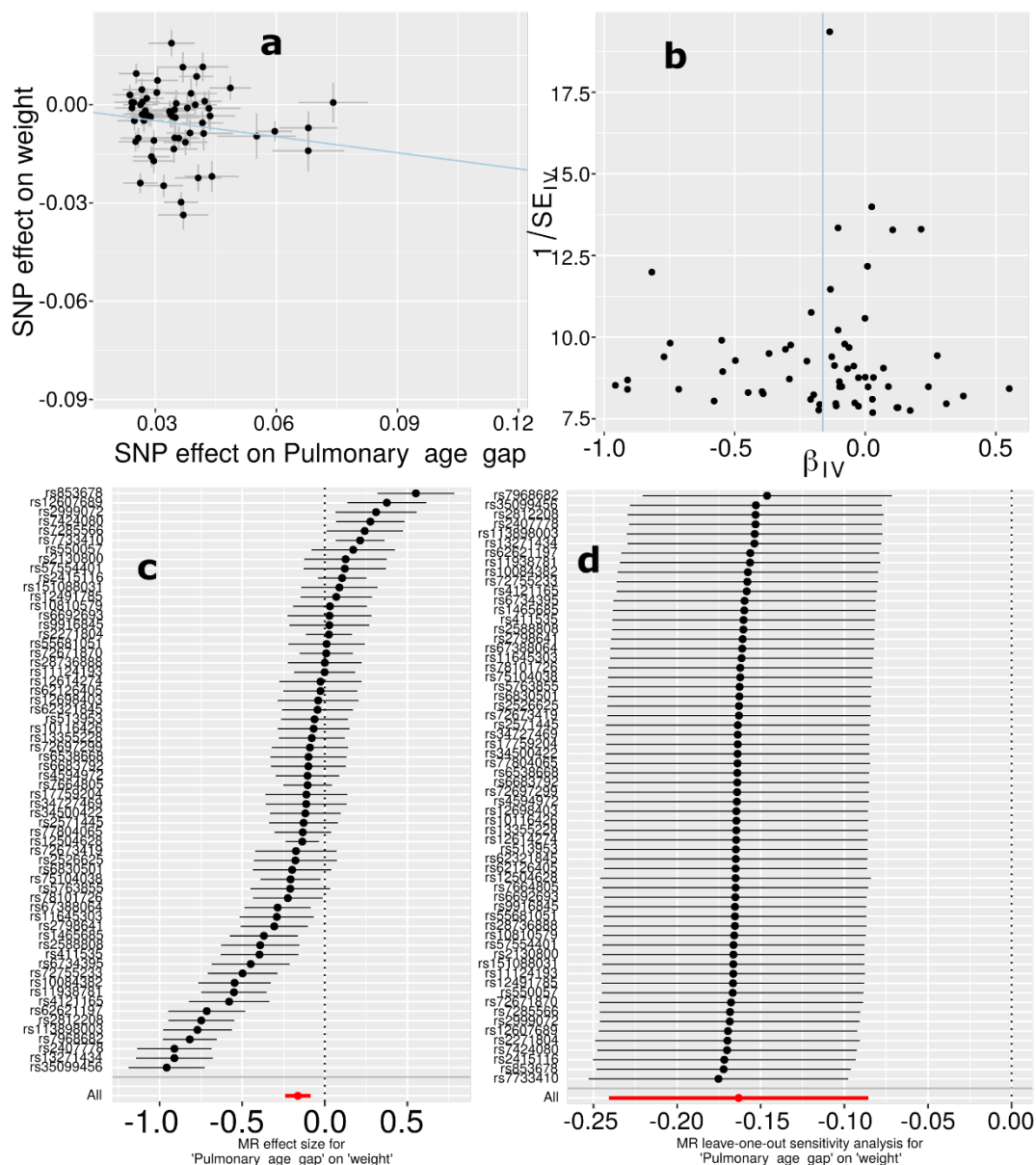


710 **a)** Scatter plot for the MR effect sizes of the exposure variable (cardiovascular BAG, x -axis, SD
 711 units) and the outcome variable (triglycerides to lipids ratio in very large VLDL, y -axis, log OR)
 712 with standard error bars. The slopes of the regression line correspond to the causal effect sizes
 713 estimated by the IVW estimator. **b)** Funnel plot for the relationship between the causal effect of
 714 the exposure variable on the outcome variable. Each dot represents MR effect sizes estimated
 715 using each SNP as a separate instrument against the inverse of the standard error of the causal
 716 estimate. The vertical red line shows the MR estimates using all SNPs. **c)** Forest plot for the
 717 single-SNP MR results. Each line represents the MR effect (log OR) for the exposure variable on
 718 the outcome variable using only one SNP; the red line shows the MR effect using all SNPs
 719

720 together. **d)** Leave-one-out analysis of the exposure variable on the outcome variable. Each row
721 represents the MR effect (log OR) and the 95% CI by excluding that SNP from the analysis. The
722 red line depicts the IVW estimator using all SNPs.
723

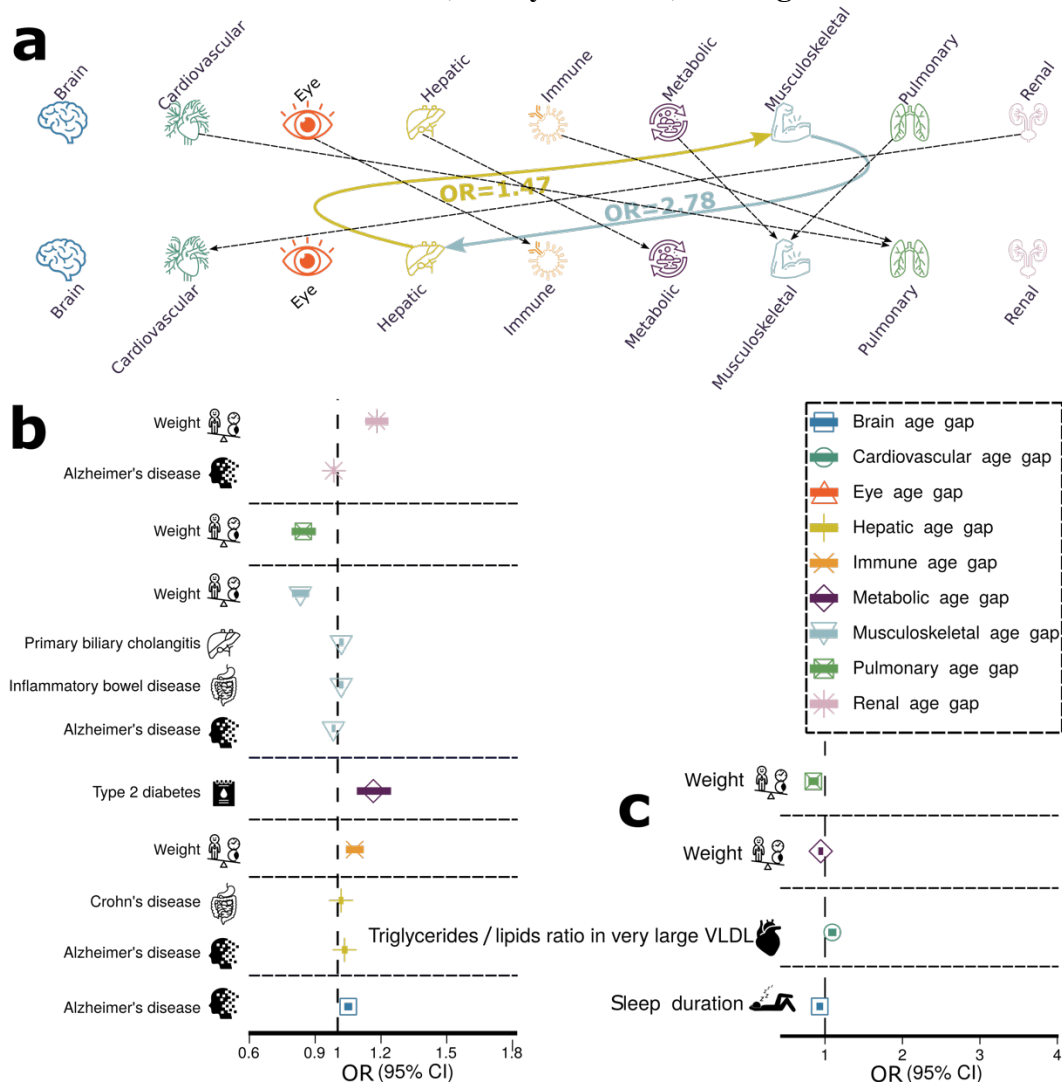
724 **eFigure 36: Mendelian randomization sensitivity check for the metabolic BAG on weight**

725
 726 **a)** Scatter plot for the MR effect sizes of the exposure variable (metabolic BAG, x-axis, SD
 727 units) and the outcome variable (body weight, y-axis, log OR) with standard error bars. The
 728 slopes of the regression line correspond to the causal effect sizes estimated by the IVW
 729 estimator. **b)** Funnel plot for the relationship between the causal effect of the exposure variable
 730 on the outcome variable. Each dot represents MR effect sizes estimated using each SNP as a
 731 separate instrument against the inverse of the standard error of the causal estimate. The vertical
 732 red line shows the MR estimates using all SNPs. **c)** Forest plot for the single-SNP MR results.
 733 Each line represents the MR effect (log OR) for the exposure variable on the outcome variable
 734 using only one SNP; the red line shows the MR effect using all SNPs together. **d)** Leave-one-out
 735 analysis of the exposure variable on the outcome variable. Each row represents the MR effect
 736 (log OR) and the 95% CI by excluding that SNP from the analysis. The red line depicts the IVW
 737 estimator using all SNPs.

738 **eFigure 37: Mendelian randomization sensitivity check for the pulmonary BAG on weight**

739
 740 **a)** Scatter plot for the MR effect sizes of the exposure variable (pulmonary BAG, x-axis, SD
 741 units) and the outcome variable (body weight, y-axis, log OR) with standard error bars. The
 742 slopes of the regression line correspond to the causal effect sizes estimated by the IVW
 743 estimator. **b)** Funnel plot for the relationship between the causal effect of the exposure variable
 744 on the outcome variable. Each dot represents MR effect sizes estimated using each SNP as a
 745 separate instrument against the inverse of the standard error of the causal estimate. The vertical
 746 red line shows the MR estimates using all SNPs. **c)** Forest plot for the single-SNP MR results.
 747 Each line represents the MR effect (log OR) for the exposure variable on the outcome variable
 748 using only one SNP; the red line shows the MR effect using all SNPs together. **d)** Leave-one-out
 749 analysis of the exposure variable on the outcome variable. Each row represents the MR effect
 750 (log OR) and the 95% CI by excluding that SNP from the analysis. The red line depicts the IVW
 751 estimator using all SNPs.

752 **eFigure 38: Causal multi-organ network between the nine biological age gaps and 17**
 753 **clinical traits of chronic diseases, lifestyle factors, and cognition**



754 **a)** Causal inference between each pair of BAGs using bi-directional two-sample Mendelian
 755 randomization by excluding overlapping populations. The colored lines represent causal effects
 756 that survived the correction for multiple comparisons using the Bonferroni method; the dotted
 757 lines denote the nominal significant causal effects (P -value < 0.05). **b)** The forward Mendelian
 759 randomization investigates the causal inference of 17 unbiasedly selected exposure variables on
 760 the nine outcome variables (i.e., the nine BAGs). **c)** The inverse Mendelian randomization
 761 examines the causal inference of the 9 BAGs on the 17 clinical traits. We present the tests
 762 passing the statistical significance after adjusting for multiple comparisons using the Bonferroni
 763 correction. The OR and the 95% confidence interval are presented. Abbreviation: VLDL: very
 764 low-density lipoprotein; CI: confidence interval; OR: odds ratio.
 765

766 **eTable 1: Heritability estimates using the GCTA software**767 **A) Original sample sizes.** Original sample sizes were used to estimate the heritability for
768 the nine organ systems.

| BAG | h^2 | h^2 SE | P-value | N |
|-----------------|-------|----------|----------------------|----------|
| Brain | 0.47 | 0.02 | $<1 \times 10^{-10}$ | 30,108 |
| Cardiovascular | 0.27 | 0.006 | $<1 \times 10^{-10}$ | 111,543 |
| Eye | 0.38 | 0.02 | $<1 \times 10^{-10}$ | 36,004 |
| Hepatic | 0.23 | 0.006 | $<1 \times 10^{-10}$ | 111,543 |
| Immune | 0.20 | 0.004 | $<1 \times 10^{-10}$ | 111,543 |
| Metabolic | 0.29 | 0.006 | $<1 \times 10^{-10}$ | 111,543 |
| Musculoskeletal | 0.24 | 0.004 | $<1 \times 10^{-10}$ | 111,543 |
| Pulmonary | 0.36 | 0.006 | $<1 \times 10^{-10}$ | 111,543 |
| Renal | 0.30 | 0.006 | $<1 \times 10^{-10}$ | 111,543 |

769 **B) Down-sampled sample sizes.** For the eight BAGs except for the brain BAG, we
770 randomly down-sampled the original sample sizes to that of the brain BAG.
771

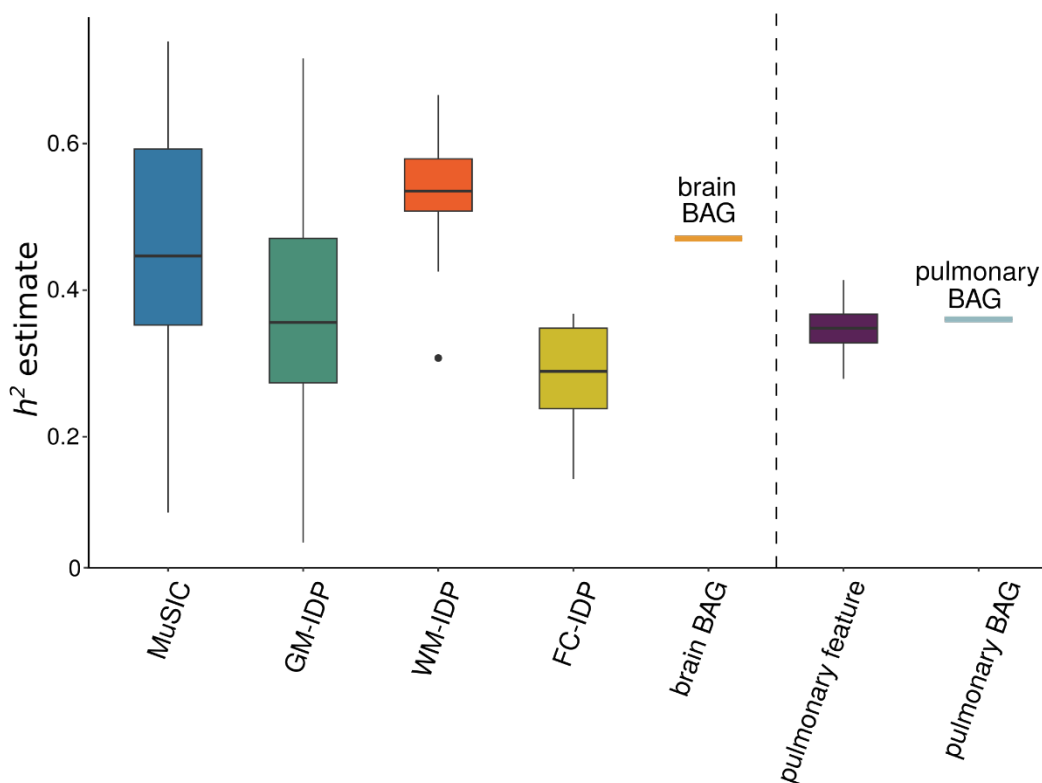
| BAG | h^2 | h^2 SE | P-value | N |
|-----------------|-------|----------|----------------------|----------|
| Brain | 0.47 | 0.02 | $<1 \times 10^{-10}$ | 30,108 |
| Cardiovascular | 0.35 | 0.07 | $<1 \times 10^{-5}$ | 30,108 |
| Eye | 0.42 | 0.02 | $<1 \times 10^{-5}$ | 30,108 |
| Hepatic | 0.18 | 0.07 | $<1 \times 10^{-5}$ | 30,108 |
| Immune | 0.19 | 0.07 | $<1 \times 10^{-5}$ | 30,108 |
| Metabolic | 0.16 | 0.07 | $<1 \times 10^{-5}$ | 30,108 |
| Musculoskeletal | 0.21 | 0.07 | $<1 \times 10^{-5}$ | 30,108 |
| Pulmonary | 0.39 | 0.07 | $<1 \times 10^{-5}$ | 30,108 |
| Renal | 0.28 | 0.07 | $<1 \times 10^{-5}$ | 30,108 |

772
773 **C) Brain imaging-derived phenotypes vs. 4 pulmonary features.** For the brain imaging
774 phenotypes, we used four sets of features from our previous studies: *i*) 32 pattern of
775 structural coavairance (PSCs) from the data-driven MuSIC atlas using T1-weighted MRI
776 and orthogonal-projective non-negative matrix factorization³; *ii*) 101 GM ROIs using the
777 ANTs (<https://stnava.github.io/ANTs/>) software⁴; *iii*) the 21 WM tracts for fractional
778 anisotropy (FA) mean values⁵; and *iv*) 21 funtional node (FN) measures from resting-
779 state functional MRI⁶. The 4 pulmonary features included forced vital capacity, forced
780 expiratory volume, peak expiratory flow, and the ratio of forced expiratory volume to
781 forced vital capacity. For comparison purposes, we also show the h^2 estimates for the
782 brain and pulmonary BAGs. The detailed results for all estimates are presented in
783 **Supplementary eFile 22**. The distribution of each phenotype group is shown in the
784 figure below.

| Organ | Phenotype group | Phenotype (mean or individual) | h^2 | h^2 SE | P-value |
|--------------|------------------------|---------------------------------------|-------|----------|----------------------|
| Brain | Brain feature | MuSIC ³ | 0.45 | 0.16 | $<1 \times 10^{-20}$ |
| | | GM-IDP ⁴ | 0.39 | 0.16 | $<1 \times 10^{-20}$ |
| | | WM-IDP ⁵ | 0.53 | 0.08 | $<1 \times 10^{-20}$ |

| | | | | | |
|-----------|---------------|---------------------|------|-------|--------------------|
| | | FN-IDP ⁶ | 0.29 | 0.06 | <1E ⁻²⁰ |
| | Brain BAG | Brain BAG | 0.47 | 0.02 | <1E ⁻²⁰ |
| Pulmonary | feature | FVC | 0.34 | 0.007 | <1E ⁻²⁰ |
| | | FEV/FVC | 0.41 | 0.007 | <1E ⁻²⁰ |
| | | PEF | 0.28 | 0.007 | <1E ⁻²⁰ |
| | | FEV | 0.35 | 0.007 | <1E ⁻²⁰ |
| | Pulmonary BAG | Pulmonary BAG | 0.36 | 0.006 | <1E ⁻²⁰ |

785



786

787 **Figure.** We compared h^2 estimates using GCTA between brain features and the brain BAG in
 788 contrast to pulmonary features and the pulmonary BAG. In general, our observations indicated
 789 that the brain BAG (0.47 ± 0.02) exhibits a higher degree of heritability than the pulmonary BAG
 790 (0.36 ± 0.06), and this pattern aligns with the heritability of the underlying features employed in
 791 their computation: Brain feature: $h^2=0.42$ across the four sets of brain features vs. pulmonary
 792 feature: $h^2=0.34$ across the four pulmonary features.

793

794 **eTable 2: The beta coefficient and its SE estimate from the full sample vs. the down-**
 795 **sampled brain BAG comparable sample**

796 N_ISS: number of independent significant SNPs

| BAG | Mean_beta_down sample | Mean_beta_full sample | SE_beta_down sample | SE_beta_fulls ample | t_beta | p_beta | t_se | p_se | N_ISS |
|-----------------|--------------------------|--------------------------|------------------------|------------------------|------------------|--------------|--------------|----------------------------|-------|
| Cardiovascular | 0.034802 | 0.035822 | 0.010533 | 0.005457 | - 0.513 17 | 0.608 293 | 14.08 46 | 1.95E -33 | 124 |
| Eye | 0.06527 | 0.064561 | 0.009967 | 0.009128 | 0.136 138 | 0.891 913 | 1.828 485 | 0.069 668 | 69 |
| Hepatic | 0.058408 | 0.057479 | 0.014495 | 0.007525 | 0.293 471 | 0.769 268 | 13.28 265 | 2.59E -35 | 289 |
| Immune | 0.043347 | 0.041526 | 0.011454 | 0.005948 | 0.682 463 | 0.495 312 | 12.78 407 | 5.79E -32 | 217 |
| Metabolic | 0.053834 | 0.052587 | 0.013227 | 0.006842 | 0.490 113 | 0.624 182 | 15.99 737 | 1.7E- 50 | 422 |
| Musculoskeletal | 0.04263 | 0.041015 | 0.011109 | 0.005817 | 0.520 949 | 0.602 797 | 11.23 119 | 1.44E -24 | 147 |
| Pulmonary | 0.035423 | 0.036056 | 0.010959 | 0.005678 | - 0.536 29 | 0.591 975 | 20.08 143 | 1.81E -67 | 272 |
| Renal | 0.067828 | 0.068927 | 0.014536 | 0.007595 | - 0.233 5 | 0.815 446 | 12.87 744 | 5.18E -34 | 331 |

797

798 **eTable 3: Genetic correlation analyses between the pulmonary BAG and the four features**
 799 **used to derive the BAG.**
 800

| BAG | Pulmonary feature | g_c mean | g_c std | P |
|-------------------|---|------------|-----------|----------------------|
| Pulmonary_age_gap | forced_vital_capacity_fvc_zscore | 0.6409 | 0.0195 | 6.1E ⁻²³⁷ |
| | fev1_fvc_ratio_zscore | 0.5371 | 0.0316 | 6.47E ⁻⁶⁵ |
| | peak_expiratory_flow_pef | -0.7903 | 0.0175 | <1E ⁻³⁰⁰ |
| | forced_expiratory_volume_in_1second_fev1_zscore | 0.8259 | 0.0111 | <1E ⁻³⁰⁰ |

801

802 **eTable 4: Selected 41 clinical traits for genetic correlation analyses.** We selected the candidate
803 studies from the GWAS Catalog for 41 clinical traits, including chronic diseases affecting multiple
804 organ systems, education, and intelligence. To ensure the suitability of the GWAS summary
805 statistics, we first checked that the selected study's population was European ancestry; we then
806 guaranteed a moderate SNP-based heritability h^2 estimate and excluded the studies with spurious
807 low h^2 (<0.05). Abbreviations are detailed in the main text.
808

| Primary organ system | Trait | PubMed ID | Sample size |
|----------------------|----------------|-----------|-------------|
| Brain | AD | 30820047 | 63,926 |
| | Smile-GAN-AD1 | NA | 33,540 |
| | SmileGAN-AD2 | NA | 33,540 |
| | SmileGAN-AD3 | NA | 33,540 |
| | SmileGAN-AD4 | NA | 33,540 |
| | SurrealGAN-AD1 | NA | 33,540 |
| | SurrealGAN-AD2 | NA | 33,540 |
| | ADHD | 30478444 | 53,293 |
| | ALS | 27455348 | 36052 |
| | ASD | 30804558 | 46,350 |
| | HYDRA-ASD1 | 37017948 | 14,786 |
| | HYDRA-ASD2 | 37017948 | 14,786 |
| | HYDRA-ASD3 | 37017948 | 14,786 |
| | BIP | 31043756 | 51,710 |
| | MDD | 22472876 | 18,759 |
| | HYDRA-MDD1 | NA | 33,540 |
| | HYDRA-MDD2 | NA | 33,540 |
| | SCZ | 23974872 | 11,244 |
| | HYDRA-SCZ1 | 32103250 | 14,786 |
| | HYDRA-SCZ2 | 32103250 | 14,786 |
| OCD | 28761083 | 9,725 | |
| Cardiovascular | WMH | 31551276 | 11,226 |
| | AF | 30061737 | 1030,836 |
| | Stroke | 29531354 | 446,696 |
| Eye | Glaucoma | 33627673 | 330,905 |
| Hepatic | Liver fat | 34128465 | 32,858 |
| | PBC | 34033851 | 24,510 |
| Immune | SLE | 26502338 | 14,267 |
| | HIV | 34737426 | 208,808 |
| Metabolic | DB | 30054458 | 655,666 |
| | Hyperlipidemia | 34906840 | 349,222 |
| Musculoskeletal | RA | 36333501 | 92,044 |
| Pulmonary | Lung carcinoma | 28604730 | 85,716 |
| Renal | CKD | 31152163 | 625,219 |
| Digestive | CD | 26192919 | 20,883 |
| | IBD | 26192919 | 34652 |
| Breast | Breast cancer | 29059683 | 139,274 |

| | | | |
|-----------|---------------|----------|---------|
| | Education | 23722424 | 126,559 |
| Cognition | Reaction time | 29844566 | 330,069 |
| | Intelligence | 28530673 | 78,308 |
| Lifestyle | Computer use | 32317632 | 408,815 |

809

810

811 **eTable 5: Genetic correlations analyses between the nine BAGs and longevity, household**
 812 **income, and telomere length.** We downloaded the GWAS summary statistics from Deelen et al.⁷,
 813 which performed two GWASs on longevity based on the 90th survival percentile. For the household
 814 income GWAS, we downloaded from Hill et al.⁸. For the telomere length, we used GWAS
 815 summary statistics from Codd et al.⁹.
 816

| BAG | Trait | g_c mean | g_c std | P | PubMed ID | Sample size |
|-------------------------|------------------|------------|-----------|---------------------|-----------|-------------|
| Brain_age_gap | | gc mean | gc_std | 0.0931 | | |
| Cardiovascular_age_gap | | -0.1588 | 0.0946 | 0.0049 | | |
| Eye_age_gap | | -0.2038 | 0.0725 | 0.0719 | | |
| Hepatic_age_gap | | -0.1657 | 0.0921 | 0.6182 | | |
| Immune_age_gap | Longevity | 0.0495 | 0.0993 | 0.9299 | 31413236 | 36,745 |
| Metabolic_age_gap | | 0.0086 | 0.0979 | 0.7605 | | |
| Musculoskeletal_age_gap | | 0.0328 | 0.1074 | 0.1128 | | |
| Pulmonary_age_gap | | -0.1193 | 0.0752 | 0.0057 | | |
| Renal_age_gap | | -0.197 | 0.0713 | 0.0323 | | |
| Brain_age_gap | | -0.2089 | 0.0403 | 2.2E ⁻⁰⁷ | | |
| Cardiovascular_age_gap | | -0.0679 | 0.0356 | 0.0563 | | |
| Eye_age_gap | | -0.066 | 0.0404 | 0.1024 | | |
| Hepatic_age_gap | Household income | -0.1026 | 0.0417 | 0.0138 | 31874048 | 286,301 |
| Immune_age_gap | | 0.0028 | 0.0414 | 0.9464 | | |
| Metabolic_age_gap | | -0.0671 | 0.0389 | 0.0841 | | |
| Musculoskeletal_age_gap | | -0.2867 | 0.0308 | 1.4E ⁻²⁰ | | |
| Pulmonary_age_gap | | -0.1567 | 0.0286 | 4.4E ⁻⁰⁸ | | |
| Renal_age_gap | | -0.0989 | 0.0321 | 0.002 | | |
| Brain_age_gap | | 0.0273 | 0.0506 | 0.5897 | | |
| Cardiovascular_age_gap | | -0.0005 | 0.0038 | 0.9897 | | |
| Eye_age_gap | | -0.0124 | 0.0439 | 0.7769 | | |
| Hepatic_age_gap | | -0.0042 | 0.0306 | 0.9089 | | |
| Immune_age_gap | Telomere length | -0.1338 | 0.0377 | 0.0004 | 34611362 | 472,174 |
| Metabolic_age_gap | | -0.0514 | 0.0393 | 0.1905 | | |
| Musculoskeletal_age_gap | | 0.0045 | 0.0333 | 0.8932 | | |
| Pulmonary_age_gap | | -0.0993 | 0.0331 | 0.0027 | | |
| Renal_age_gap | | -0.029 | 0.0293 | 0.3222 | | |

817

818 **eTable 6: Causal analysis using the LCV method.** We performed causal analysis using the LCV
 819 method for the bi-directional causality between hepatic and musculoskeletal BAGs, the 9 BAGs
 820 and longevity, and the 9 BAGs and telomere length. GCP: genetic causality proportion.
 821

| Trait1 | Trait2 | GCP | GCP_se | P | PubMed ID | Sample size |
|-------------------------|---|----------|----------|-----------------|-----------|-------------|
| Musculoskeletal age gap | Hepatic_age_gap | -0.75144 | 0.143475 | 9.37E-12 | NA | 111,543 |
| Brain_age_gap | Longevity (99 th percentile) | -0.45597 | 0.208644 | 0.047488 | 31874048 | 286,301 |
| Cardiovascular_age_gap | | -0.21694 | 0.395088 | 0.547241 | | |
| Eye_age_gap | | -0.07761 | 0.565366 | 0.639544 | | |
| Hepatic_age_gap | | -0.53253 | 0.321599 | 0.089042 | | |
| Immune_age_gap | | -0.15001 | 0.356513 | 0.868225 | | |
| Musculoskeletal_age_gap | | -0.26633 | 0.440294 | 0.827824 | | |
| Metabolic_age_gap | | -0.3153 | 0.391594 | 0.866896 | | |
| Pulmonary_age_gap | | -0.18056 | 0.375253 | 0.210053 | | |
| Renal_age_gap | | -0.33425 | 0.403767 | 0.573389 | | |
| Brain_age_gap | Telomere length | -0.05796 | 0.55584 | 0.713688 | 34611362 | 472,174 |
| Cardiovascular_age_gap | | -0.32007 | 0.294362 | 0.421771 | | |
| Eye_age_gap | | -0.11877 | 0.49709 | 0.926991 | | |
| Hepatic_age_gap | | -0.00755 | 0.332263 | 0.792948 | | |
| Immune_age_gap | | -0.3321 | 0.126005 | 0.002502 | | |
| Metabolic_age_gap | | -0.07943 | 0.45872 | 0.705827 | | |
| Musculoskeletal_age_gap | | -0.15992 | 0.478106 | 0.821179 | | |
| Pulmonary_age_gap | | -0.67193 | 0.198345 | 3.57E-16 | | |
| Renal_age_gap | | -0.17496 | 0.500093 | 0.6767 | | |

822

823 **eTable 7: Selected 17 clinical traits for Mendelian randomization analyses.** We unbiasedly
 824 and systematically selected 17 clinical traits, including chronic diseases affecting multiple organ
 825 systems, cognition, and lifestyle factors. The selection procedure is detailed in the main text
 826 **(Method 2J).**
 827

| Primary organ system | Trait | PubMed ID | IEU-ID (If applicable) | Number of IVs (forward MR) |
|----------------------|------------------------------|-----------|--|----------------------------|
| Brain | AD | 24162737 | ebi-a-GCST002245 | 10 |
| | BIP | 31043756 | ieu-a-1126 | 12 |
| Metabolic | Type 2 diabetes | 22885922 | ieu-a-26 | 10 |
| | Triglyceride-to-lipid ratio | 32114887 | XL_VLDL_TG_pct finn-b- H7_GLAUCOMA | 41 |
| Eye | Glaucoma | NA | finn-b- H7_GLAUCOMA | 9 |
| Musculoskeletal | RA | 23143596 | ebi-a-GCST005569 | 11 |
| Hepatic | PBC | 26394269 | ebi-a-GCST003129 | 16 |
| Digestive | CD | 26192919 | ieu-a-12 | 77 |
| | IBD | 23128233 | ieu-a-292 | 81 |
| Breast | Breast cancer | 29059683 | ieu-a-1126 | 86 |
| Cognition | Reaction time | NA | Local-UKBB | 18 |
| Lifestyle | Coffee intake | NA | Local-UKBB | 11 |
| | Fresh fruit | NA | Local-UKBB | 15 |
| | Tea intake | NA | Local-UKBB | 12 |
| | Sleep duration | NA | Local-UKBB | 8 |
| | Summer outdoor activity hour | NA | Local-UKBB | 14 |
| | Body weight | NA | Local-UKBB | 161 |

828
 829
 830

831 **References**

- 832 1. Bowden, J. *et al.* A framework for the investigation of pleiotropy in two-sample summary
833 data Mendelian randomization. *Stat Med* **36**, 1783–1802 (2017).
- 834 2. Burgess, S. & Thompson, S. G. Interpreting findings from Mendelian randomization using the
835 MR-Egger method. *Eur J Epidemiol* **32**, 377–389 (2017).
- 836 3. Wen, J. *et al.* Novel genomic loci and pathways influence patterns of structural covariance in
837 the human brain. 2022.07.20.22277727 Preprint at
838 <https://doi.org/10.1101/2022.07.20.22277727> (2022).
- 839 4. Zhao, B. *et al.* Genome-wide association analysis of 19,629 individuals identifies variants
840 influencing regional brain volumes and refines their genetic co-architecture with cognitive and
841 mental health traits. *Nat Genet* **51**, 1637–1644 (2019).
- 842 5. Zhao, B. *et al.* Common genetic variation influencing human white matter microstructure.
843 *Science* **372**, (2021).
- 844 6. Zhao, B. *et al.* Common variants contribute to intrinsic human brain functional networks. *Nat*
845 *Genet* **54**, 508–517 (2022).
- 846 7. Deelen, J. *et al.* A meta-analysis of genome-wide association studies identifies multiple
847 longevity genes. *Nat Commun* **10**, 3669 (2019).
- 848 8. Hill, W. D. *et al.* Genome-wide analysis identifies molecular systems and 149 genetic loci
849 associated with income. *Nat Commun* **10**, 5741 (2019).
- 850 9. Codd, V. *et al.* Polygenic basis and biomedical consequences of telomere length variation. *Nat*
851 *Genet* **53**, 1425–1433 (2021).

852